NASA Contractor Report 189220

Creep Fatigue Life Prediction for Engine Hot Section Materials (Isotropic)

Second Interim Report

R.S. Nelson, G.W. Levan, and J.F. Schoendorf
United Technologies Corporation
Pratt & Whitney
Commercial Engineering

August 1992

NASA

National Aeronautics and
Space Administration
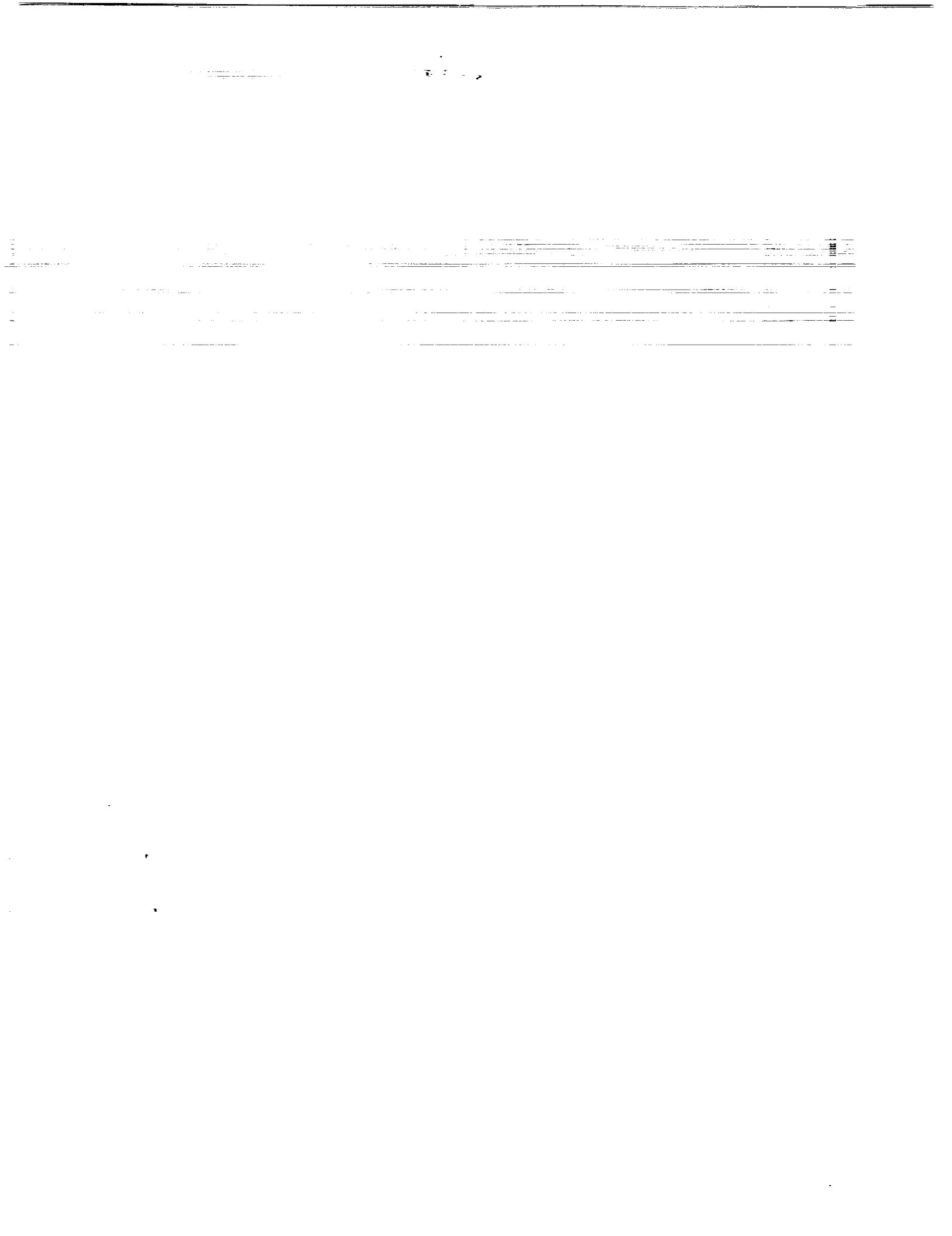
PREFACE

The Second Interim Report contained in this document details the activities performed under the optional program of the NASA HOST Contract, "Creep Fatigue Life Prediction for Engine Hot Section Materials (Isotropic)", under Contract NAS3-23288. The time period covered is from October 1985 through April 1987. The objective of this effort was to improve the high temperature crack initiation prediction technology for gas turbine hot section components. This program was conducted under the direction of Dr. Gary R. Halford, who served as the NASA Program Manager. The Program Manager at United Technologies Corporation was Mr. Richard S. Nelson who also served as prinicipal investigator, having responsibility for the life prediction model development and oversight of most of the technical tasks. Mr. Gregory W. Levan directed the metallographic examinations of the test material and specimens and provided interpretation of the results. Mr. John F. Schoendorf was responsible for the technical effort under Task VI, Multiaxial Stress State Model; Task VIII, Screening of Potential Environmental and Protective Coating Models; and Task IX, Environmental Attack Model.

TABLE OF CONTENTS

TABLE OF CONTENTS (Continued)

iv

SECTION 1.0
SUMMARY

A series of high temperature, strain controlled fatigue tests have been completed to study the effects of complex loadings such as thermomechanical fatigue, multiaxial loading, and imposed mean stresses along with reactive environments. Most of these tests used the cast nickel-base superalloy B1900+Hf (with and without coatings) as a baseline alloy. A small number of alternative alloy tests were run on wrought INCO 718.

A strong path dependence was demonstrated during the thermomechanical fatigue testing, using several different strain-temperature cycles, including in-phase, out-phase, and non-proportional (elliptical and "dogleg") cycles. Other test variables included temperature range, strain range, strain ratio and hold time. A series of multiaxial tests also demonstrated cycle path to be a significant variable, using both proportional and non-proportional tension-torsion loading.

Environmental screening tests were conducted in moderate pressure oxygen and purified argon; the oxygen reduced the specimen lives by a factor of two, while the argon testing produced ambiguous data. Both NiCoCrAlY overlay and diffusion aluminide coatings were evaluated on B1900+Hf material under isothermal and TMF conditions. In general, the lives of the coated specimens were higher than those of uncoated specimens tested under the same conditions, giving further evidence that environmental mechanisms are very important in the temperature range of 538-871°C(1000-1600°F).

Controlled mean stress TMF tests were conducted under load control instead of strain control so that a fixed mean stress could be maintained during each test. These tests showed that small mean stress changes could affect initiation lives by orders of magnitude. Such results are not conservatively predicted using traditional linear damage summation rules.

Extensive microstructural evaluations were completed for many specimens in this program using optical, Scanning Electron Microscopy (SEM), and Transmission Electron Microscopy (TEM) techniques. These techniques were used to categorize failure modes and to correlate the various types of dislocation configurations with fatigue capability. Crack initiation lives were determined using surface replication techniques; tensile load drop lives were recorded automatically by the test rig software. Life prediction models were then developed based on this information.

SECTION 2.0
INTRODUCTION

2.1 Contract Objectives

The overall operating cost of the modern gas turbine engine is greatly
influenced by the durability of combustor and turbine structural components
operating at high temperatures. Inadequate durability results in reduced
engine efficiency and increased maintenance costs due to premature repair and
replacement. To increase the durability of these components, more accurate
structural analysis and life prediction methods must be developed for compo-
nents operating at higher temperatures. However, improvements in the state-of-
the art technology for elevated temperature durability prediction have been
hampered by: 1) the severe operating conditions of the engine; 2) the inability
of analytical and life prediction tools to be successfully used in the design
of lower temperature components to predict complex material behavior and inter-
action of damage mechanisms of components at elevated temperatures; and 3) the
high cost of engine development testing which prohibits the accumulation of
adequate failure data and local operating conditions required for the system-
atic development and calibration of durability prediction models.

This contract began as part of the NASA Hot Section Technology (HOST) program
which was aimed at developing improved life prediction technology for
structures operating at elevated temperatures. It investigated fundamental
approaches to high temperature crack initiation life prediction, identified
modeling strategies and developed specific models for component relevant
loading conditions. The program was a 6-year, 2-part effort (2-year base
program plus a 4 year optional program) that considered two isotropic hot
section materials and protective coating systems. Under the base program,
various life prediction approaches for high temperature applications were
investigated, and basic models for simple cycle, isothermal loading conditions
were selected and developed. Models that addressed thermomechanical cycling,
multiaxial loading conditions, cumulative loading, environmental effects and
cyclic mean stress were developed under the optional program. Finally, to
demonstrate the applicability of these models to other materials, additional
tests were performed on an alternative material.

This report details the activities performed under the optional portion of
NASA Contract NAS3-23288, "Creep Fatigue Life Prediction for Engine Hot
Section Materials (Isotropic)", during the period from October 1985 through
April 1987. The specific areas covered include the following technical tasks:

        Task V   – Thermal-Mechanical Cycling Model
        Task VI   – Multiaxial Stress State Model
        Task VIII   – Screening of Potential Environmental and Protective Coating
                      Models
        Task IX   – Environmental Attack Model
        Task X   – Protective Coating Models
        Task XI   – Cyclic Mean Stress Model
        Task XII   – Final Verification and Evaluation of Alternative
                      Material/Protection Coating System/Component Combination

2

2.2 Overview of Previous Contract Activity

This section provides a brief review of the progress made during the first four years of this contract effort. It describes the early work performed during this period of the HOST contract and serves as background for the work covered by this report. The data generated during the base program will not be repeated in this report but may be found in the Second Annual Report (Moreno et al, 1984) and in the previous Interim Report (Nelson et al, 1986).

The following materials were recommended and approved for use in both the base and option portions of the program:

Base Material	=	Cast B1900 + Hf	(PWA 1455)
Alternate Material	=	Wrought INCO 718	(AMS 5663)
Coatings	=	Diffusion Aluminide	(PWA 273)
		MCrAlY Overlay	(PWA 286)

Details of the selection and characterization of these materials and of the preparation and testing of the specimens will be presented in Section 3.0.

A total of 21 tensile tests were completed on PWA 1455, covering the temperature range from room temperature to 1093°C (2000°F). Figure 1 shows typical stress-strain response curves for the standard strain rate of 0.005 min^{-1}. Also, a total of 19 specimens were creep tested at temperatures between 649°C (1200°F) and 982°C (1800°F). Both actual test data and post-test metallurgical examination of these monotonic specimen tests were used to understand the deformation mechanisms active at various temperatures for this material.
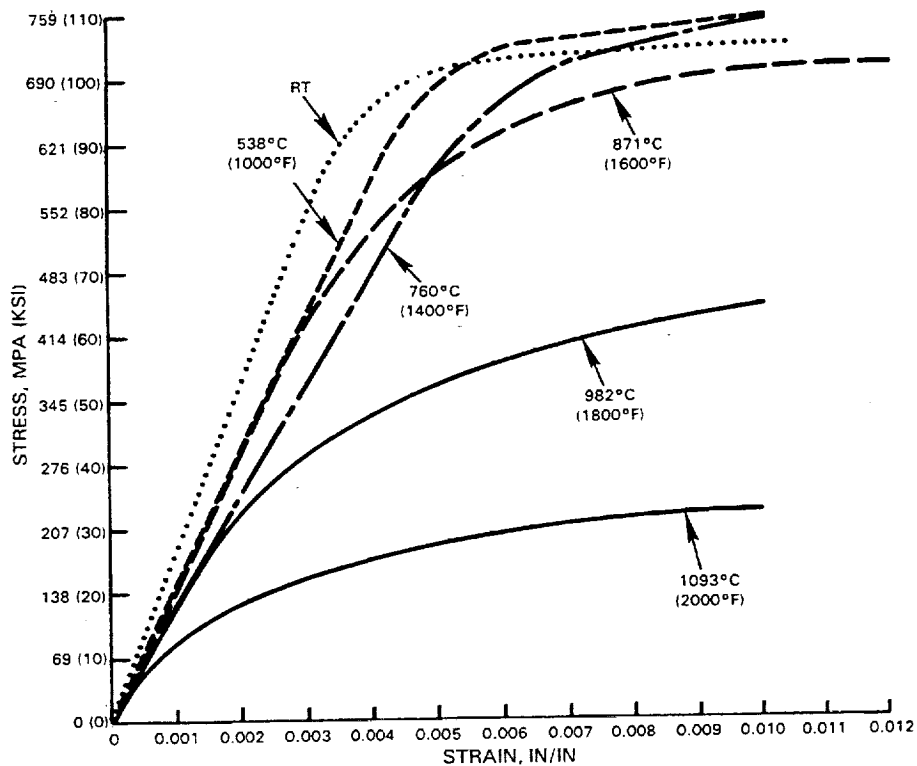
Figure 1.- Monotonic Tensile Response, $\dot{\varepsilon}$= .005 min^{-1}.

3

A total of 99 isothermal fatigue tests were conducted on PWA 1455 during the base program covering the temperature range from 538°C (1000°F) to 982°C (1800°F), with the bulk of the tests being run at 871°C (1600°F). The additional variables studied included strain range, ratio, and rate, as well as hold time effects. For each specimen, a crack initiation life was determined by means of surface replicas taken during tests conducted at similar conditions. The definition of initiation was chosen to be the generation of a 0.76 mm (0.030 in.) surface length crack. This surface length corresponds to a crack depth of about 1-2 grain diameters and is considered to represent the point at which the crack may be analyzed using linear elastic fracture mechanics.

Many specimens were examined metallographically using optical, SEM, and TEM techniques to determine failure sites, crack paths, and dislocation networks. No statistically significant difference could be seen between failures which originated at porosity and those which originated at carbides. The initiation and propagation modes (transgranular or intergranular) were shown to be a function of both temperature and strain rate. Figure 2 shows that there is a greater tendency toward intergranular behavior as temperature increases and strain rate decreases. The appearance of the dislocation networks created by various loading conditions suggested that the maximum stress achieved during the initial cycling was very important to the subsequent fatigue capability of the material.
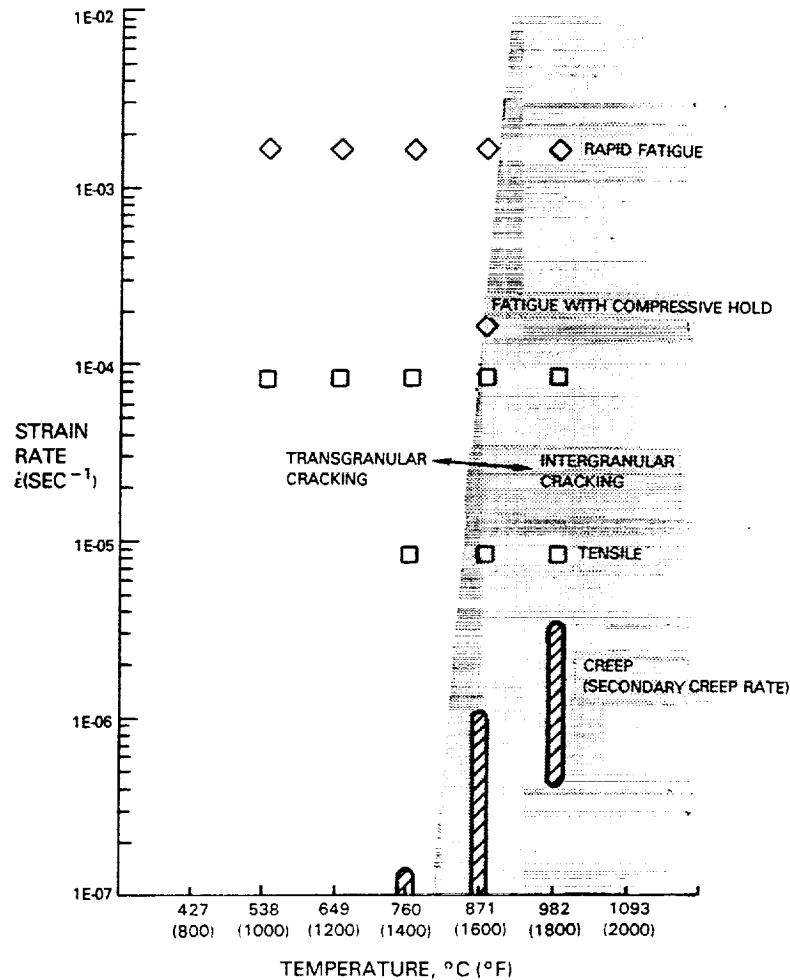
Figure 2.- Cracking Map for B1900+Hf.

4

The life prediction approach which developed during the base program is called Cyclic Damage Accumulation (CDA). One of the fundamental assumptions of the CDA model is that the damage capability is related to the grain dislocation structure. Determination of the grain capability must therefore include consideration of the entire loading history of the specimen, especially the maximum stress excursions. In particular, it was assumed that the grain cyclic capability can be calculated from the maximum stress attained in the initial loading cycle and the amount of primary creep strain that could have been developed if that stress level had been held constant. It was further assumed that, for temperatures below 649°C (1200°F) where little or no creep occurs, the grain cyclic capability would be represented by the residual inelastic strain (percent elongation) measured after a tensile test. The result of these two assumptions is that grain cyclic capability varies as a function of temperature and stress as shown in Figure 3.
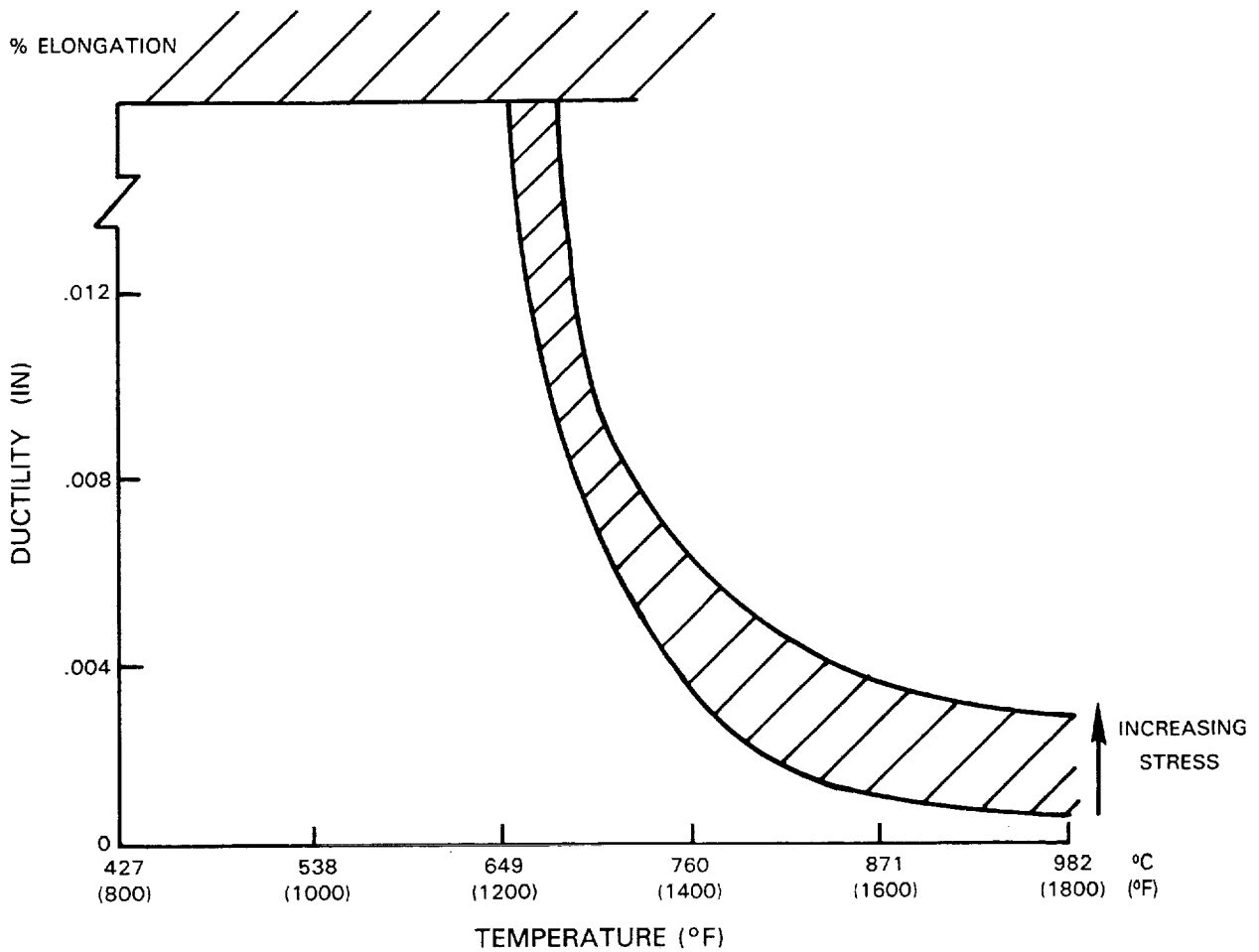
Figure 3.- Assumed Grain Cyclic Fatigue Capability.

5

Another feature incorporated in the CDA life model was the use of damage
ratios rather than absolute damage levels. By plotting the available data for
cycles having either time-independent or time-dependent damage, it was
possible to arrive at the following mathematical form of the CDA model:

$$\bar{\varepsilon}_p - \int_0^{N_i} \left(\frac{dD}{dN}\right)_{REF} \left\{ \left(\frac{\sigma_T}{\sigma_{T,REF}}\right)\left(\frac{\Delta\sigma}{\Delta\sigma_{REF}}\right) + \left[\left(\frac{\Delta\sigma_{REF}}{\Delta\sigma}\right)\left(\frac{\sigma_T}{\sigma_{T,REF}}\right)\right]^{B'}\left[\left(\frac{t}{t_{REF}}\right)^{C'} - 1\right]\right\} dN = 0 \qquad (1)$$

Where:

$\bar{\varepsilon}_p$ = primary creep strain ductility

$\left(\dfrac{dD}{dN}\right)_{REF}$ = reference cyclic damage rate

σ_T = maximum tensile stress

$\Delta\sigma$ = stress range

t = time = 0.5 * (total cycle period + hold times)

N_i = initiation life

REF = reference values

B' = stress exponent in primary creep power law

C' = time exponent in primary creep power law with shifted time origin

This equation was then calibrated using the baseline fatigue data and used to
generate life predictions for various verification cycles. Sensitivity studies
were also conducted to determine the effects of crack size to grain size
ratio, definition of initiation, choice of reference condition, and data
requirements for life predictions. Preliminary work was also done on possible
means of using this or a similar equation to predict intergranular cracking as
well as transgranular.

During the initial part of the optional program, work began on the expansion
of the basic CDA life prediction method to account for the effects of
thermomechanical fatigue, multiaxiality, cumulative damage, environment,
coatings, and mean stresses. The B1900+Hf specimen database was significantly
expanded during this time to provide clear data regarding material behavior
under such complex conditions. Under Task IV, eighteen additional isothermal
fatigue verification tests were completed and are covered by the previous
report. These tests explored the effects of hold times with R=0 or high strain
range, R-ratios at low strain rate and high temperature, load control, and
surface finish. The first four multiaxial tests were completed during the

6

previous reporting period, and much of the information generated is included in Section 5 of this report. Similarly, the investigation of environmental effects began during the last period and is covered in detail in Sections 6 and 7 of this report. Two comprehensive literature reviews, covering state-of-the-art life prediction methods for both multiaxial stresses and environmental effects, were also included in the previous report.

Prediction of initiation life under conditions of thermomechanical fatigue (TMF) is one of the most important practical applications of any advanced creep-fatigue life model since conditions of simultaneously varying strain and temperature are typical of what is experienced by many components of modern turbomachinery and powerplants. To understand the behavior of B1900+Hf under TMF conditions, thirty uncoated TMF specimen tests were completed during the period covered by the previous interim report. These simulated many types of strain-temperature cycle paths, including in-phase, out-of-phase, "dogleg" (non-isothermal holds), and elliptical cycles. The results shown in Figure 4 are typical of the effects produced by such variables for which successful life models must be able to account. The modifications to the CDA model which were initiated at this time will enable it to accept completely arbitrary histories of stress-strain-temperature and thereby make accurate TMF life predictions.
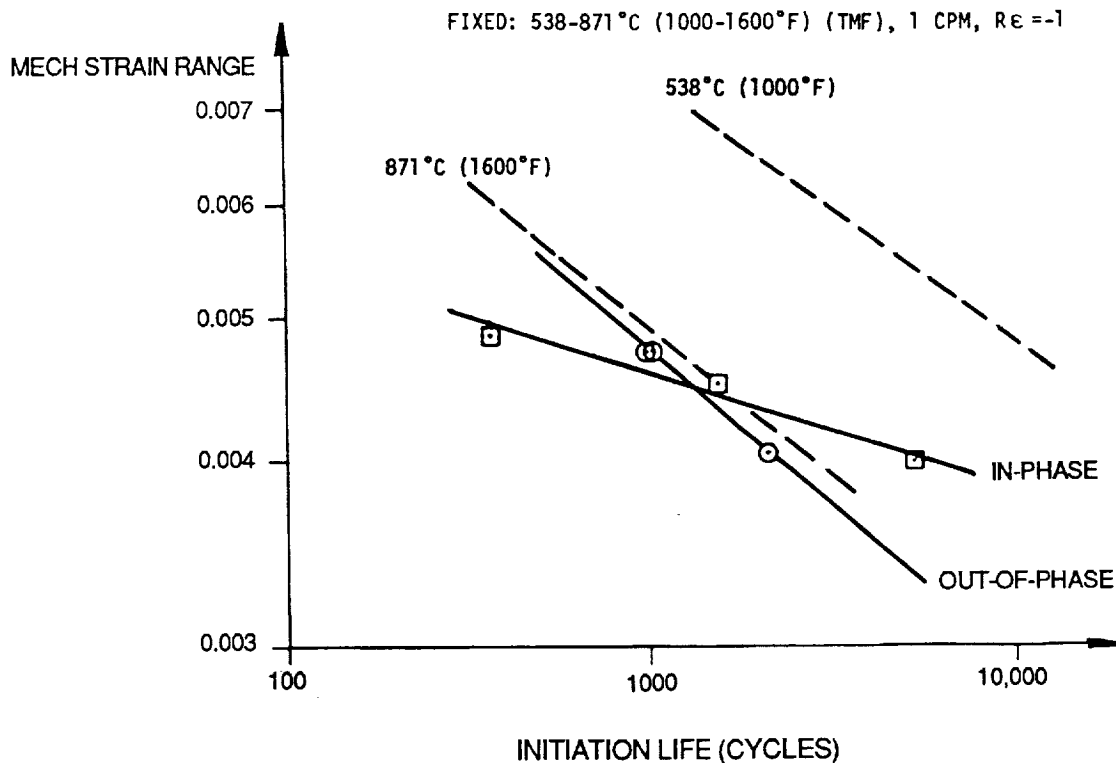
Figure 4.- TMF Results for In-Phase and Out-of-Phase Cycles.

Under Task VII, fifty cumulative damage tests were completed, including blocktests (strain ratio, temperature, and hold time), sequenced tests (strain range and rate), and interrupted tests (prior creep and interspersed exposure time). An interaction curve for the block strain ratio results are shown in

7

Figure 5, where the level of prior loading and its duration are seen to have pronounced effects on the life of subsequent block loading. This effect is easily captured using the CDA concept of primary creep ductility, since this variable depends on the prior loading history. The cumulative damage tests also showed the need to incorporate a non-linear damage accumulation function to predict sequence effects correctly. This required the introduction of two modifications of the original form of the CDA model: the concept of ductility fraction, and the non-linear rate modifier function, $G(N/Ni)$.
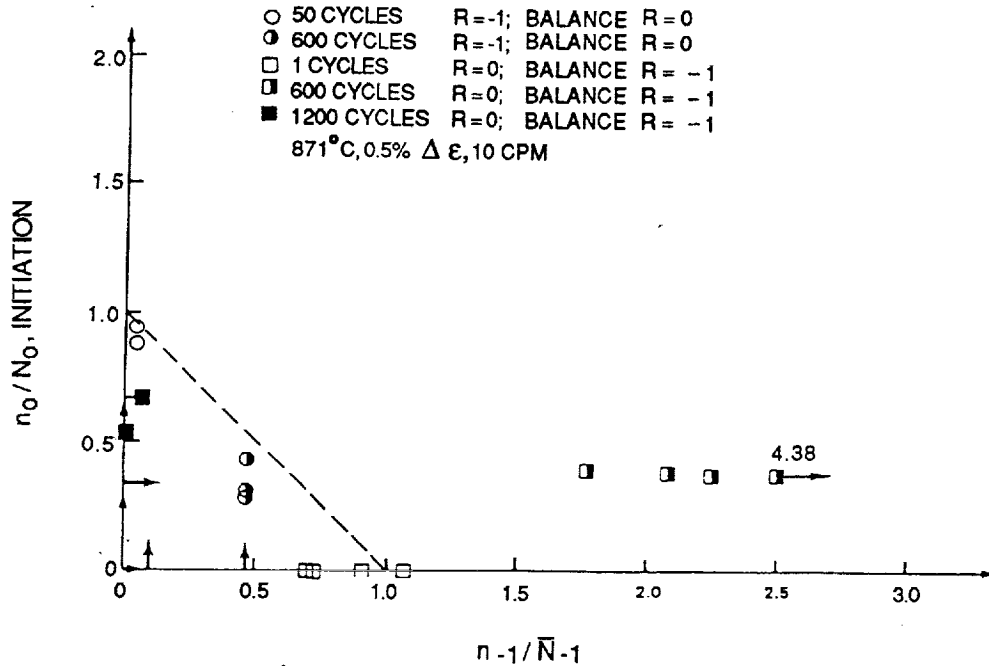
Figure 5.- Interaction Diagram for Strain Ratio Block Tests.

The ductility fraction concept permits the primary creep strain ductility to vary during the course of the test by bringing it under the integral. The ductility fraction, f_ε, is defined as the fraction of the available ductility which has been consumed:

$$Ductility\ Fraction, f_\varepsilon = \frac{Ductility\ Exhausted}{Available\ Ductility} \tag{2}$$

The equation used to calculate this quantity may be written as follows, using CDA nomenclature:

$$f_\varepsilon = \int_0^{N_i} \left(\frac{1}{\dot{\varepsilon}_p} \right) \left(\frac{dD}{dN} \right)_{REF} \Gamma(\sigma_T, \Delta\sigma, t) dN \tag{3}$$

8

where:

$$F(\sigma_T, \Delta\sigma, t) = \left(\frac{\sigma_T}{\sigma_{T,REF}}\right)\left(\frac{\Delta\sigma}{\Delta\sigma_{REF}}\right) + \left[\left(\frac{\Delta\sigma_{REF}}{\Delta\sigma}\right)\left(\frac{c_T}{\sigma_{T,REF}}\right)\right]^{B'}\left[\left(\frac{t}{t_{REF}}\right)^{C'} - 1\right] \qquad (4)$$

It can be seen that when f_ε reaches 1, N will equal the predicted initiation life, Ni. Note also that the current initial ductility is now inside the integral, which permits the algorithm to switch from one loading condition to another which has a different initial ductility.

We may also rewrite equation 3 to perform the integration over f_ε instead of N, and at the same time introduce a non-linear function G(N/Ni) which has the property that its integral over the interval from 0 to 1 is always 1, no matter what values are chosen for its constants:

$$N_i = \int_0^1 \left[\frac{\bar{\varepsilon}_p}{\left(\frac{dD}{dN}\right)_{REF} F(\sigma_T, \Delta\sigma, t)}\right] G\left(\frac{N}{N_i}\right) df_\varepsilon \qquad (5)$$

The function G(N/Ni) chosen for the initial trials of this method is a combination of a power law and a linear function:

$$G\left(\frac{N}{N_i}\right) = (1 - LF)(M + 1)\left[1 - \left(\frac{N}{N_i}\right)\right]^M + LF \qquad (6)$$

The effect of the inclusion of the non-linear function G(N/Ni) on the CDA life prediction for a strain ratio block test is shown by Figure 6. This plot shows how the ductility fraction increases as a function of cycles, both for linear and non-linear damage accumulation. In this case the non-linear prediction is lower than the linear prediction, because the basic damage rate (slope of the linear accumulation line) during the first block of the test is lower than the rate during the second block. This causes the ductility to be consumed earlier with the non-linear function than without it, and the net result is a lower prediction. The opposite effect is seen in Figure 7, where reversal of the order of the blocks causes the non-linear life prediction to be higher than the linear one. Note that this is the same effect which was observed during the specimen testing.
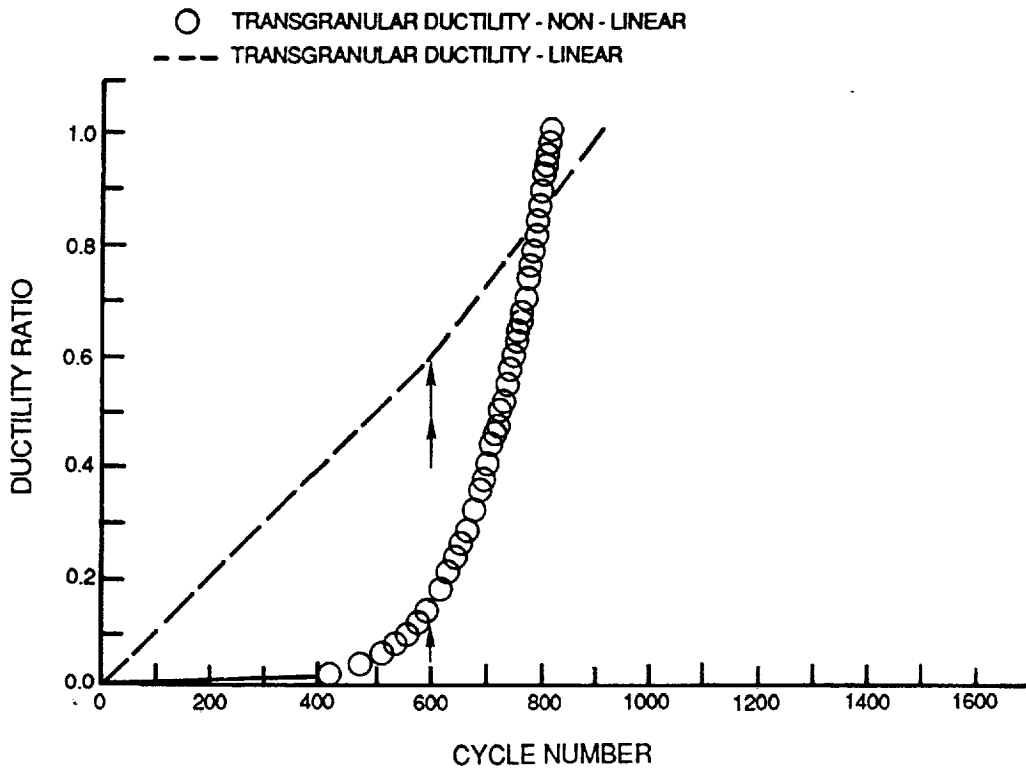
Figure 6.- Example of Lower Life Prediction with Non-Linear Accumulation
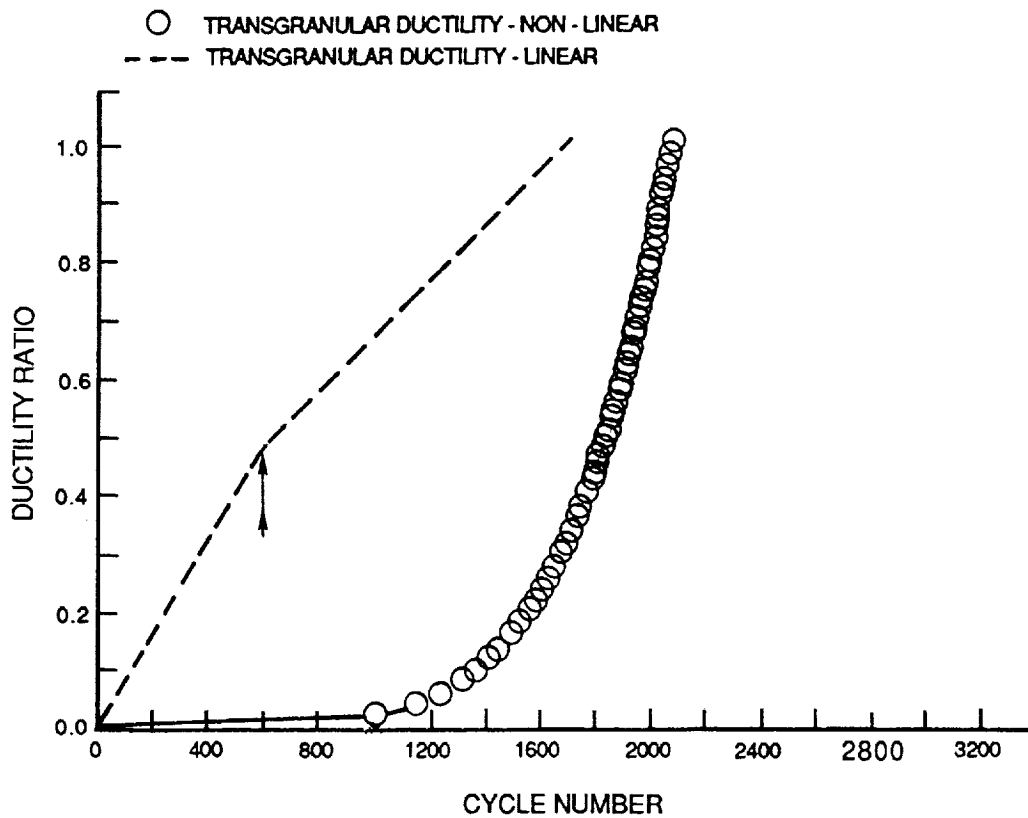
Figure 7.- Example of Higher Life Prediction with Non-Linear Accumulation

SECTION 3.0
MATERIALS AND TEST METHODS

3.1 Material Selection and Characterization

Based on a comprehensive survey conducted early in this program, the following materials and coating systems were selected as representative of hot section materials in general use today:

Base Material	: Cast B1900+Hf (PWA 1455)
Coating Systems	: Diffusion Aluminide (PWA 273) and NiCoCrAlY Overlay (PWA 286)
Alternative Material	: Wrought INCO 718 (AMS 5663)

The use of cast and wrought alloys allows the development and examination of life prediction models for two materials having the same matrix (nickel) but significantly different composition and microstructure (e.g., high vs. low volume fraction gamma prime). The selection of a diffusion and an overlay coating also provides a variation in composition and microstructure to determine their effects on creep-fatigue life.

3.1.1 Base Material

The B1900 + Hf material selected for the program was part of a single heat, designated W-0098, obtained from Certified Alloy Products, Inc., Long Beach, California. The chemical composition of this heat is compared to nominal specifications in Table I a). A total of 2500 pounds of material was obtained for specimen preparation.

As mentioned in Section 2.2, the monotonic behavior of this heat of material was fully characterized during the base program using 21 tensile tests and 19 creep tests. Detailed listings of the data for these tests were reported in the Second Annual Report (Moreno et al, 1984).

For the uniaxial fatigue specimens, the alloy stock was cast into individual test bars using standard investment casting techniques. The geometry of these bars is shown in Figure 8. Each bar was given a unique identification number consisting of the mold sequence number, followed by A, B, C, or D to differentiate the four bars from each mold. A somewhat larger cast tubular test bar was developed for the multiaxial specimens in cooperation with Hitchiner Manufacturing Co., Milford, New Hampshire. For all cast geometries, the casting parameters (pour temperature, mold temperature, cooling rate, etc.) were established to produce a uniform small grain size (ASTM 1-2) in each bar.

11

TABLE I
COMPOSITION AND HEAT TREATMENT OF B1900+Hf

a) Chemical Composition by Weight

Element	Nominal %	Actual % Heat W-0098
C	0.11	0.09
Cr	8.0	7.72
Co	10.0	9.91
Mo	6.0	5.97
Al	6.0	6.07
Ta	4.25	4.21
Ti	1.0	0.99
B	0.015	0.016
Zr	0.08	0.04
Fe	0.35*	0.17
W	0.1*	0.04
Cb	0.1*	0.08
Bi	0.5 ppm	0.1
Pb	10.0 ppm	0.1
Hf	1.15	1.19
Ni	Remainder	Remainder

b) Heat Treatment Cycles for B1900+Hf (coated or uncoated)

Solution   : 1079 ±14°C (1975 ±25°F) for 4 hours in hydrogen atmosphere; air cool

Precipitation : 899 ±14°C (1650 ±25°F) for 10 hours in air; air cool

(A) "Standard" Bar Configuration

(B) Constant Section Bar
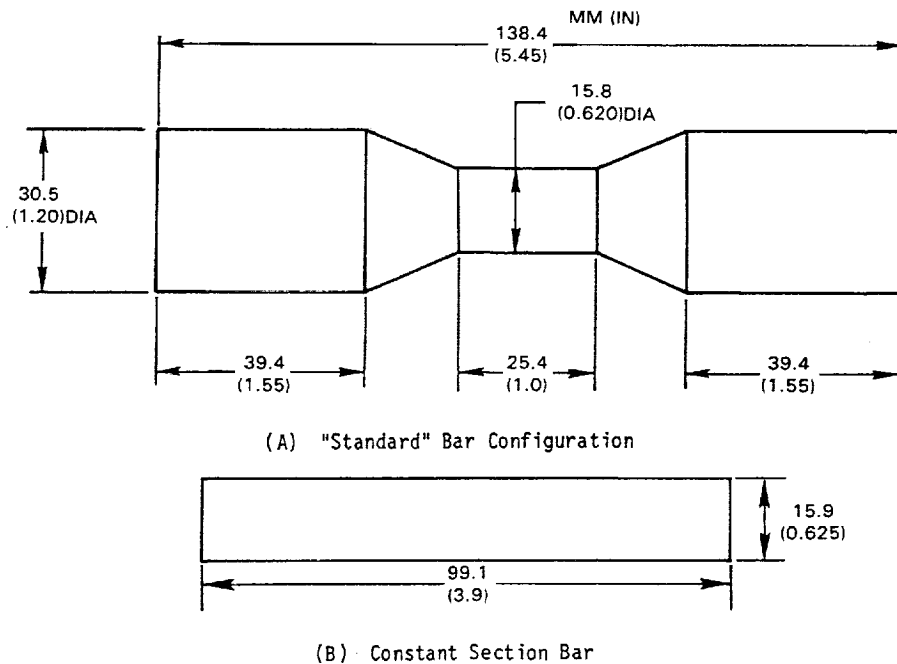
Figure 8.- Costing Geometry Used for Test Specimens.

12

The heat treatment cycles used for all the B1900+Hf specimens are shown in Table I b). All the bars for specimens to be tested without coatings were fully heat treated prior to machining. Specimens which were to be tested with protective coatings were first machined, then coated using standard production methods, and finally heat treated (which also served as part of the coating application process). The compositions and deposition processes for the two coating systems are shown in Table II. The nominal thickness shown for the PWA 286 coating was determined directly by comparing the specimen diameters before and after coating. The actual as-applied thicknesses varied from 0.12 to 0.15 mm (0.0046-0.0060 in.). The PWA 273 thickness was measured by including a small disk sample of B1900+Hf during the coating application cycle. This disk was sectioned and examined metallography. As shown in Figure 9, the average coating thickness including the diffusion zone was approximately 0.04 mm. (0.0015 in.).

TABLE II
DESCRIPTION OF PWA 286 AND 273 COATING SYSTEMS

Coating	Type	Composition	Deposition Process	Nominal Thickness (mm.(in.))
PWA 286	Overlay	NiCoCrAlY+Si+Hf	Vacuum Plasma Spray	0.13 (0.005)
PWA 273	Aluminide	AlSi	Pack Cementation	0.04 (0.0015)

1 mil

500X
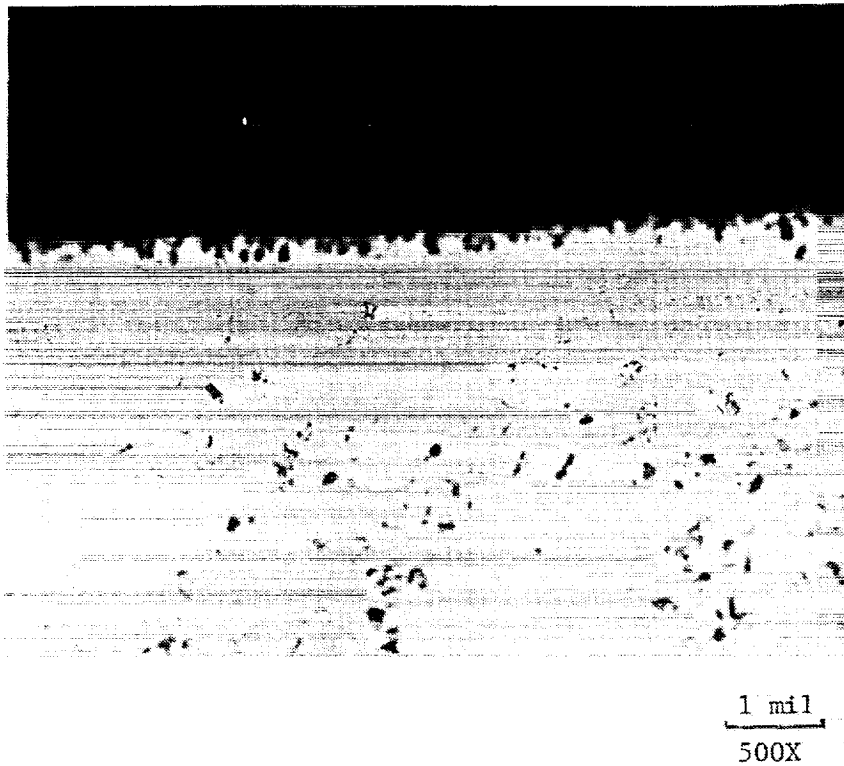
Figure 9.- PWA 273 Coated PWA 1455 Coating/Base Metal Interface. Average coating thickness including diffusion zone is 1.5 mils.

13

3.1.2 Alternative Material

To provide material for this task, a production quality ring rolled forging of AMS 5662 was obtained (heat code RLVO-9938). This forging weighed more than 190 kilograms (420 pounds), thus providing sufficient material for machining all test specimens. The forging was sectioned into manageable chunks of material and was then heat treated to AMS 5663 specifications. The detailed chemical composition and heat treatment schedule are given in Table III. Optical examination was made of the fully heat treated microstructure of the forged INCO 718 material. Typical micrographs are shown in Figure 10. The needle shaped precipitates along the grain boundaries are delta phase, and the larger particles in the matrix are believed to be carbides. The grain size is approximately ASTM 2-5 (as compared to ASTM 1-2 for the B-1900 Hf alloy).

As with the B1900+Hf, the INCO 718 material will be fully characterized regarding tensile and creep properties. These tests will be completed during the final reporting period and will be covered in detail in the Final Report.

TABLE III
COMPOSITION AND HEAT TREATMENT OF INCO 718

A. Chemical Composition by Weight

Element	Nominal %	Actual % (H/C RLVO-9938)
Cr	19.0	18.6
Fe	19.0	19.0
Cb+Ta	5.2	5.2
Ti	0.9	0.98
Al	0.6	0.53
Mo	3.0	3.0
C	0.05	0.054
Ni	Remainder	Remainder

B. Heat Treatment Cycles for INCO 718

Solution : 954 ±14°C (1750 ± 25°F) for 1 hour in protective atmosphere; air cool

Precipitation : 718 ±8°C (1325 ±15°F) for 8 hours; furnace cool at 55°C (100°F) per hour to 621 ±8°C (1150 ±15°F); hold until a total aging time of 18 hours is reached; air cool

14
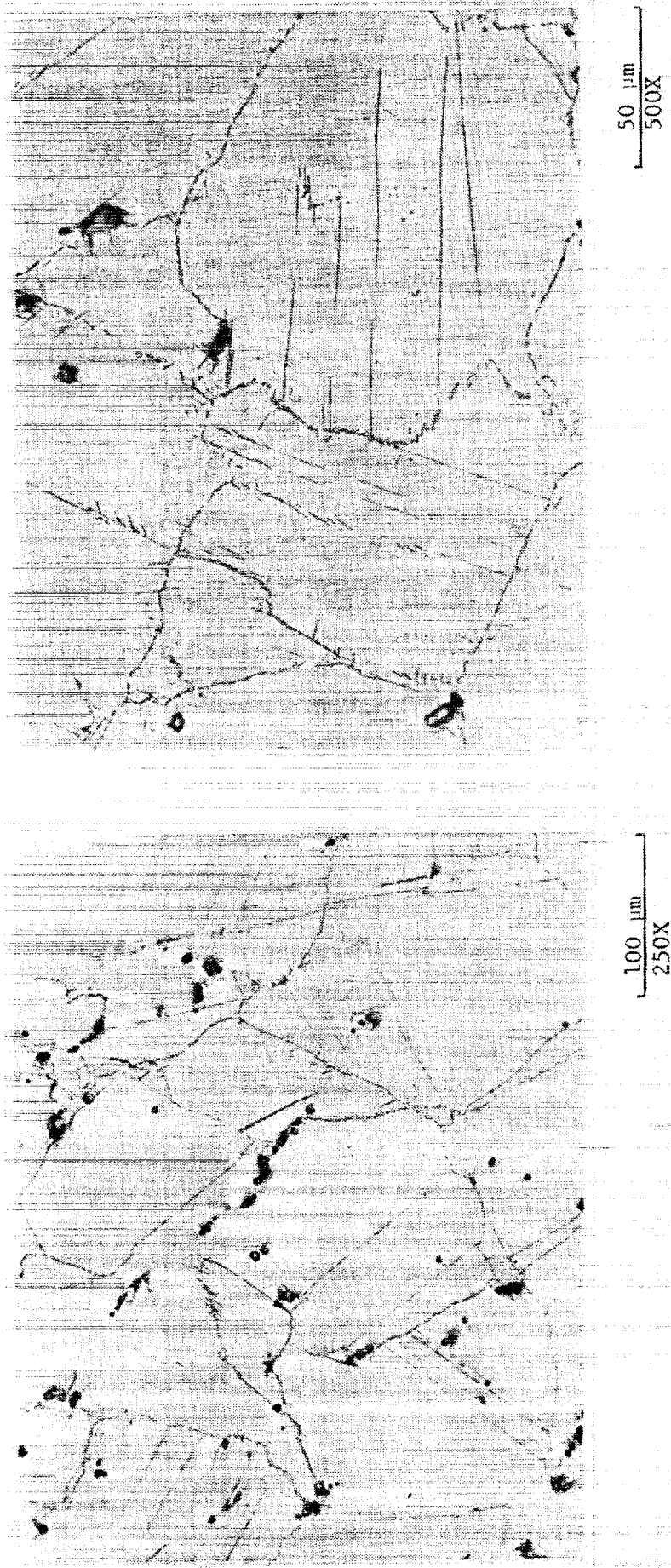
Figure 10   Optical micrographs of IN718 in the as received condition. Long
             needle shape precipitates are δ phase, small precipitates in matrix
             are carbides.

15

3.2 Specimen Preparation

All fatigue specimens were prepared using low stress, centerless grinding techniques. Following the machining operations, all uncoated specimens were electropolished using parameters developed to remove about 10 microns (0.0004 in.) from the surface without any deleterious effects on the microstructure. Tubular specimens were electropolished on the outer diameter.

Three basic specimen geometries were used, as shown in Figure 11. The solid specimen shown in Figure 11(a) was used for all uniaxial, isothermal fatigue testing, including cumulative damage tests and environmental tests. The smaller tubular specimen shown in Figure 11(b) was designed for TMF testing using an external extensometer. Its wall thickness was chosen to represent that of a typical airfoil, thereby permitting rapid temperature changes. The larger tubular specimen shown in Figure 11(c) was designed for strain controlled tension-torsion multiaxial testing. The actual gage section was approximately 33 mm. (1.3 in.) long, but this was corrected to an effective gage section of 25.4 mm. (1.000 in.) using factors developed from strain gage tests of an actual specimen. All tubular specimens were honed on the I.D. to help prevent failures from that surface.

3.3 Test Equipment and Procedures

All fatigue specimens were tested in computer controlled servohydraulic load frames similar to the TMF rig shown in Figure 12. The computer controlled the test and recorded stress and strain data at specified logarithmic intervals. Most of the tests were strain controlled using external extensometry; for those few tests run under load control, the extensometry was still used to record strain data. Specimen heating was by low frequency induction, with closed loop temperature control accomplished with infrared pyrometry. The B1900+Hf tests were generally held at zero load at the test temperature until the surface emissivity stabilized prior to beginning the actual test. The INCO 718 tests were much lower in temperature and therefore required a high emissivity target (spot of black paint) to provide stable temperature readings.

The multiaxial experiments under Task VI were conducted at the University of Connecticut by Prof. Eric Jordan of the Mechanical Engineering Department and his students. A very stiff tension-torsion load frame was employed, using collet-style specimen grips. Initial specimen tests used an extensometer which required attachment and alignment of two concentric target rings onto the specimen. This procedure proved to be time consuming during the surface replications which are taken periodically during the tests, and the capacitance probes used for displacement measurements caused some problems as well. Therefore, other multiaxial extensometer designs which did not require any special targets on the specimen were evaluated, including those in use at Oak Ridge and NASA-Lewis. An improved version based on these earlier designs was fabricated and installed toward the end of the series of B1900+Hf tests. The new design was much easier to operate and simplified the testing procedure. Comparison of results from the new extensometer with those from the earlier extensometer showed good agreement.
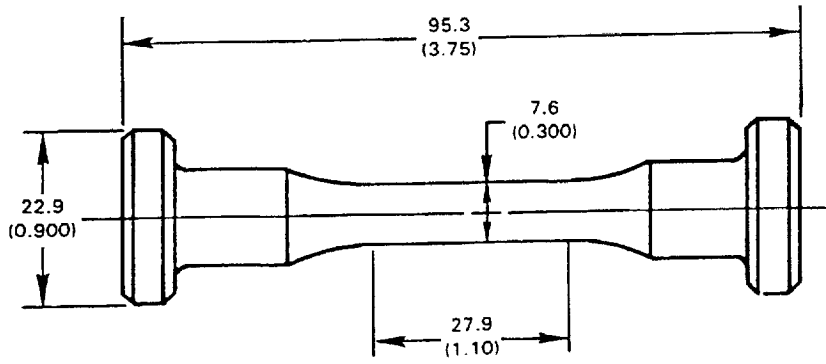
(A) Isothermal Specimen
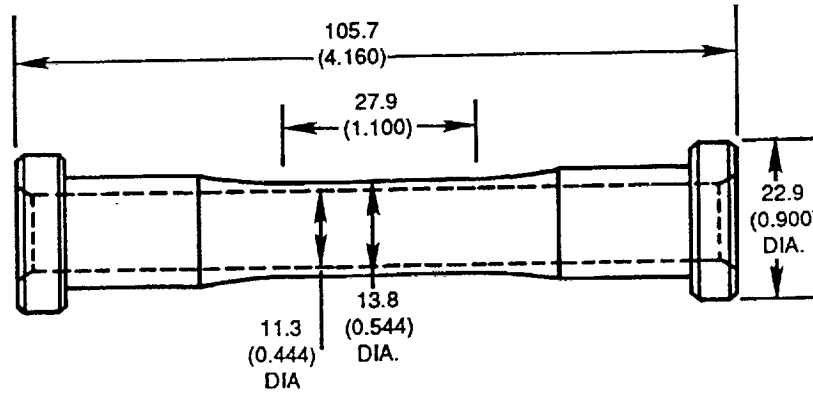
(B) TMF Specimen
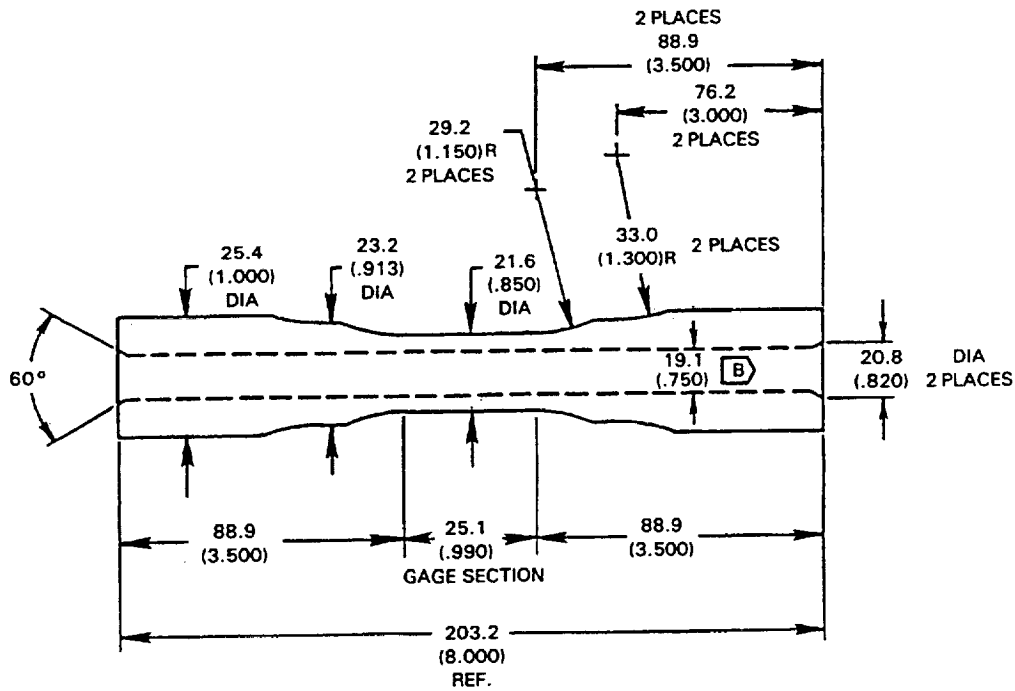
(C) Biaxial Tension Torsion Specimen

Figure 11.- Test Specimen Geometries [all dimensions in mm (in.)]

17
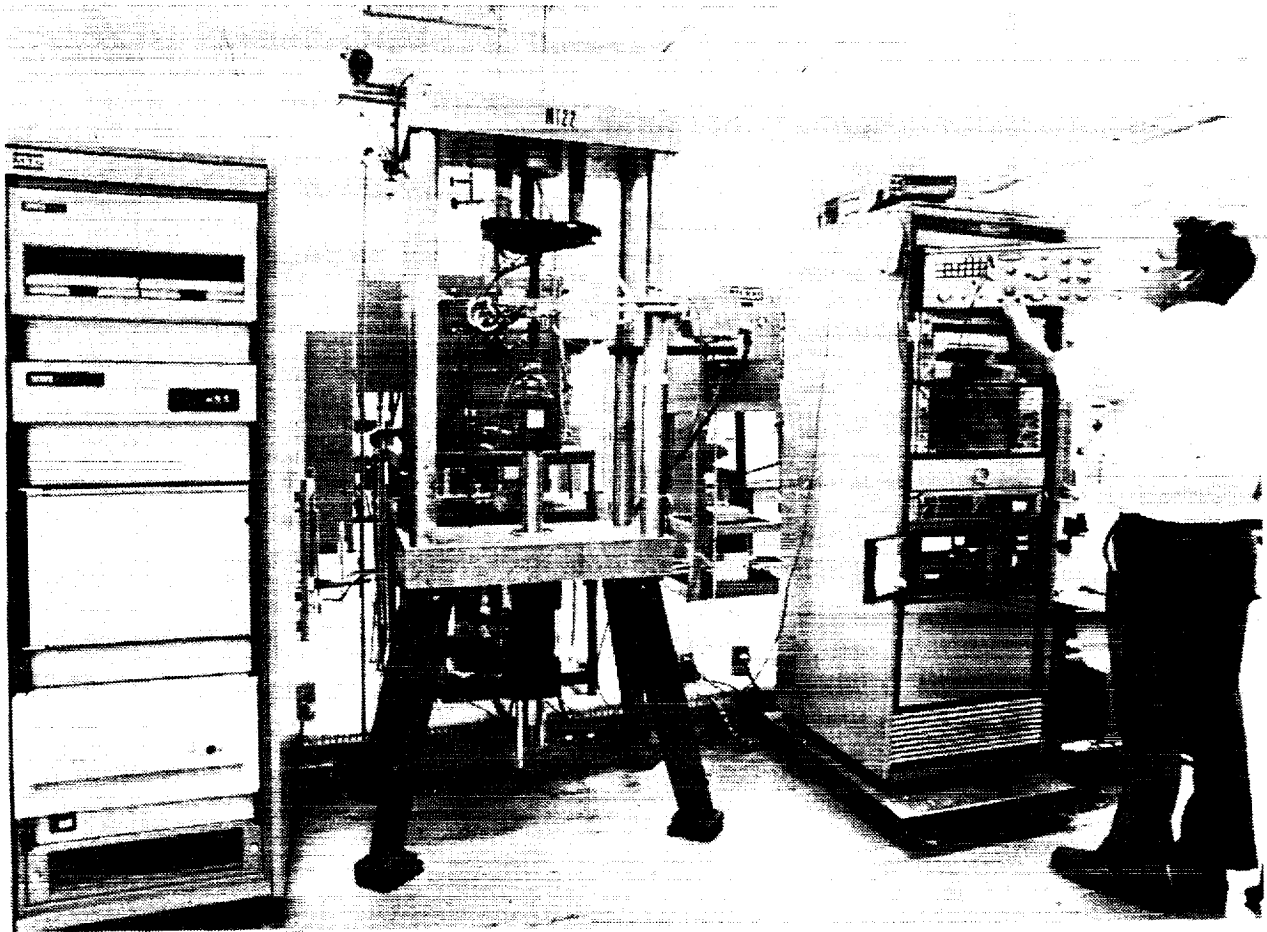
Figure 12.- TMF Specimen Test Rig.

As shown in Figure 13, a stainless steel, low pressure chamber for the environmental testing under Task IX was completed and overpressure tested. The chamber itself is water-cooled and has ports for induction power feed-through, strain and temperature signals, infrared pyrometer and internal cooling water. The chamber was fitted with an argon purifier to assure very low oxygen levels, and initial trials showed that the environment was satisfactory. Figure 14 shows the water-cooled MTS extensometer in place in front of the specimen.

The mean stress experiments under Task XI required simultaneous independent control of both mean stress and strain range. The isothermal tests under this task were conducted at the University of Rhode Island by Prof. Hamouda Ghonem of the Mechanical Engineering Department and his students. They had developed control software which uses history data from earlier cycles of a particular test to forward extrapolate where to set the maximum and minimum strain limits for the next cycle. This arrangement worked very well, producing reliable data under a wide range of isothermal test conditions. However, because the capability to run a full load controlled TMF test was already available in the P&W lab, it was decided to run the TMF mean stress tests under load control using the current software. This provided direct control of the mean stress while the fixed stress range gave a strain range which was approximately constant provided as there was little cyclic hardening or softening.

18
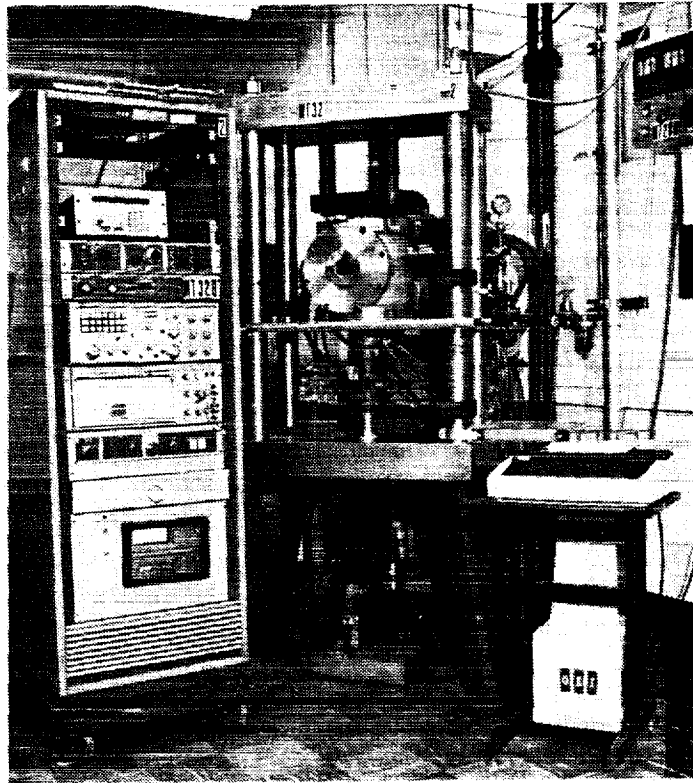
Figure 13.- Environmental Test Rig.
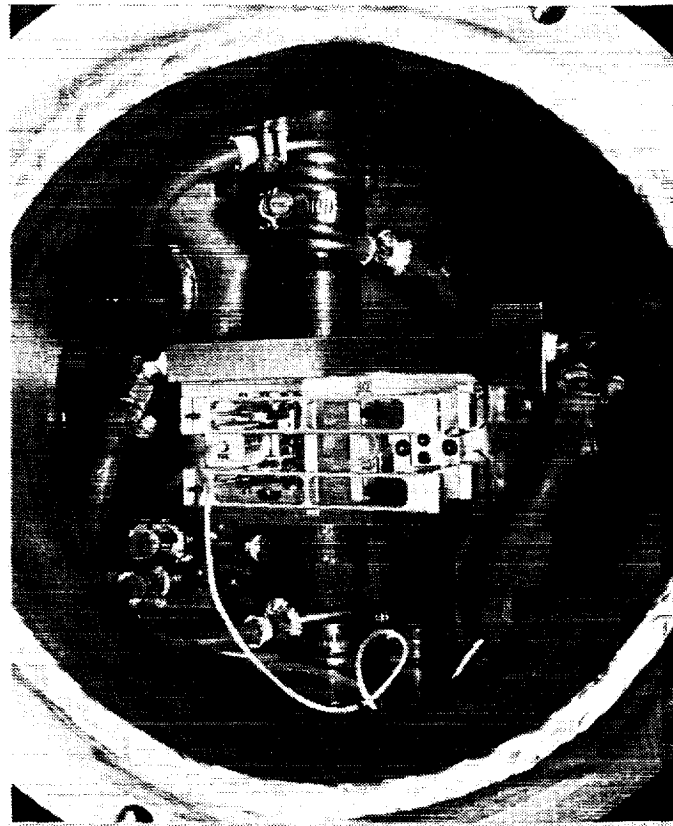
Figure 14.- Water Cooled Extensometer in Environmental Test Chamber.

SECTION 4.0
EXPERIMENTAL RESULTS

4.1 Task V - Thermal - Mechanical Cycling Model

The purpose of this task was to simulate engine operating conditions by
varying both strain and temperature simultaneously. These tests were conducted
to provide an increased understanding of the damage mechanisms of actual
components and to characterize the influence of cycle type, strain range,
R-ratio, and temperature range. The initial effort of this task which
concentrated on uncoated samples was reported by Nelson et al (1986). The type
of basic cycles used for this task are shown in Figure 15.
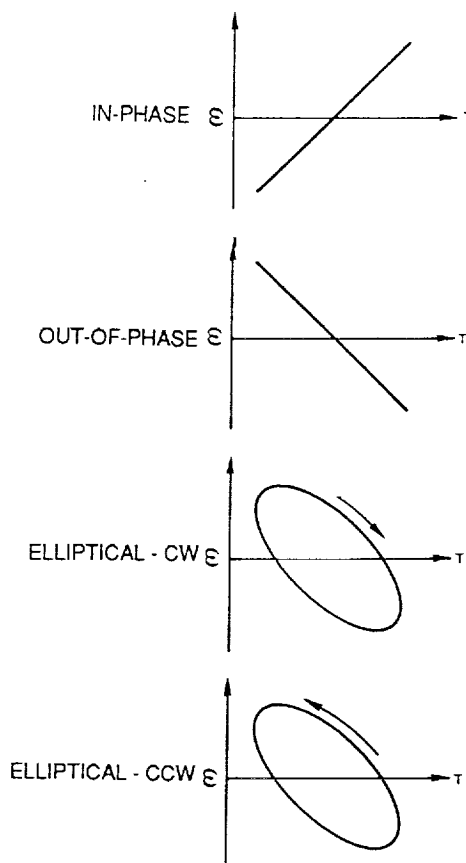
Figure 15.- Comparison of Basic TMF Cycle Types.

Specimen testing under this task was completed in December, 1986, with a total
of 55 B1900+Hf TMF specimen tests. Of these 55 specimens, 32 specimens were
tested in the uncoated condition, and data for all uncoated specimen tests
(except for the two hold time tests) were included in the first interim
report. The TMF tests reported in this interim report focused on the effects
of two major types of protective coatings currently in use in gas turbine
engines. During this reporting period, a total of 25 specimens were evaluated,
12 coated with NiCoCrAlY overlay coating (PWA 286), 11 coated with diffusion
aluminide coating (PWA 273), and 2 without coating. The test variables
included strain range, temperature range, mean strain, cycle type, and hold

20

times. The conditions were chosen to complement both the uncoated TMF tests and the baseline isothermal fatigue tests. Particular attention was focused on the low strain, high life regime, since modern turbomachinery is designed for good durability. Some of the non-standard cycle types used (such as elliptical and dogleg cycles) have demonstrated that TMF damage cannot always be accounted for in the same manner as isothermal tests. The model chosen must be sensitive to accumulation of damage from any arbitrary strain-stress-temperature cycle and yet be practical for use in design applications.

Strain range and cycle type were both shown to be significant factors in determining coated TMF life. As with the uncoated TMF tests, the phase angle between strain and temperature for elliptical cycle tests (clockwise vs. counterclockwise) was also very important, especially at low strain ranges.

For the conditions used in this task, the presence of the coatings in general increased the specimen lives by 2-5X. This is in contrast to most actual service conditions, in which the coating will crack prematurely when exposed to high local strains. This was confirmed by judicious selection of a cycle type which resulted in high coating strains and hence lower life than an uncoated specimen.

Optical and SEM examinations were made on two of the PWA 286 overlay coated specimens (119A and 119B) to determine if recrystallization occurred at the worked surfaces of the specimens because of the post-coating heat treatment. Examinations of the fracture surfaces and polished and etched sections below the fractures did not reveal evidence of recrystallization. Figure 16 shows SEM micrographs at the OD of polished and etched sections of 119A and 119B. At the uncoated OD surface of both specimens, a thin depletion zone (about 10 microns in the thickest regions) was observed. This zone forms as the result of oxidation of the specimen surface at elevated temperatures.

For comparison, matrices of TMF tests for both uncoated and coated specimens are shown in Tables IV and V. Details of the test results for all tests completed during this reporting period are given in Appendix A.

4.1.1 Out-of-Phase Testing on Specimens Coated With PWA 286 NiCoCrAlY Overlay Coatings

A total of six overlay coated specimens were tested using out-of-phase strain-temperature cycling. In the first test, the initiation life of specimen 120A [538-871°C (100-1600°F), 0.4% strain range, R=-1, 1 cpm] using PWA 286 (NiCoCrAlY) overlay coating was 3700 cycles. During the test, a crack developed on the outer fillet of one of the ID ridges which caused a premature failure of the specimen at 4033 cycles. These ridges were machined out of the remaining specimens to preclude a recurrence of this problem. A second PWA 286 coated specimen (120B) was tested at the same conditions which revealed initiation and separation lives of 2938 and 4452 cycles, respectively. Comparison of the replica data of specimen 120B with those of specimen 120A showed that the separation life of Specimen 120A would have been 5584 cycles if it had not failed prematurely due to the internal ridges. These lives are approximately 2X higher than the lives of uncoated specimens run at the same conditions, indicating that the coating inhibited some damage mechanism(s) (such as oxidation) found in the uncoated TMF tests.

21
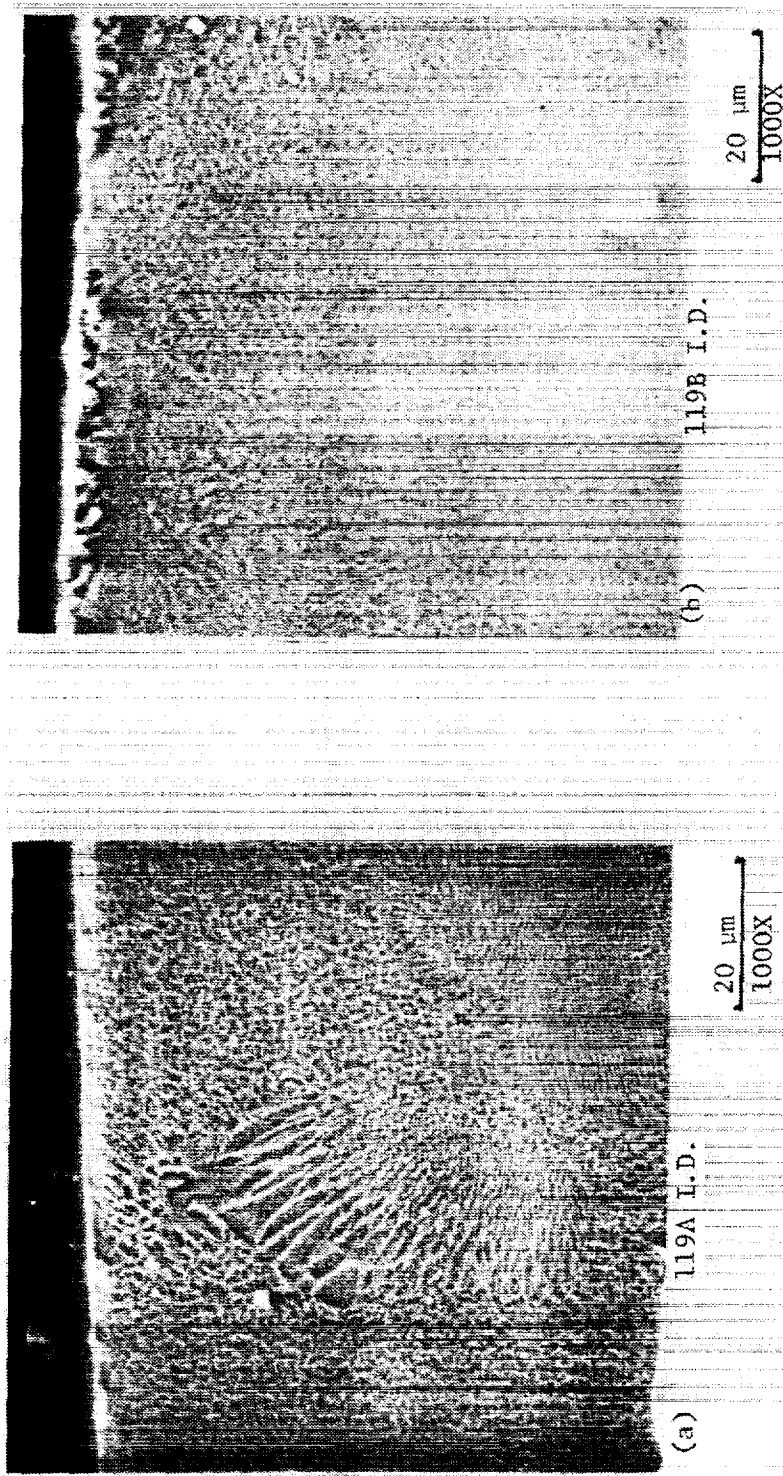
Figure 16 SEM micrographs of PWA 286 overlay coated TMF specimens at the O.D. surface. Depletion zones resulting from oxidation of the specimen surfaces are seen, no evidence of recrystallization was found. Maximum thickness of depletion zones ι 10μm.

22

TABLE IV
UNCOATED PWA 1455 TMF SPECIMEN TEST MATRIX

Temp. Range (°F)	Strain Range	R	I	II	CW	CCW	I+Hold	II+Hold	LT	LC	HT	HC
1000-1600	0.004	0	126A									
		-1	122A	128B	122B 109B	126D 124C	123D	124A				
		-	107C									
	0.005	0	46C 42C	42D 104A								
		-1	45A 105D	42B 102C	127D 129B	108D 125D			42A 101B	45D	108A	46A 105C
		-	46D									
1000-1700	0.004	-1		103B								
1000-1800	0.005	-1	106C									
800-1700	0.005	-1	45C									

TABLE V
COATED PWA 1455 TMF SPECIMEN TEST MATRIX

O = Overlay (PWA 286)   A = Aluminide (PWA 273)

Temp. Range(°F)	Strain Range	R	I	II	CW	CCW	I+Hold	II+Hold	LT	LC	HT	HC
1000-1600	0.004	0	0-120A	0-120D	A-115B	0-119C	0-120C	A-116A				
		-1	0-120B A-114A	A-114D	0-113D	A-114C	0-113B					
		-	0-112D									
	0.005	0										
		-1	0-119A 0-113A A-115C			A-115D				0-113C		
		-	A-116C									
1000-1800	0.004	-1	A-116D			A-116B						
	0.005	-1	0-119B A-115A									

23

Optical examination of specimen 120B revealed the presence of initiation sites at the inner and outer diameters. The inner diameter initiation resulted in the larger crack which may have influenced the life of the specimen. SEM examinations were made of the outer diameter initiation area only, as this involves the coated surface. SEM micrographs of this area are shown in Figures 17(a) and 17(b). As shown, the fracture surface is heavily oxidized and the exact location of the initiation cannot be determined; a secondary crack is also visible. The coating in the fatigue area has a porous appearance as compared to the coating fractured at room temperature when the specimen was pulled apart, as can be seen by comparing Figures 17(b) and 17(c).

Additional out-of-phase TMF tests on PWA 286 overlay coated specimens were run at different temperatures and at a higher strain range of 0.5%. Specimen 119A was run at 538-871°C (1000-1600°F), 0.5% strain range, R = -1, and out-of-phase strain-temperature cycling at 1 cpm. This specimen separated at 2570 cycles, and subsequent SEM observations revealed multiple initiation sites on the ID. Porosity was also observed at the primary initiation site, as shown in Figure 18. However, replica data taken from the specimen OD showed a 0.010 in. crack at 1601 cycles. By using the growth rate observed during similar testing on uncoated samples (45A, 105D), the initiation life for the coated OD surface was estimated to be at 2073 cycles and the separation life at 3240 cycles if the ID failure did not end the test prematurely. These lives are significantly higher than the lives of the uncoated specimens run at these conditions, with the initiation life being approximately double that of the uncoated specimens. This is in agreement with the life increase noted at the lower strain range (0.4%) for coated specimens relative to uncoated specimens. Various methods such as bleeding inert gas into the ID cavity during the test and additional honing of the ID following heat treatment were evaluated to prevent ID-initiated failures.

Specimen 113A was tested at 538-871°C (1000-1600°F), 0.5% strain range, R = -1, and 1 CPM, with out-of-phase cycling. Its initiation and separation lives were 1495 and 1967 cycles, respectively. These compare favorably with specimen 119A, whose initiation and separation lives were 2073 and 3240, respectively.

Specimen 119B was run at a higher strain range (0.5%) and a higher temperature range 538-982°C (1000-1800°F). The initiation and separation lives were 577 cycles and 731 cycles, respectively. As shown in Figure 19, SEM observations once again confirmed the presence of porosity and multiple ID initiation sites similar to that seen in specimen 119A. The lives of this specimen are similar to the lives of the uncoated specimen (106C) tested at the higher temperature range of 538-982°C(1000-1800°F) and do not reflect the 2X life increase for coated specimens tested at 538-871°C (1000-1600°F) such as specimens 119A and 113A. Apparently different mechanisms are active at this higher temperature range which diminishes the effect of the coating. One possible explanation is that the actual stress state of the coating is quite different at the higher temperature range, which could account for the lack of initiation life increase with the coating.

(b)
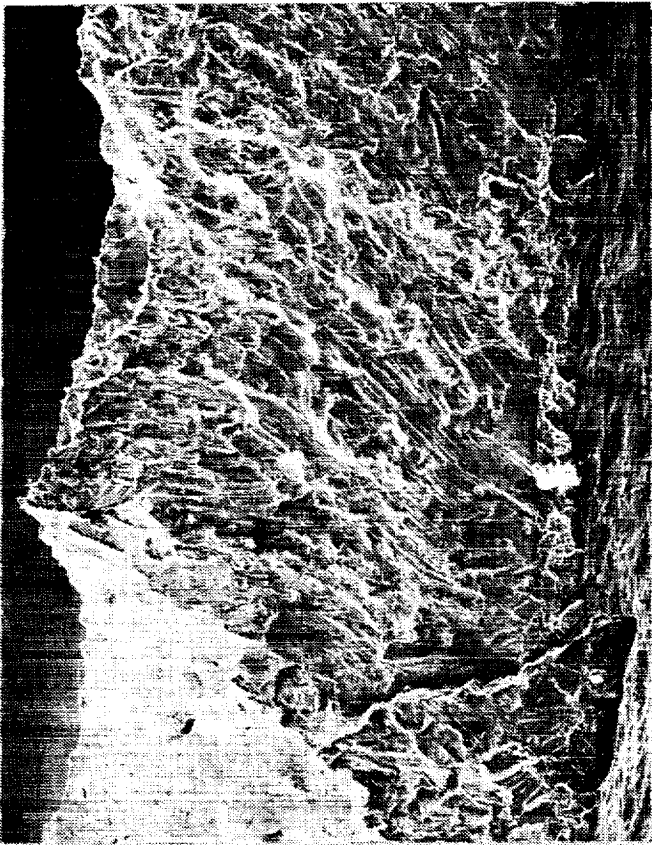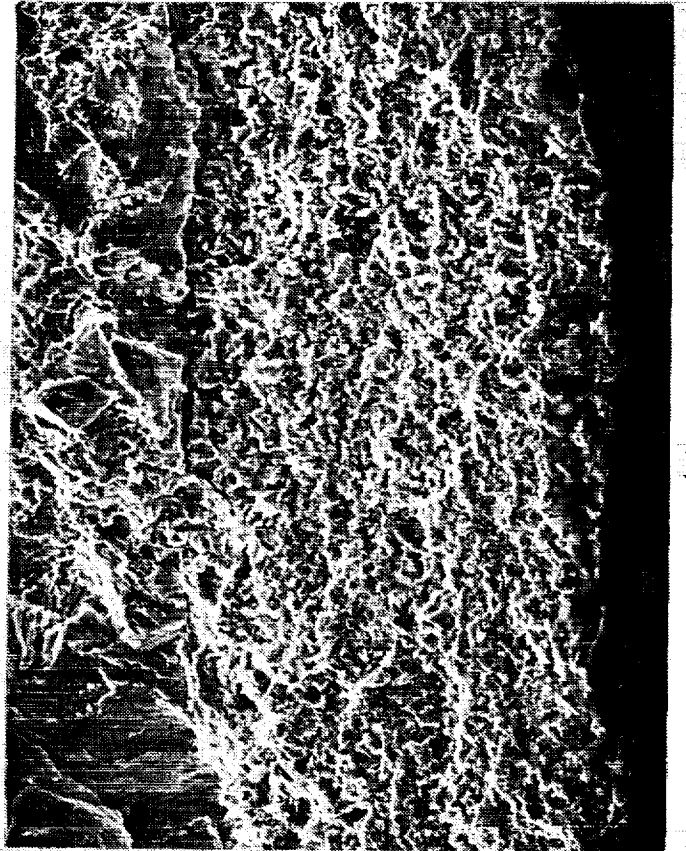
Figure 17   PWA 286 coated TMF specimen 20B. Cycle I,
$\Delta\varepsilon = 0.4\%$, 538-871°C (1000-1600°F), R = -1,
initiation life = 2938 cycles.

(a)   SEM micrograph of O.D. initiation site.

(b)   Higher magnification of (a) showing
porous appearance of coating in initiation
area.

(c)   SEM micrograph of coating in area fractured
at room temperature.

(a)

(c)
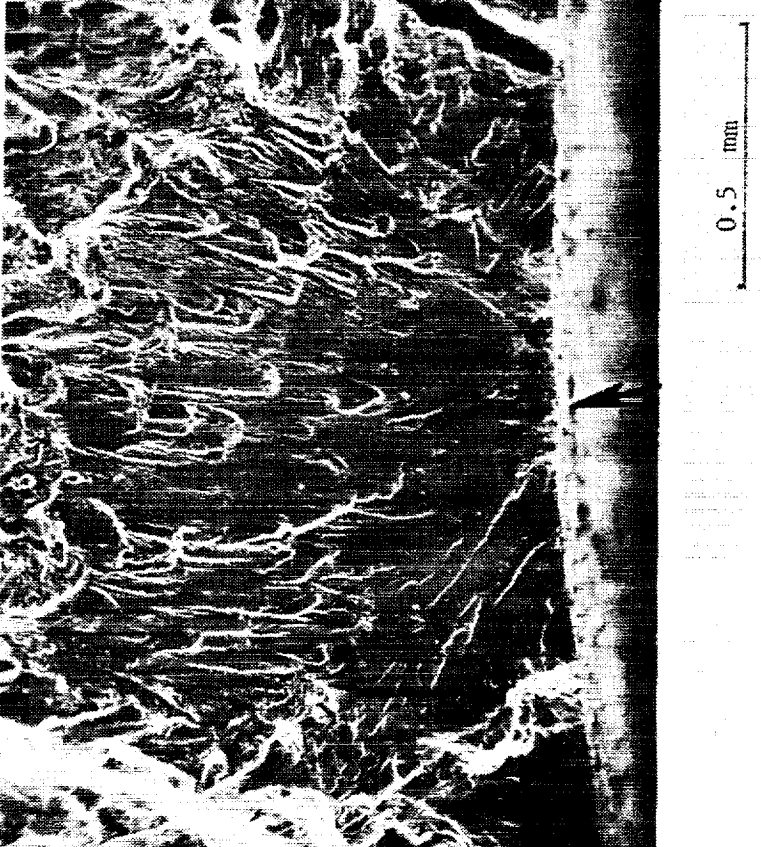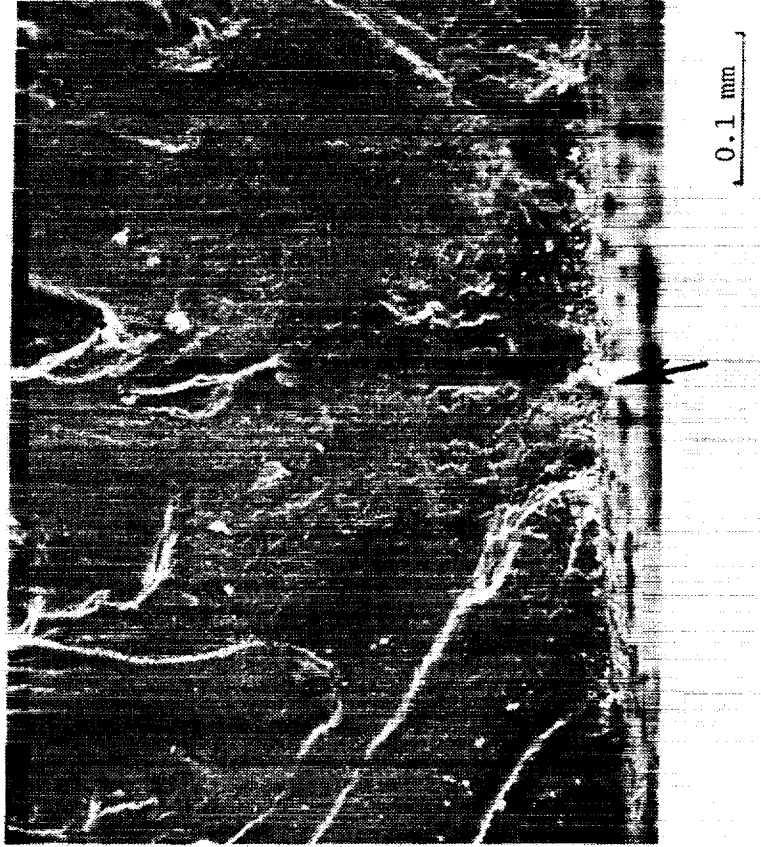
Figure 18   Specimen 119A.   SEM micrographs showing porosity at primary initiation site on I.D.

0.1 mm

0.5 mm

26
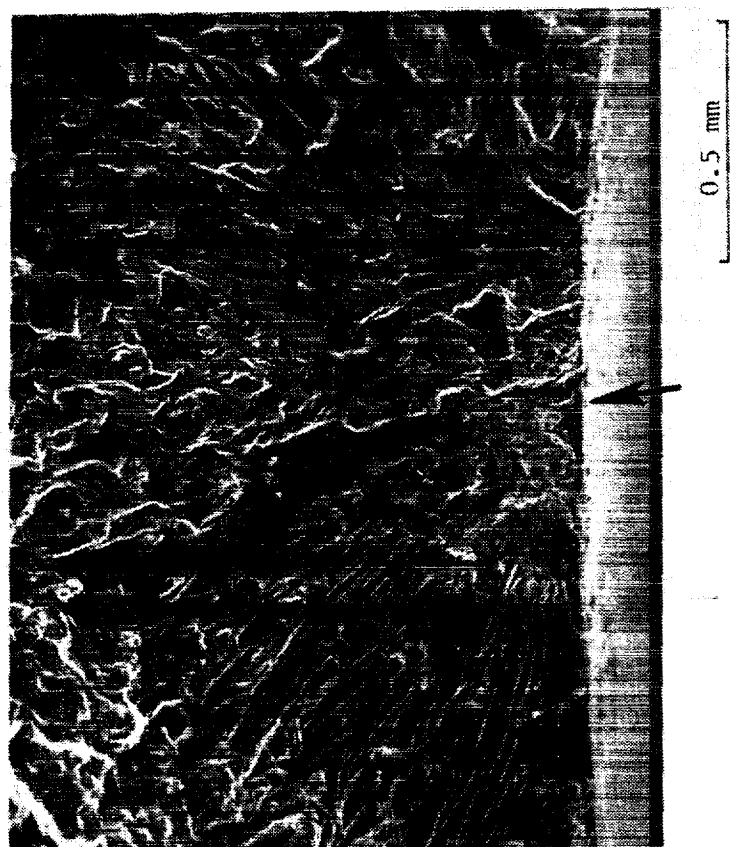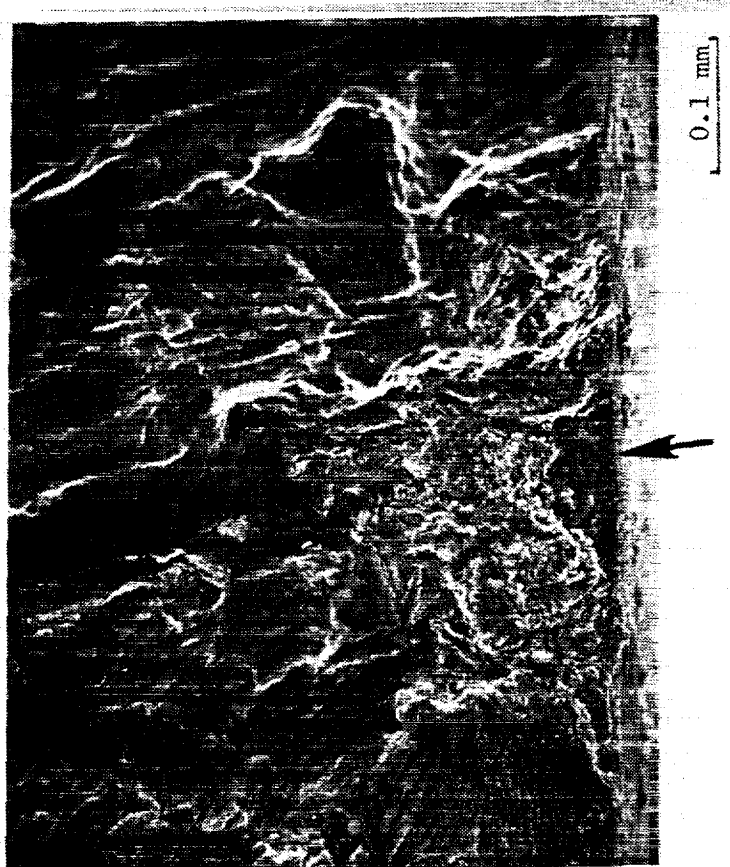
Figure 19   Specimen 119B. SEM micrographs showing extensive oxidation at initiation site on I.D. Porosity is also evident at the initiation site.

27

Specimen 112D was tested at 538-871°C (1000-1600°F), 0.4% strain range, and R = -infinity. Its lives were 3661 and 5319 cycles which are lower than the lives of uncoated specimens at similar conditions. This agrees with the assumption that the coating relaxes rapidly at the high temperature end of the cycle when the substrate is in compression. This results in high tensile stresses in the coating at low temperatures and, hence, a coating life which is not much different than when the cycle is fully reversed. The separation life of the Specimen 112D was shorter than that of the uncoated test, Specimen 107C.

4.1.2   Out-of-Phase Testing on Specimens Coated With PWA 273 Aluminide Coating

Specimen 114A, the first PWA 273 aluminide coated TMF specimen, was tested at 538-871°C (1000-1600°F), 0.4% strain range, R = -1, and out-of-phase cycling. Its observed separation life was 8195 cycles, which is nearly twice that of the overlay coated (PWA 286) specimens tested under the same conditions (120A, 120B). Replica data shows that the initiation life was 4753 cycles which is 1.4X higher than the lives of the PWA 286 coated specimens tested at similar conditions. Optical examination of specimen 114A shows that there were multiple initiation sites on both inner and outer diameters, but the majority of initiations as well as the primary initiation occurred on the outer diameter. Only the primary outer diameter initiation was examined by SEM as only the OD surface involves the coating. As shown in Figure 20, the fracture surface is heavily oxidized and the exact location of the crack origin cannot be identified. The dark band between the coating and base material is the diffusion zone.

Specimen 116D was tested at the same conditions as specimen 114A except at a higher temperature range of 538-982°C (1000-1800°F). Its initiation and separation lives were 1105 and 1535 cycles, respectively.

An aluminide coated specimen was out-of-phase tested at both a higher strain range and temperature range. This specimen (115A) was tested at 538-982°C (1000-1800°F), 0.5% strain range, and R = -1. Its initiation and separation lives were 537 and 647 cycles, respectively, which are slightly lower than the lives of uncoated specimens tested at similar conditions (specimen 106C). Inspection of the fracture shows that the specimen failed from the ID.

Specimen 116C was tested at 538-871°C (1000-1600°F), a higher strain range of 0.5%, and R = -infinity. Its observed initiation and separation lives were 1359 and 3997 cycles, respectively. The separation life was somewhat longer than that of the uncoated specimen (46D). Also, specimen 115C was tested at these same conditions but with R=-1; its initiation and separation lives were 1881 and 2687 cycles, respectively.

28

Figure 20   PWA 273 coated TMF specimen 114A, Cycle I, $\Delta\epsilon = 0.4\%$, 538-871°C (1000-1600°F), R = -1, initiation life = 4753 cycles. SEM micrographs of primary O.D. initiation site. Dark band between coating and base metal is the diffusion zone.

29

4.1.3 In-Phase Testing on Specimens Coated With PWA 286 NiCoCrAlY Overlay Coating

In-phase testing on PWA 286 coated specimen 120D was conducted at 538-871°C (1000-1600°F), 0.4% strain range, R = -1. At these conditions, the primary crack indication showed the initiation life to be 10,012 cycles. However, after the crack reached 0.040", no growth was observed. To verify the appearance of a crack, the specimen was uploaded to 0.5% strain range at 14,497 cycles at which time the crack immediately began to grow again; separation occurred at 16,687 cycles. As in previous tests, these lives are about twice the lives observed from the uncoated tests at these conditions (specimen 128B). This suggests that the low ductility of the coating at low temperatures is not a significant factor at low strains.

SEM examination of the fracture surface of specimen 120D showed it to be heavily oxidized and did not reveal any unusual features that could be associated with the crack growth behavior, except that location of the crack origin was believed to be at subsurface porosity. Figure 21 is a SEM micrograph of the initiation site showing the porosity.

4.1.4 In-Phase Testing on Specimens Coated With PWA 273 Aluminide Coating

An aluminide coated (PWA 273) specimen was tested at 1000 - 1600°F, 0.4% strain range, R = -1, with in-phase strain-temperature cycling (specimen 114D). Its observed initiation and separation lives were 11,712 and 26,028 cycles, respectively,which are significantly higher than the lives of the uncoated specimen tested at these conditions (128B, initiation life = 5127 and separation life = 8138 cycles). Note that when comparing the coated to the uncoated specimen the increase in separation life is much larger than that for the initiation life (3.2X vs 2.3X) which indicates that, at these conditions, the environment is important for crack propagation as well as initiation.

4.1.5 Elliptical Cycle Tests

Six coated specimen tests were completed under this series, two using clockwise (CW) and four using counterclockwise (CCW) cycles. These cycles were compared with the traditional in-phase and out-of-phase TMF cycles (see Figure 15). The CCW cycle is a good simulation of the strain-temperature history experienced by many actual hot section components, although there are some components which have a CW movement around their strain-temperature history. The CW cycle results are most valuable when compared to the CCW results.

4.1.5.1 CW Elliptical Cycles

When subjected to CW elliptical strain-temperature cycling at 538-871°C (1000-1600°F), 0.4% strain range, R=1, 1 cpm, both coating systems were found to show life reductions as compared to uncoated specimens, as can be seen from the test results of Specimens 115B and 113D. Specimen 115B was coated with PWA 273 and specimen 113D was coated with PWA 286. The initiation and separation lives for Specimen 115B were 2339 and 4253 cycles, respectively, and those for Specimen 113D were 1450 and 4394 cycles, respectively. The lives for the PWA 286 coated specimen were slightly lower than the lives of the PWA 273 coated specimen and were approximately one-half of the lives of the uncoated specimens at these test conditions.
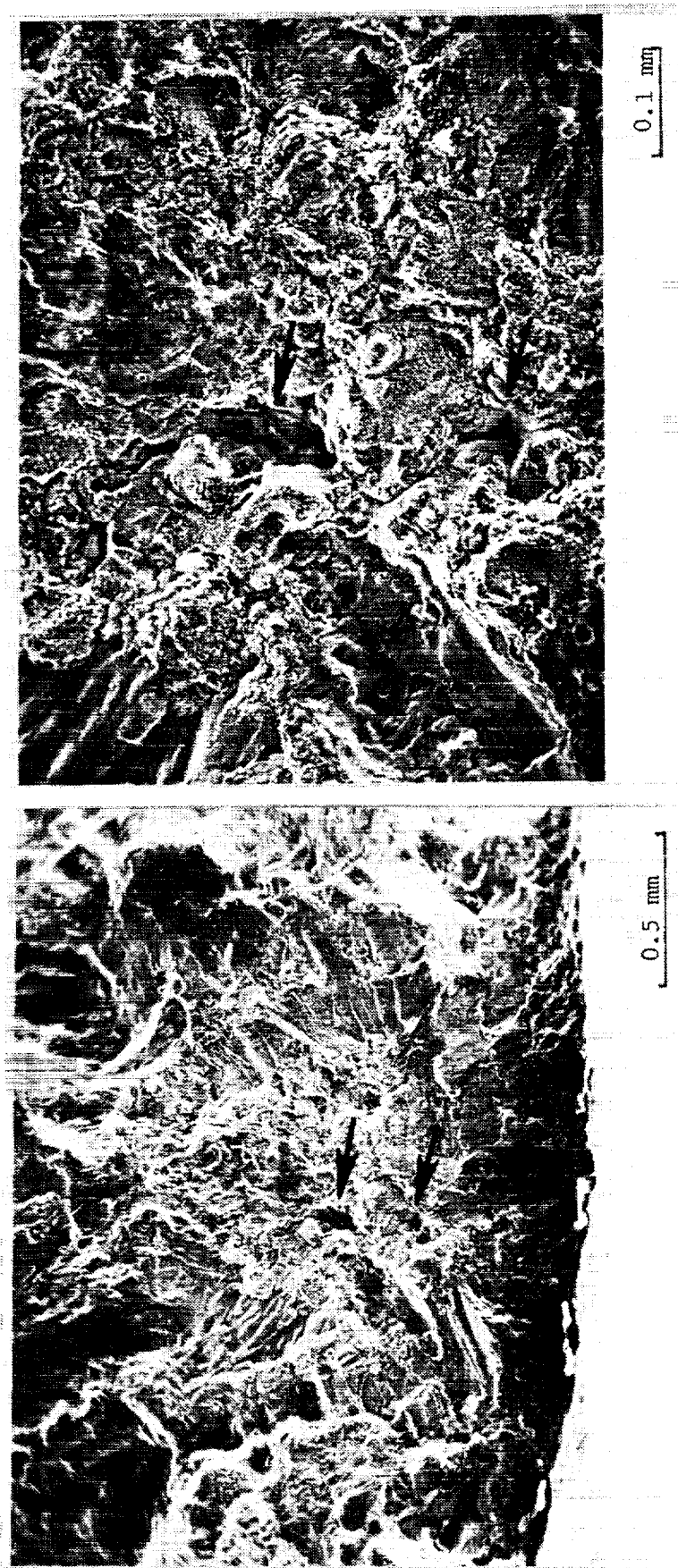
Figure 21   Specimen 120D (PWA 286 overlay coated, $\Delta\varepsilon$ = 0.4%, R = -1, 538-871°C (1000-1600°F), in phase, initiation life = 10,012 cycles, separation life = 16,682 cycles). SEM micrograph showing porosity at crack origin near O.D. with extensive oxidation. Location of porosity indicates that crack may have initiated subsurface.

31

4.1.5.2   CCW Elliptical Cycles

One PWA 286 coated specimen and three PWA 273 coated specimens were tested under CCW strain-temperature cycling conditions. CCW loading produced the highest lives for uncoated specimens.

Specimen 119C was coated with PWA 286 and tested at 538-871°C (1000-1600°F), 0.4% strain range, R = -1. Its initiation and separation lives were 11,125 and 16,123 cycles, respectively. Visual inspection of the fracture surface indicated that the failure was from the OD. Although these lives are higher than those of uncoated specimens at these conditions, they are less than what was observed for out-of-phase and in-phase conditions.

Specimens 114C, 115D and 116B were all aluminide coated (PWA 273). Specimen 114C was tested at 538-871°C (1000-1600°F), 0.4% strain range, R = -1. Its initiation and separation lives were 9270 and 15,982 cycles, respectively, which are 1.2 - 1.5X higher than the lives of uncoated specimens tested at these conditions but slightly lower than the lives of the overlay coated specimen (specimen 119C). These results suggest that the life increase generated by CCW elliptical cycling affects the same mechanism that benefits from coatings.

Specimen 115D (PWA 273 coating) was tested at 538-871°C (1000-1600°F) but at a higher strain range of 0.5% (R=-1) as compared to 0.4% for specimen 114C. Its lives were 1946 and 3538 cycles. The initiation life of this specimen is similar to that resulting from out-of-phase cycling of PWA 273 coated specimens at 0.5% strain range. It does not show the life increases seen for uncoated specimens subjected to CCW cycling. The life increases resulting from CCW elliptical cycling and from coating the specimens do not appear to add directly.

Specimen 116B was tested at higher temperature conditions; 538-982°C (1000-1800°F), 0.4% strain range, R = -1. Its lives were 2622 and 2703 cycles which is a substantial life credit relative to the standard out-of-phase cycle at these conditions. The short propagation time may indicate that the crack originated on the ID or in the substrate and was propagating for quite some time before detection by surface replication.

4.1.5.3   Comparison of CW and CCW Fracture Surfaces

Optical micrographs of a CCW tested specimen (114C) and a CW tested specimen (115B), both PWA 273 coated, are shown in Figure 22. Both specimens had multiple OD initiation sites. SEM examination of the primary initiation site on the outside diameter of Specimen 114C shows a heavily oxidized fracture surface with MC carbides at the locations indicated by the arrows in Figure 23. The fracture surface oxide prevents detailed examination of the fracture that would pinpoint the exact nature of the initiation site. The PWA 273 coating at this location was measured to be 1.7 mils thick.

The SEM micrographs of specimen 115B shown in Figure 24 show that the fracture is similar to that of specimen 114C. The surface is heavily oxidized and MC carbides are seen in the vicinity of the origin (indicated by arrows). The PWA 273 coating measured 1.4 mils thick at this location. Possible dross was observed at the inside diameter initiation site.

32
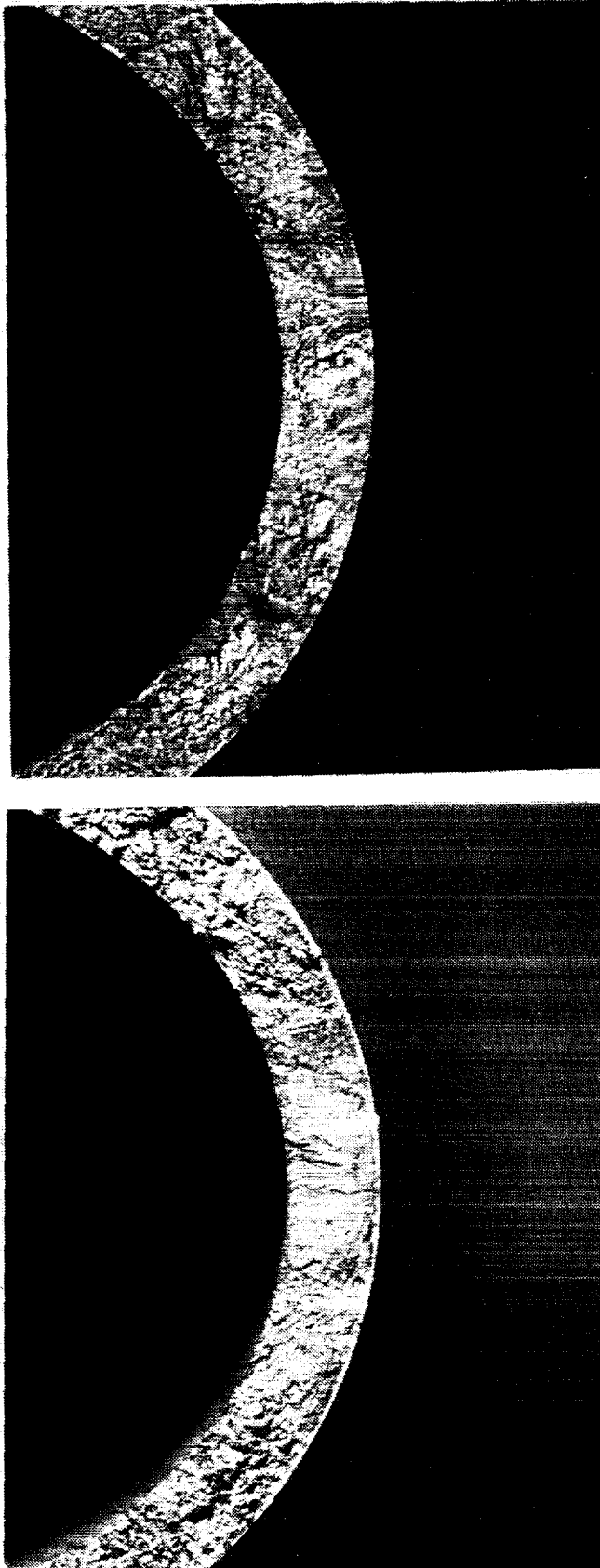
Figure 22   Optical Micrographs of PWA 273 Coated PWA 1455 Elliptical Cycle TMF specimens.

(a)   114C (± 0.2%ε, 538-871°C (1000-1600°F), 1cpm, CCW, initiation 9270 cycles, total test length, 15982 cycles).

(b)   115B (± 0.2%ε, 538-871°C (1000-1600°F), 1cpm, CW initiation 2339 cycles, total test length, 4253 cycles).
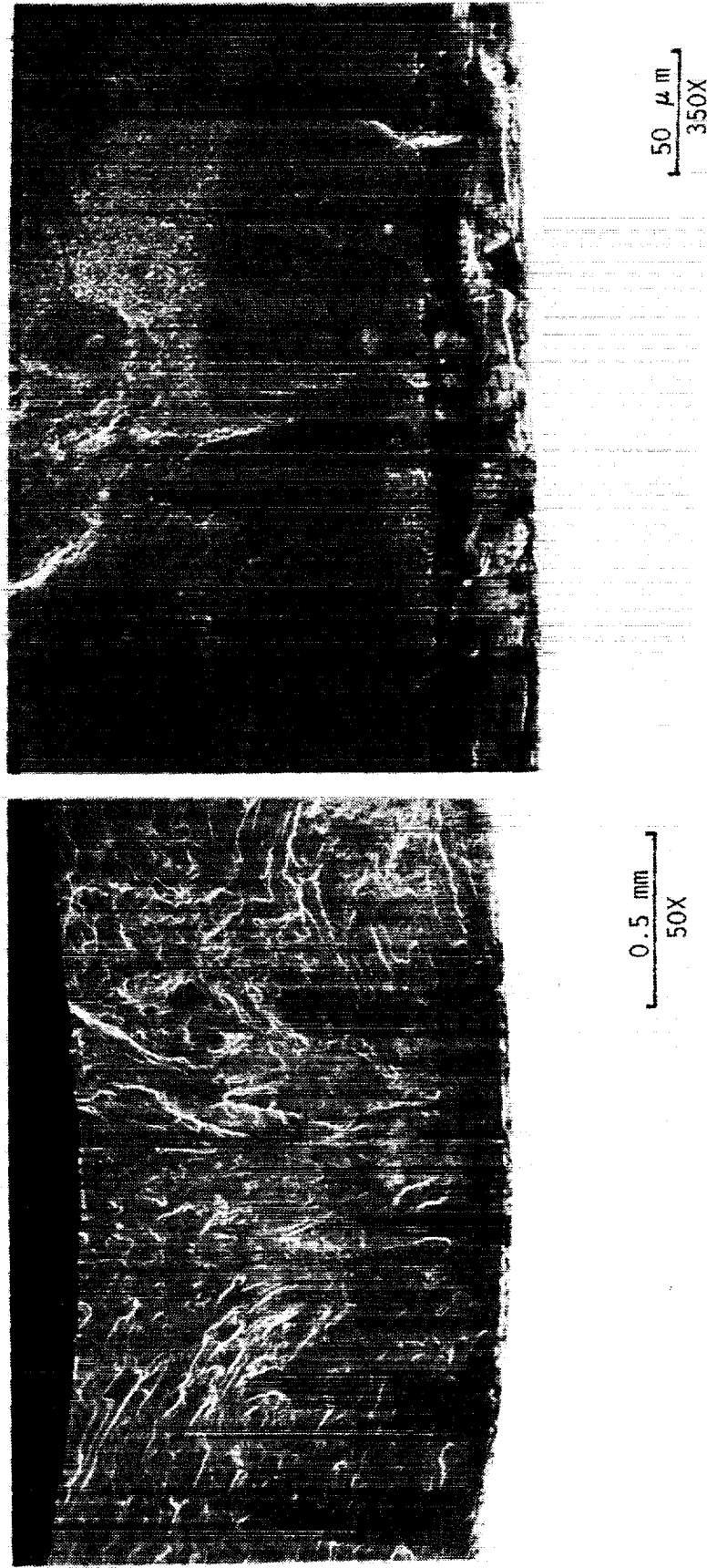
Figure 23   SEM Micrographs of Primary Initiation Site of 114C. Fracture surface is heavily oxidized, MC carbides are indicated by arrows. PWA 273 coating thickness ⌐1.7 mils.

34
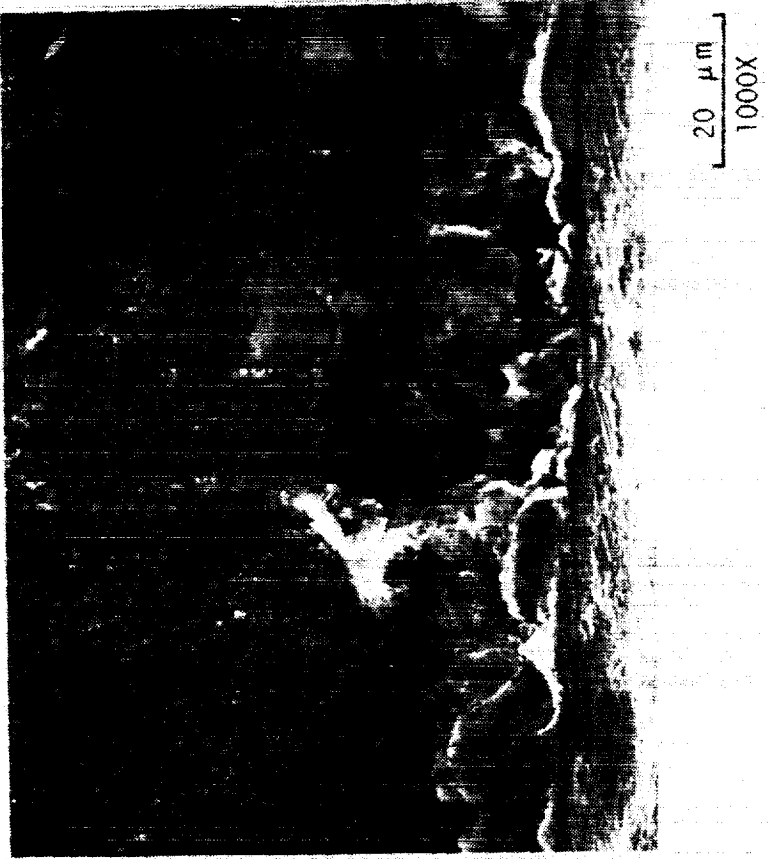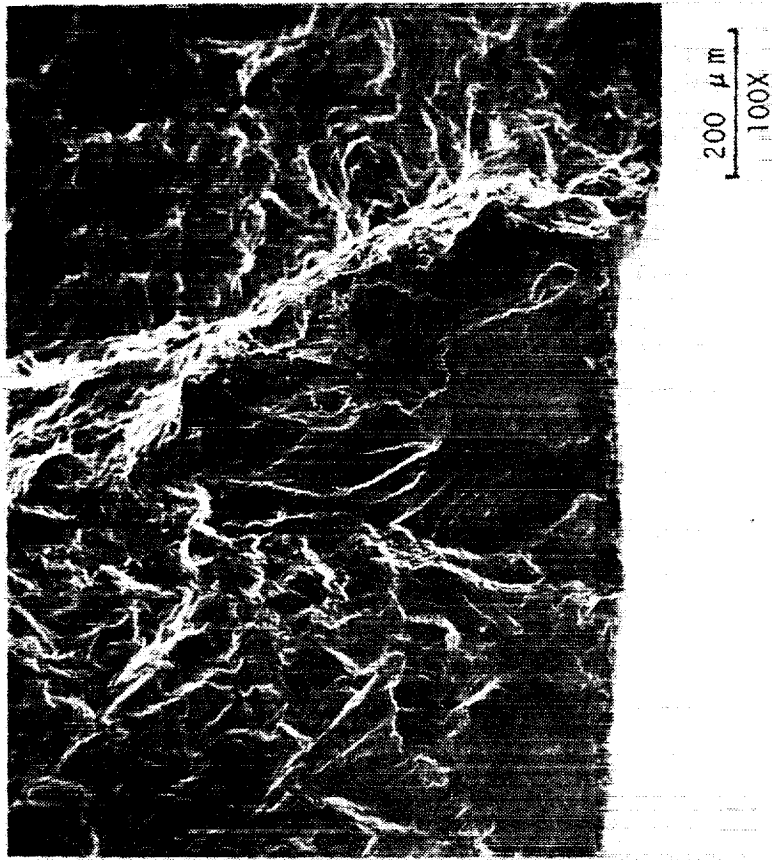
Figure 24   SEM Micrographs of an Initiation Site on 115B.   Fracture surface is heavily oxidized, MC carbides are indicated by arrows.   PWA 273 coating thickness ₁1.4 mils.

Optical and SEM examinations were also made on two uncoated CCW elliptical specimens tested at 538-871°C (1000-1600°F), 0.5% strain range, R=-1: 108D (initiation life = 3652 cycles, separation life = 7024 cycles, and 125D (initiation life = 1097 cycles, separation life = 2551 cycles). Both specimens exhibited multiple initiation sites. The major initiation site of 108D is shown in Figure 25 and that of 125D is shown in Figure 26. The shiny areas on the fracture surface of 108D shown in Figure 25(a) are the result of damage to the fracture surface that occurred after testing. Note that there is only minimal porosity at the initiation site of 108D, while Figure 26 shows that there is a high amount of porosity at the initiation site of 125D. This condition may be the cause of the lower fatigue lives observed in this specimen. No other features that may have played a role in the initiation of cracks in these specimens (such as the carbides observed in two of the PWA 273 coated specimens) were seen. The fracture surfaces of these specimens are similar overall to those of the other elliptical cycle specimens.

4.1.6 Hold Tests, Out-Of-Phase and In-Phase

Hold time TMF testing was conducted on five specimens at test conditions of 538-871°C (1000-1600°F), 0.4% strain range, one minute hold at maximum temperature and using in-phase or out-of-phase loading. Two specimens were tested uncoated, two specimens were coated with PWA 286, and one specimen was coated with PWA 273. These tests demonstrated the effect of a high maximum stress fatigue cycle accompanied by simultaneous creep damage.

Three specimens were tested using out-of-phase cycling with hold times; 123D, 120C and 113B. Specimen 123D was tested in an uncoated condition at 538-871°C (1000-1600°F), 0.4% strain range, R = -1, with one minute hold at 1600°F and -0.2% strain. Its initiation and separation lives were 1237 and 2689 cycles, respectively. While the initiation life with hold time is shorter than those of specimens not subjected to hold times, the crack propagation life (from 0.030" to 50% load drop is longer). This may have been due to inherent data scatter since the increasing maximum tensile stress observed during the test that results from out-of-phase cycling would usually be expected to shorten the propagation life. Also a change in crack conditions may occur because of the additional time spent at 871°C (1600°F).

Specimens 120C and 113B were both coated with PWA 286 overlay and were tested using the same conditions as for specimen 123D: 538-871°C (1000-1600°F), 0.4% strain range, R = -1, with one minute hold at 871°C (1600°F) and -0.2% strain. These specimens had nearly identical initiation and separation lives. The initiation and separation lives of specimen 120C were 2338 and 3270 cycles, respectively and those of Specimen 113B were 2364 and 3377 cycles, respectively. The PWA 286 coated specimens show an approximately 2X increase in initiation life as compared to the uncoated specimen.
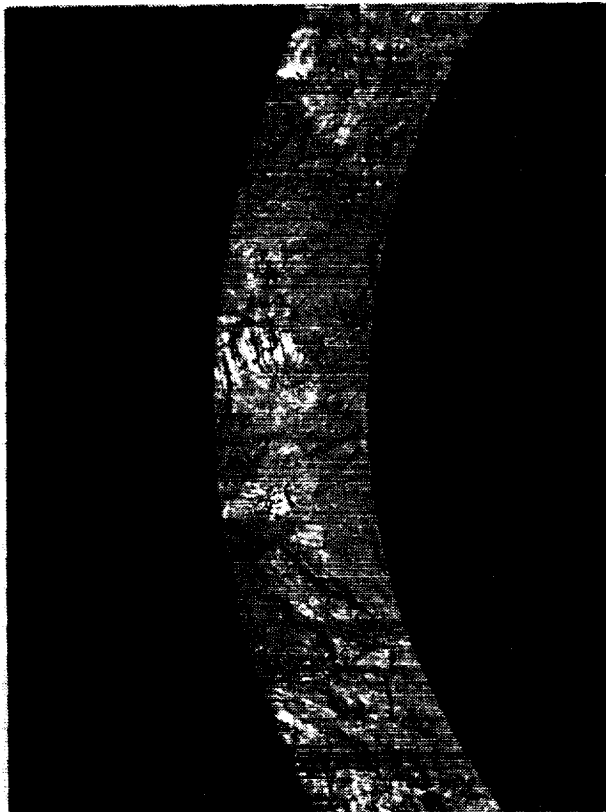
Figure 25   Specimen 108D (CCW elliptical, ϵ = 0.5%, initiation life = 3652 cycles, separation life = 7024 cycles), (a) optical and (b) SEM of initiation site. Minimal porosity was observed.
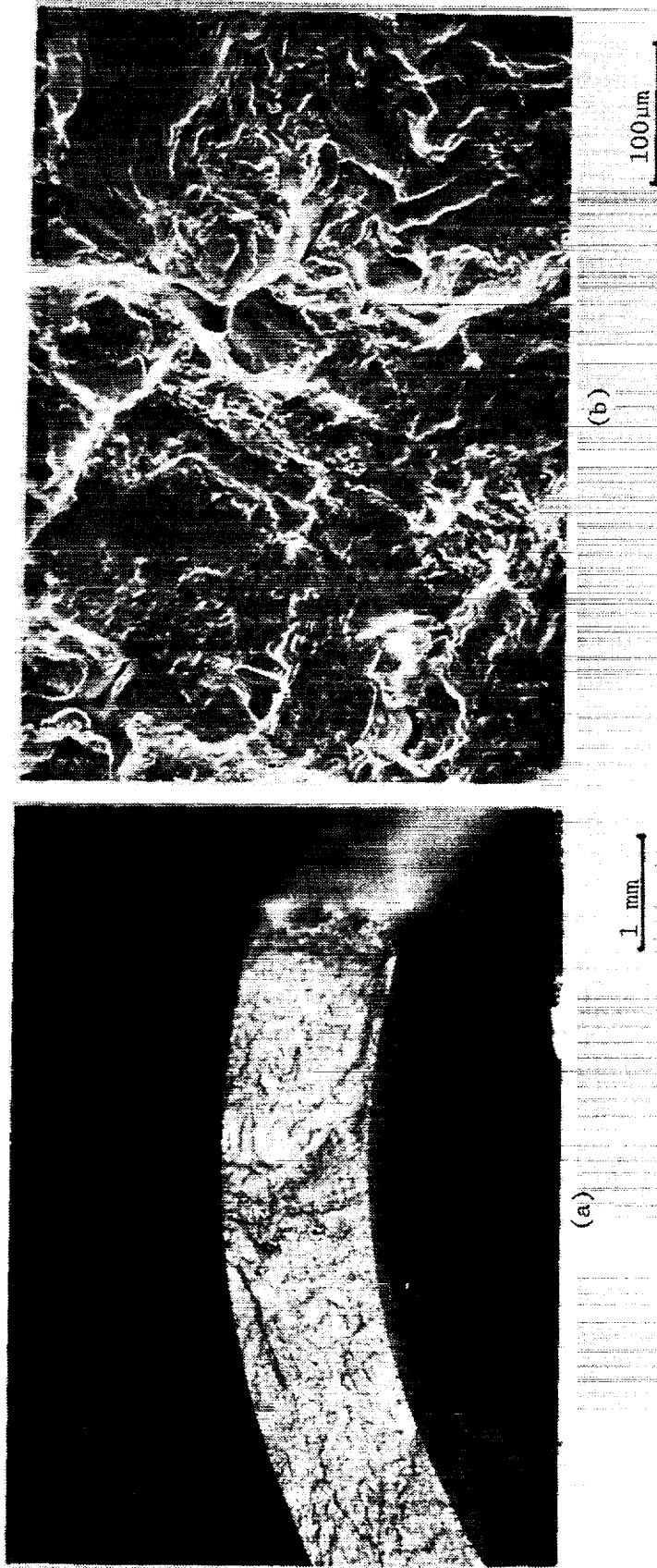
Figure 26   Specimen 125D (CCW elliptical, $\varepsilon = 0.5\%$, initiation life = 1097 cycles, separation life = 2551 cycles), (a) optical and (b) SEM of initiation site showing unusually high degree of porosity.

Specimen 124A (uncoated) was run using in-phase cycling with a hold time at 538-871°C (1000-1600°F), 0.4% strain range, R = -1, with one minute hold at 871°C (1600°F) and +0.2% strain. Its initiation life was 4411 cycles and its separation life was 11,054 cycles which were considerably longer than uncoated Specimen 123D which had a one-minute compression hold at -0.2% strain and 871°C (1600°F). Figure 27 shows a plot of the specimen stresses vs. time for Specimen 124A and it can be seen that the mean stress drifted downward throughout the test. From the standpoint of the total specimen life, this modified stress response apparently outweighed any detrimental effects caused by having the crack held open at the high temperature, resulting in a significant reduction in average damage per cycle.

CONDITIONS: 538-871°C (1000-1600°F), 0.4% Δε, R = -1, ONE MIN. HOLD AT +0.20%
SPECIMEN NO.   =124A
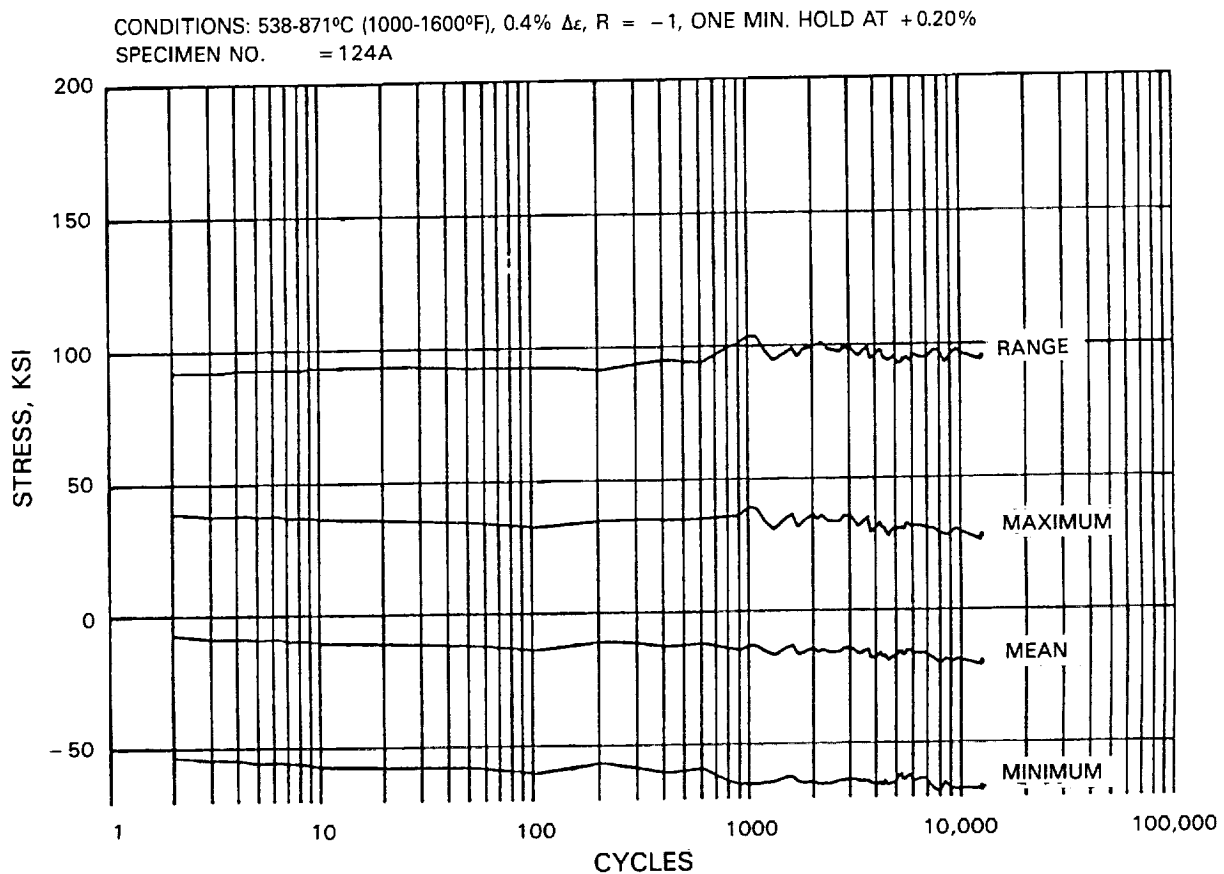
Figure 27.- Stress Response for Tensile Hold TMF Test.

Figure 28 compares crack growth data from replicas of both in-phase and out-of-phase uncoated TMF specimen tests, with and without a one minute hold at the maximum temperature. It appears that the effects of the hold time at maximum temperature on the specimen stress response has a strong influence on the crack growth rate. The tensile hold that occurs for in-phase cycling decreases the crack propagation rate due to the reduction in mean stress that occurs as the test progresses. Note, however, that the initiation lives of the hold time tests were lower than those of the corresponding tests without hold times, indicating that the hold times also increased the damage rates during the early portions of the test.

39
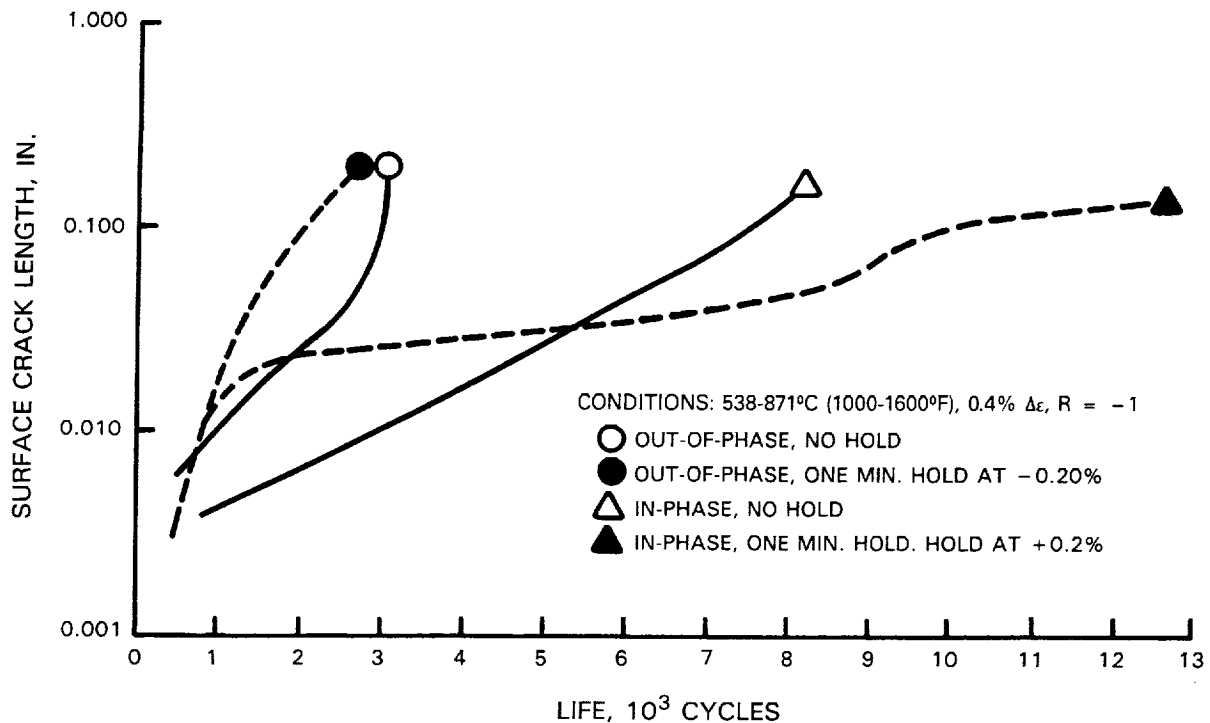
Figure 28.- TMF Crack Growth Data - Uncoated Specimens.

Specimen 116A was PWA 273 aluminide coated and tested to show the effects of this coating on fatigue life during tensile hold conditions similar to those conditions that an actual engine component may experience. This specimen was tested at 538-871°C (1000-1600°F), 0.4% strain range, R = -1, in-phase strain-temperature cycling with a one minute hold at +0.2% and 871°C (1600°F). Its lives were 4659 and 11,092 cycles which are essentially the same as the lives for the uncoated specimen (124A) tested at these conditions. This indicates that for these conditions the damage mechanism is more related to phenomena at the grain boundaries within the bulk rather than to surface properties.

4.1.7 Dogleg Test

Specimen 113C utilized PWA 286 overlay coating and was tested at 538-871°C (1000-1600°F), 0.5% strain range, R = -1, with "LC" type dogleg strain-temperature cycling. As shown in Figure 29, this cycle begins with a -0.25% strain hold with temperature varying from 538-871°C (1000-1600°F) and back, then 6 seconds strain excursion to +0.25% at 538°C (1000°F). These test conditions were chosen to induce high coating stresses and hence early coating cracking. The initiation and separation lives for this specimen were 742 and 1856 cycles, respectively, which are lower than the lives for the uncoated specimen tested at the same conditions (45D; 1300 and 2096 cycles). The lower lives for the coated specimen (0.6X for initiation) confirm that these test conditions result in early coating cracking.

40
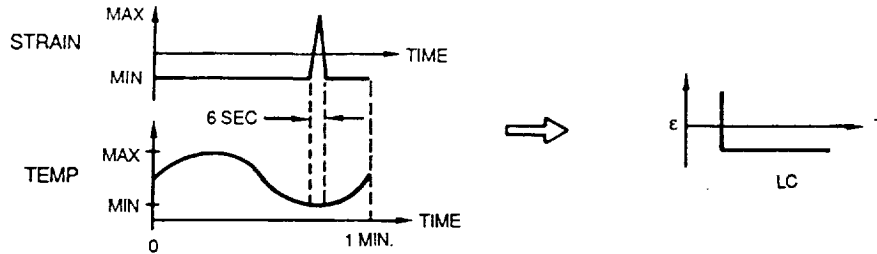
A. STRAIN AND TEMPERATURE HISTORIES LC DOGLEG CYCLE
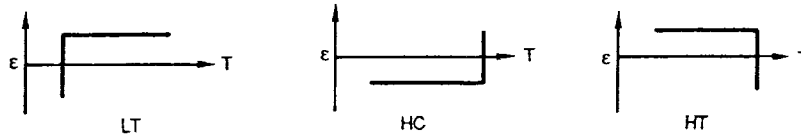
B. OTHER DOGLEG CYCLES USED FOR TESTING

Figure 29.- Dogleg TMF Cycles.

4.2 Task VI - Multiaxial Stress State Model

The purpose of this testing was to simulate engine operation conditions encountered by certain areas of high temperature components such as intersections of platforms and airfoils which have a high degree of multiaxiality. For such locations some method is needed to determine the parameters which best characterize the initiation life under those conditions. Therefore a total of 26 tests using thin-walled (0.050") tubular specimens were conducted to obtain crack initiation data for use in developing and verifying a multiaxial stress state creep fatigue life prediction model. As illustrated in Figure 30, four types of strain cycles were employed; simple tension, simple torsion, combined in-phase tension-torsion (proportional loading) and combined 90° out-of-phase tension-torsion (non-proportional loading). Additional variables were investigated which included temperature, strain range, and strain rate. Table VI shows a matrix of all 26 tests completed under this task. Appendix B lists the detailed test results for all PWA 1455 multiaxial tests, including revised data for the four tests previously reported.

Strain range and cycle type were both shown to be significant factors in determining multiaxial life. The phase angle between axial strain and torsional strain was also important, although frequently there was little interaction between the two. Unusual levels of dross and/or porosity were found to have caused premature cracking in four of the tests. This was no doubt caused by the casting process used to create the bars for these specimens.

The configuration of the multiaxial specimen is considerably different from that of the uniaxial specimens used in the baseline LCF testing and therefore optical and TEM replica examinations were made in order to document the microstructure. Both the grain size and gamma prime size were found to be comparable to those for the uniaxial specimens. The specimen wall thickness contains approximately two grains and elastic anisotropy effects may require more careful consideration in the case of the multiaxial specimens than for the uniaxial specimens.

41
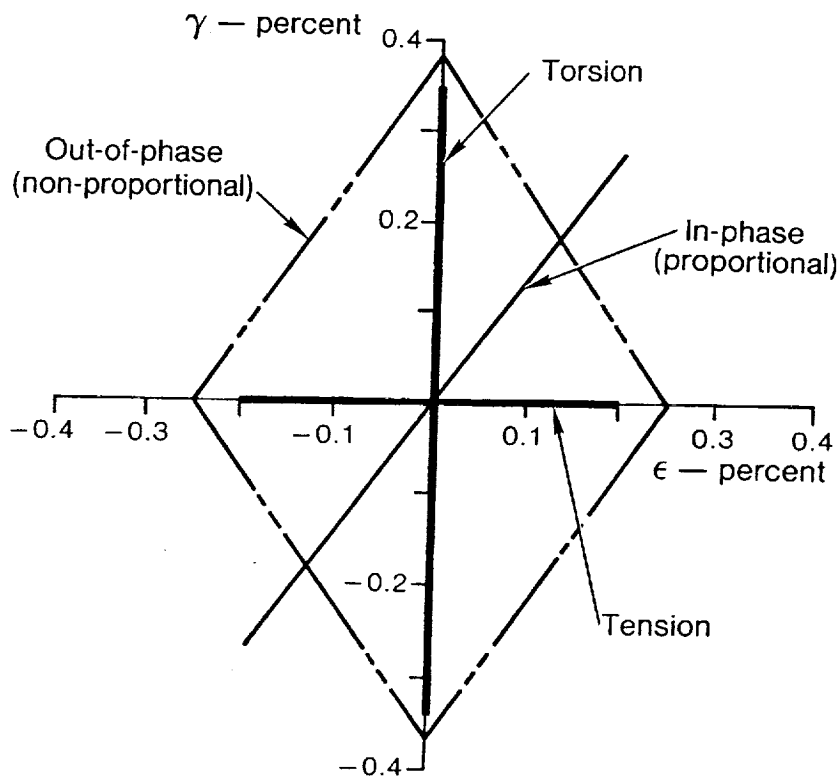
Figure 30.— Strain Cycles Used for Multiaxial Testing.

TABLE VI
PWA 1455 MULTIAXIAL TEST MATRIX

Temp (°F)	Nominal $\Delta\varepsilon$ (%)	Freq. (CPM)	Strain Cycle Type Tension ($\gamma=0$)	Torsion ($\gamma=\infty$)	In-Phase ($\gamma=1.5$)	Out-of-Phase ($\gamma=1.5$; $\phi=90°$)
1000	0.50	10	#12: 201	#16: 209	#22: 225	#14: 214
		1				#21: 211
	0.675	10	#9 : 220	#7 : 221	#10: 223	#11: 202 (X) #23: 206
		1				#13: 215
1600	0.40	10	#8 : 222	#2: 203 #6: 219	#5: 218 (X) #26: 228	#15: 205 (X) #19: 227
		1		#25: 210		#20: 213
	0.50	10	#3: 217	#24: 212	#1: 204 (X) #17: 226	#4: 216
		1				#18: 207

Notes: 1. Table entries show #(test number): (specimen ID number)
2. (X) indicates a bad test (due to dross, porosity, etc.)

42

4.2.1 Simple Tension Cycling

A total of four specimens were tested using simple tension cycling. Specimen 201 was tested at 538°C (1000°F), 10 CPM and axial strain range of 0.523%. Its initiation life was 4100 cycles; 50% tensile load drop was achieved at 5941 cycles. However, as with most of the multiaxial specimens, cycling was inadvertantly continued beyond 50% tensile load drop.

Specimen 220 was tested for a total of 6837 cycles at 538°C (1000°F), 10 CPM and axial strain range of 0.679%; its initiation life was 1790 cycles. Optical examination showed the fracture surface to be perpendicular to the longitudinal specimen axis. Multiple initiation sites were observed on the specimen OD. Figure 31 shows optical and SEM micrographs of the initiation sites.

Specimen 217 was tested for a total of 2442 cycles at 871°C (1600°F) and 10 CPM using an axial strain range of 0.494%. The initiation life of approximately 1107 cycles was consistent with the uniaxial tests of solid specimens at the same conditions. Figure 32 shows optical and SEM micrographs of the crack initiation site of specimen 217. As shown in Figures 32(b) and 32(c), the crack initiated from porosity which is considered typical for the test material. Two separate cracks eventually coalesced, and their initiation sites were found on specimen surface replicas taken during test. Figure 33 presents replica micrographs that show a crack evolving at one of the initiation sites exhibiting an atypical surface appearance. As shown in Figure 33c, a 10-mil long crack evolved after 800 cycles. Figure 34 shows these crack surface length measurements from replicas versus cycles.

During the testing, it was discovered that the hysteresis loops for test numbers 3, 4 and 5 showed successively higher levels of tensile mean stress shift, as shown in Figure 35. Examination of the test rig revealed a malfunctioning axial capacitance displacement probe which was repaired. The cyclic life results of the tests run with tensile stresses are still valid because R-ratio testing previously conducted on uniaxial, solid specimens showed only moderate effects on cyclic life for these mean stress levels. Life predictions for these specimens will account for these mean stresses.

Specimen 222 was tested for a total of 19,390 cycles at 871°C (1600°F), 10 CPM and axial strain range of 0.402%. This test used the repaired axial capacitance displacement probe so that no significant increase in tensile mean stress occurred prior to crack initiation at 9629 cycles.
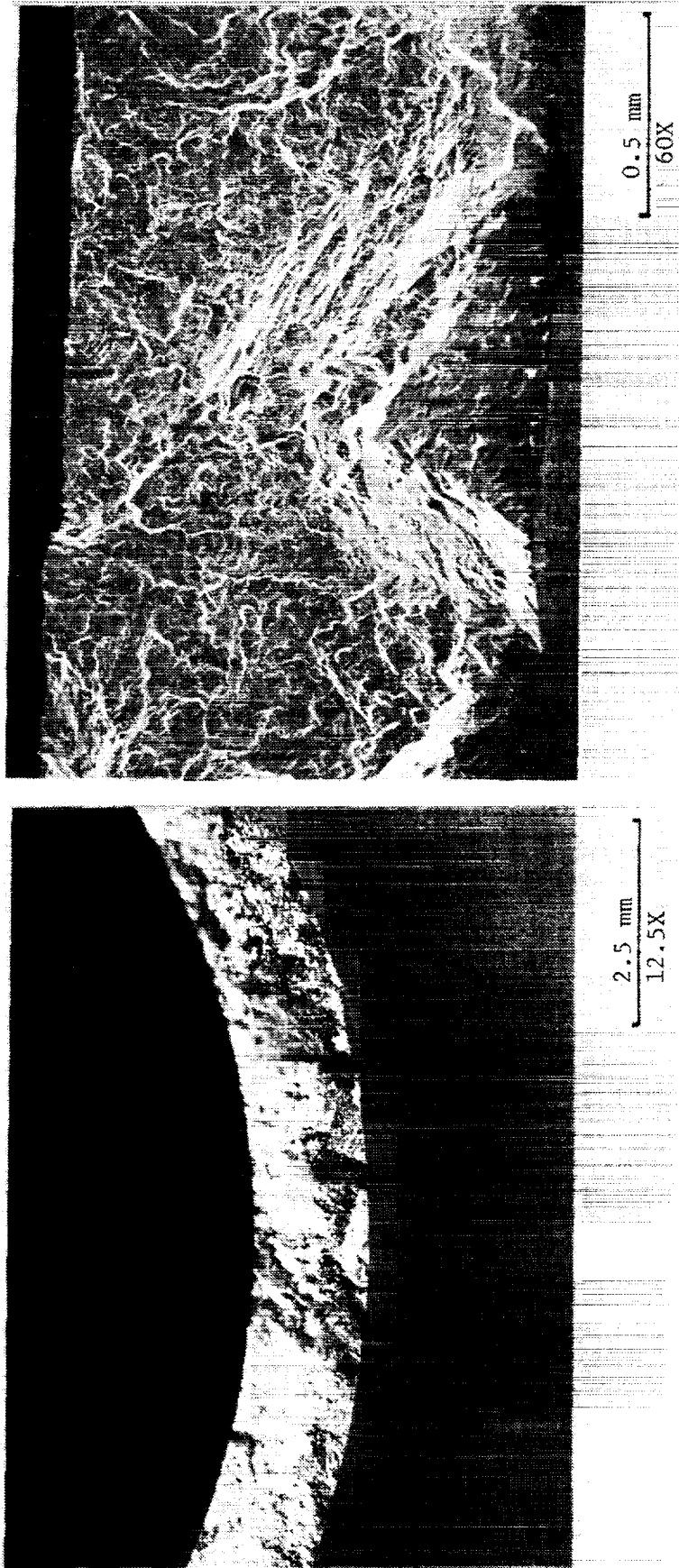
Figure 31   Multiaxial specimen 220 (538°C (1000°F), tensile only, $\varepsilon_x = \pm .34$, 10 cpm, estimated initiation life = 1790 cycles). Optical and SEM micrographs showing typical initiation sites.

44
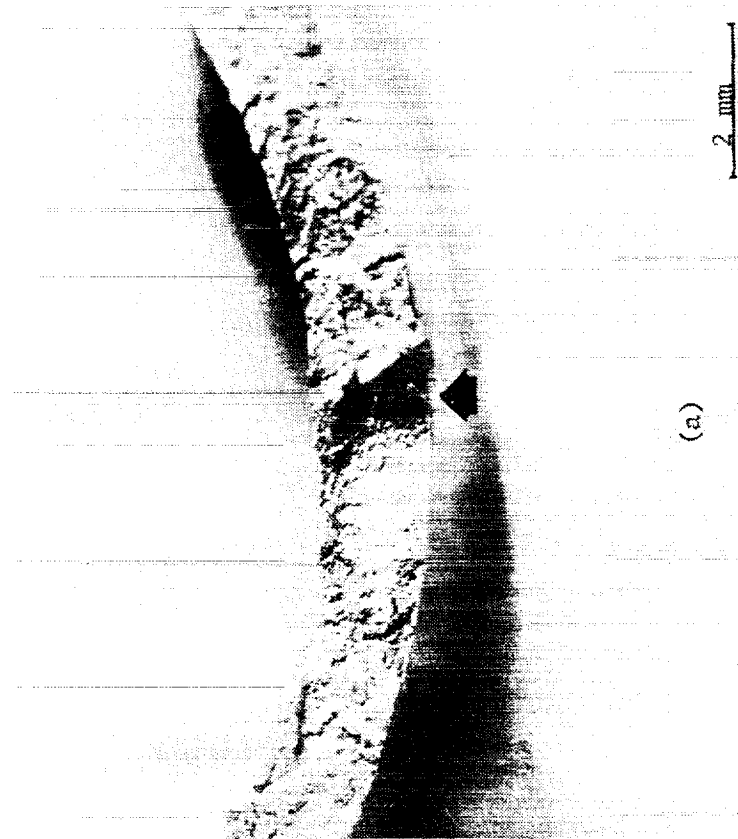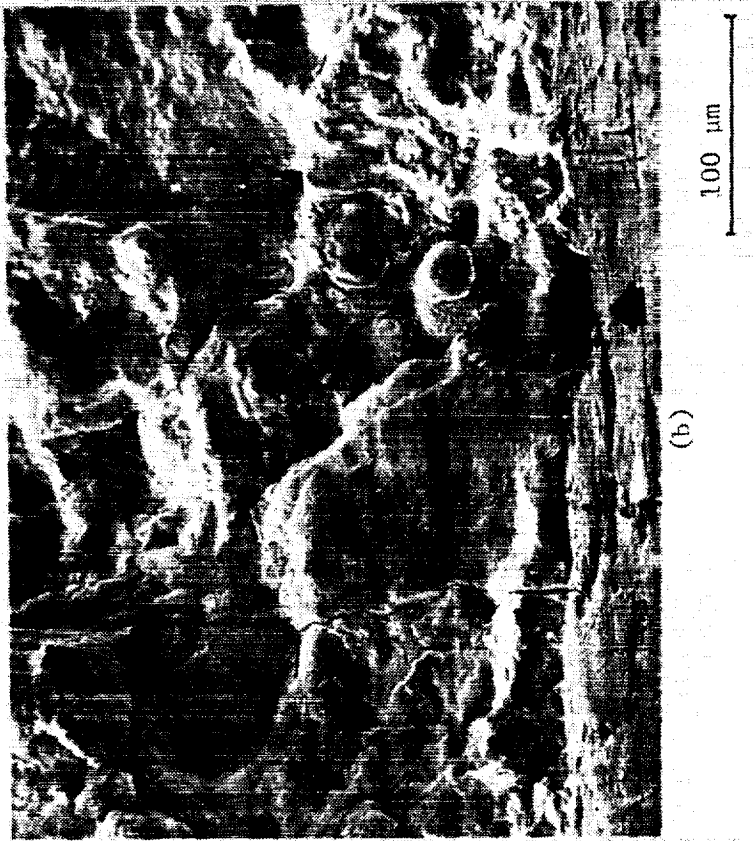
Figure 32

Multiaxial specimen #217 (tension only ± 0.25%, 2442 cycles).

(a) Optical micrograph of area of initiation site.

(b) and (c) SEM micrographs showing porosity at initiations site as well as secondary cracking.
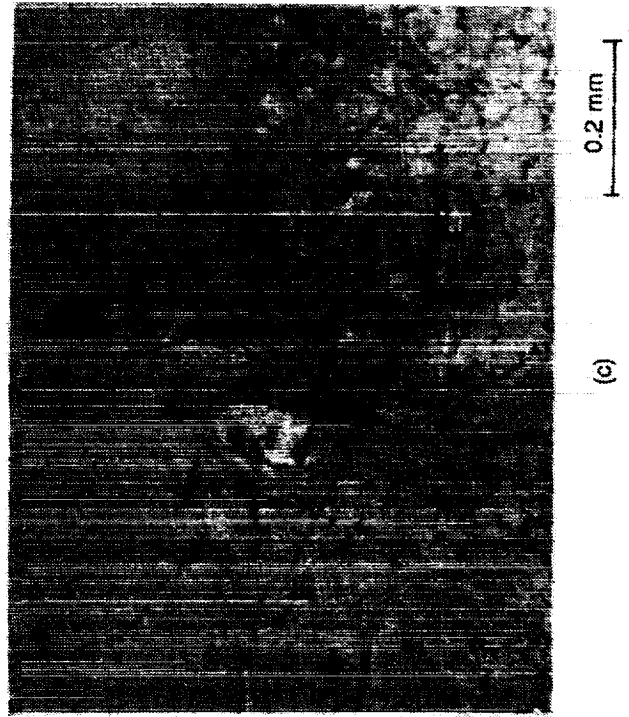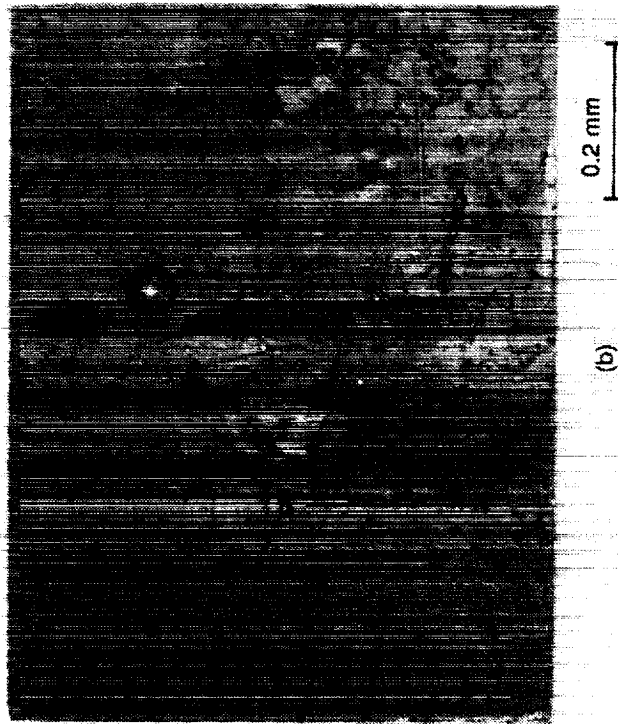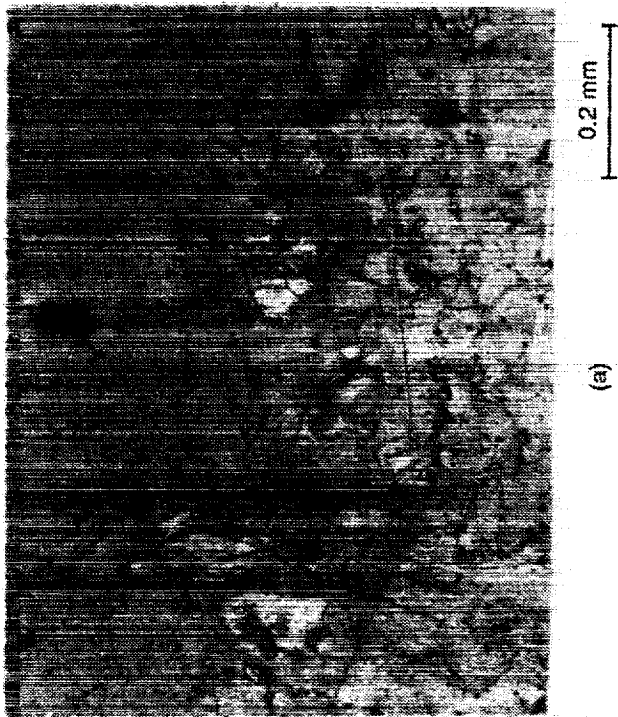
Figure 33

Surface replicas of multiaxial specimen 217 (tension only)

Micrographs at initiation site:

(a) At 0 cycles showing a typical surface appearance.
(b) At 400 cycles showing small cracks had developed.
(c) At 800 cycles showing ⎤10 mil long surface crack.
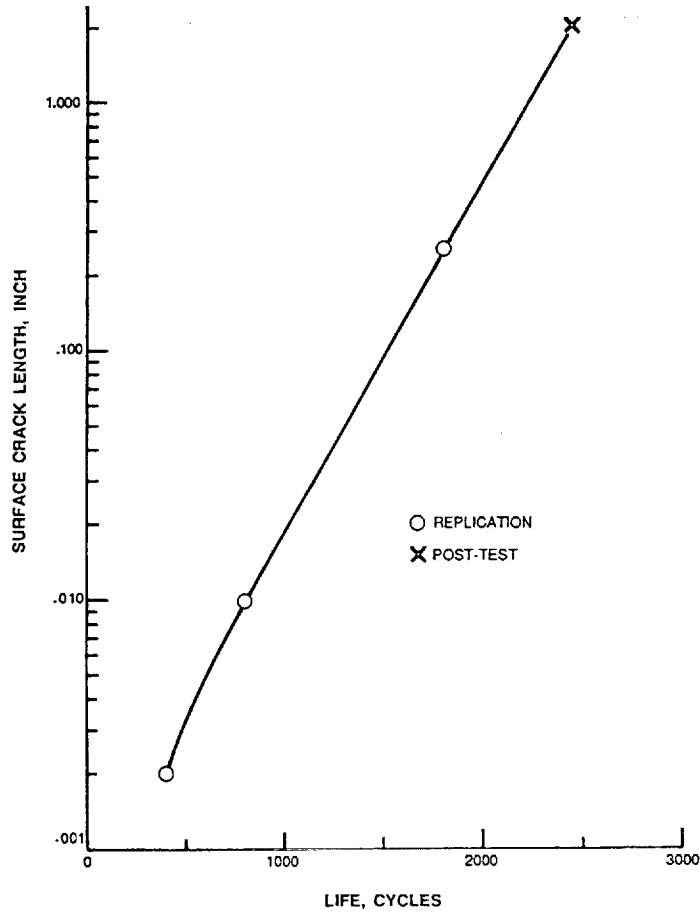
Figure 34.- Crack Growth Data for Multiaxial Specimen 217 (tension only).
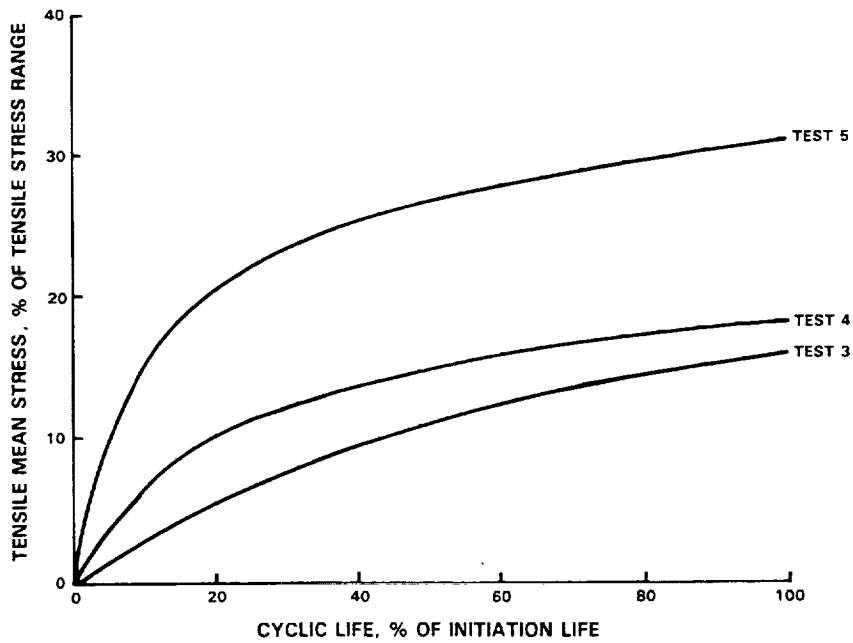
Figure 35.- Tensile Mean Stresses Developed During Multiaxial Specimen Tests.

47

4.2.2 Simple Torsion Cycling

4.2.2.1 538°C (1000°F)

Specimen 209 was tested for a total of 24,366 cycles at 538°C (1000°F), 10 CPM and a torsional strain range of 1.008%. The crack initiation life of 20,188 cycles appeared to be high but may be attributable to the greater degree of scatter in this life regime. Optical and SEM observations of specimen 209 are shown in Figure 36. As shown in Figure 36(a), this specimen had five crack segments. The short center segment is 71° from the longitudinal specimen axis while the other longer segments are 39° and 49° from the longitudinal specimen axis. Optical examination of the fracture surface revealed that some rubbing of the opposing fracture surface features occurred during testing, as shown in Figure 36(b). Multiple OD initiation sites were examined by SEM but the origins could not be identified due to rubbing damage. A typical SEM fractograph showing multiple initiation sites and some secondary cracking is shown in Figure 36(c).

Specimen 221 was tested for a total of 2332 cycles at 538°C (1000°F) and 10 CPM at a torsional strain range of 1.362%. This strain range was significantly larger than the levels used at 871°C (1600°F) because of the increased life capability at 1000°F. As shown in Figure 37, the final crack configuration was complex with three cracks meeting at one point. Two of the cracks were at 45°-50° from the longitudinal specimen axis which corresponded to the maximum normal strain planes and was consistent with the cracking planes observed for pure torsion at 871°C (1600°F). In examinations of other multiaxial specimens, the fracture surfaces were found to be perpendicular overall to the longitudinal specimen axis (i.e., they did not slant from I.D. to O.D.). However, the fracture surface of specimen 221 was observed to have a slant. Multiple origins were found along the O.D. of the sample. SEM micrographs of a typical initiation site on the 45° fracture surface are shown in Figure 38. The exact nature of the initiation sites (carbide or porosity) could not be determined. The crack growth mode was transgranular.

4.2.2.2 871°C (1600°F)

Specimen No. 203 was tested for a total of 11,224 cycles at 871°C (1600°F) and 10 CPM with a torsional strain range of .805%. The final crack was 1.6" long and was slanted at an angle of 45° with respect to the longitudinal axis of the specimen, as shown in Figure 39(a). This corresponded to the maximum normal strain planes. The most likely site for initiation was determined by finding the location along the crack where separation between the two crack faces was greatest. The suspected initiation site is shown in Figure 39(b). Note the secondary crack propagating at right angles to the primary crack.
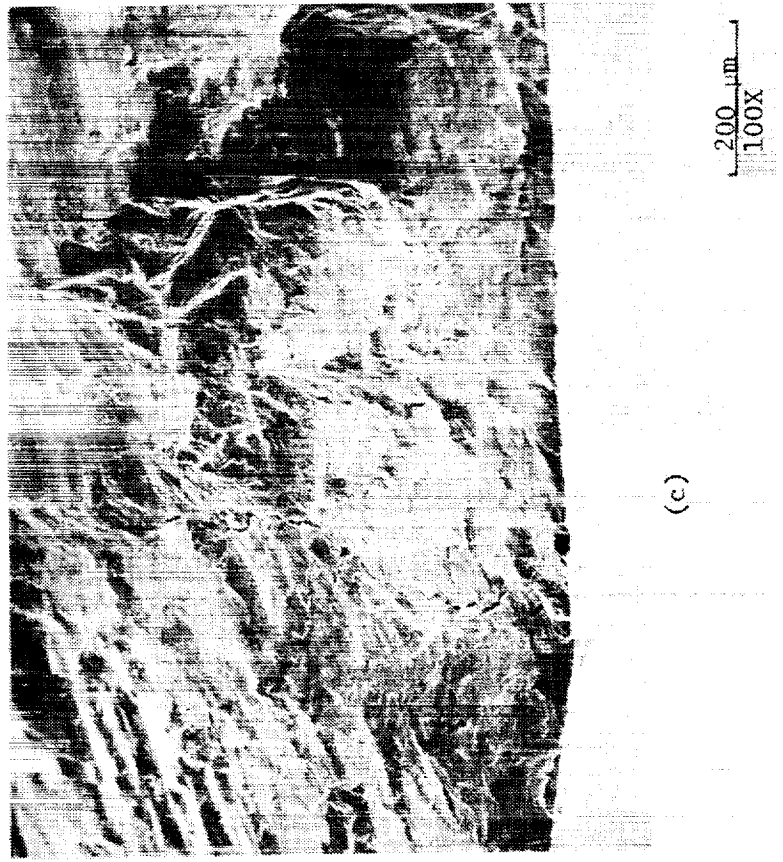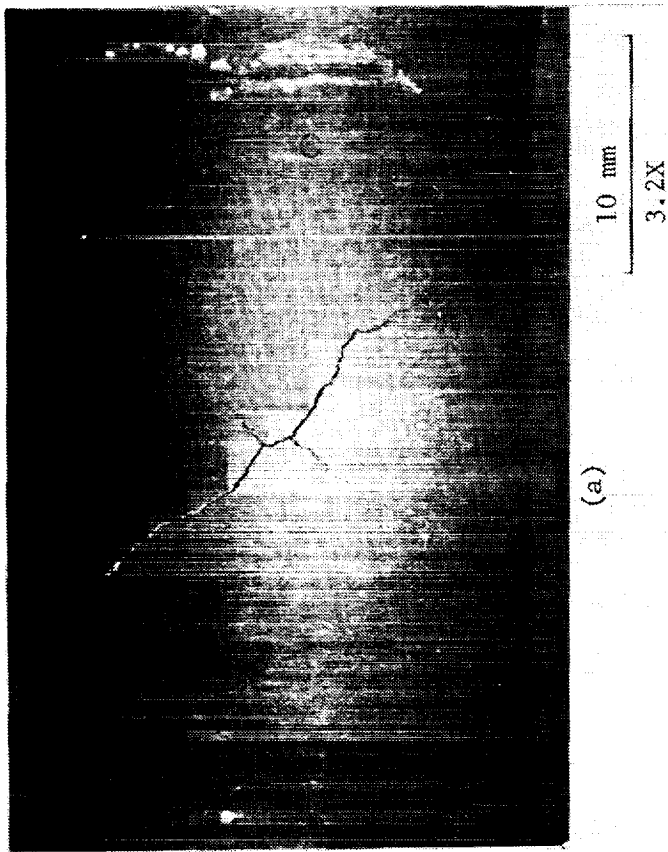
Figure 36

Multiaxial specimen 209 (538°ε (100°F), Δε = 0,
Δγ = 1.008%, 10 cpm, 20,188 cycles, total test
life = 24,366 cycles.

(a) Optical micrograph showing crack segments.

(b) Optical micrograph of fracture surface
     showing evidence of rubbing.

(c) SEM micrograph showing multiple O.D.
     initiation sites and some secondary
     cracking.

49
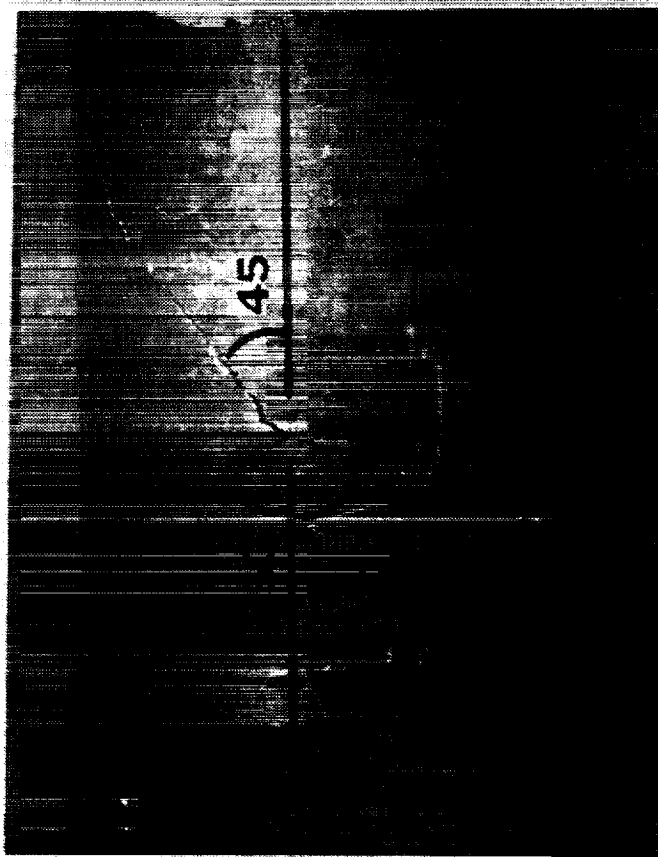
Figure 37   Multiaxial specimen 221 (pure torsion, $\Delta\gamma = 1.362\%$, 538°C (1000°F), life = 2332 cycles). Three cracks are present at 45°, 50° and 70° from the longitudinal specimen axis. Multiple origins were found along specimen outer diameter.
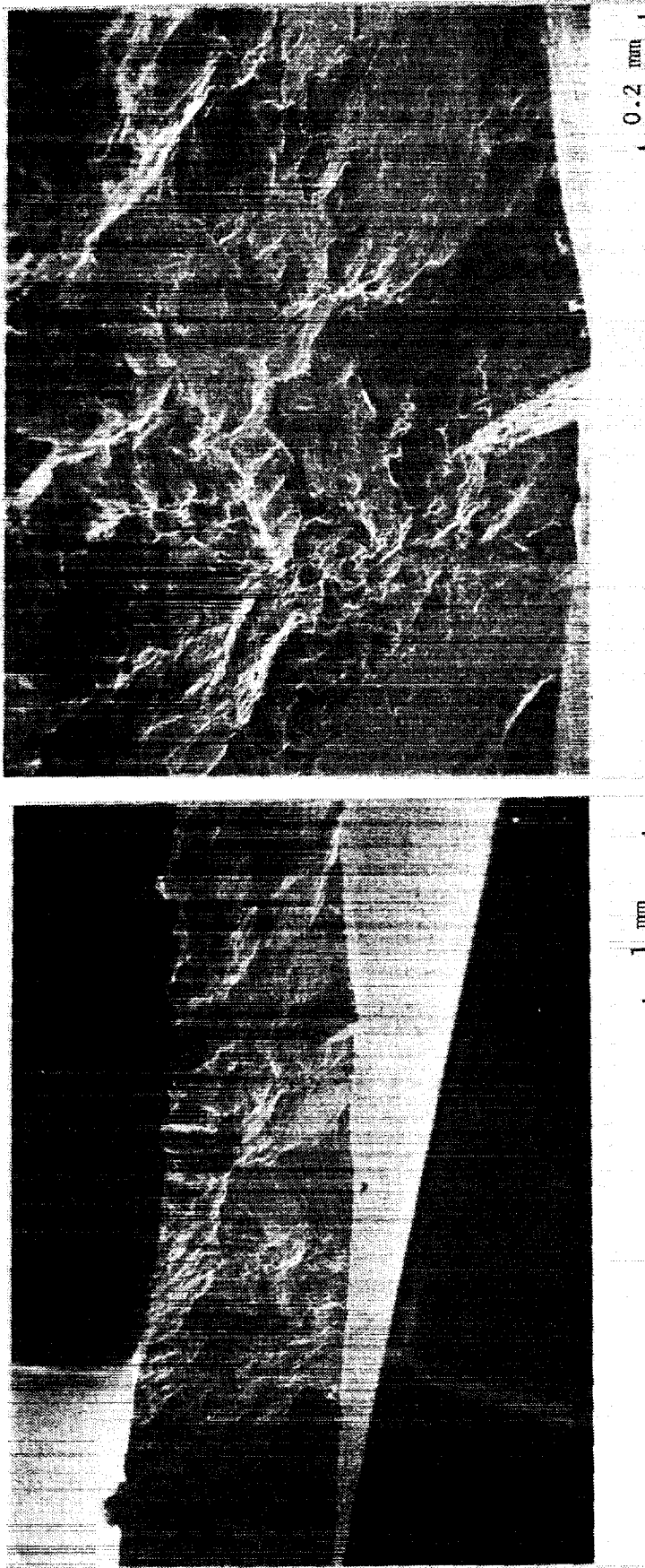
Figure 38   Multiaxial specimen 221 (pure torsion, $\Delta\gamma$ = 1.362%, 538°C (1000°F),
            life = 2332 cycles). Typical initiation site on fracture surface
            45° from longitudinal specimen axis.
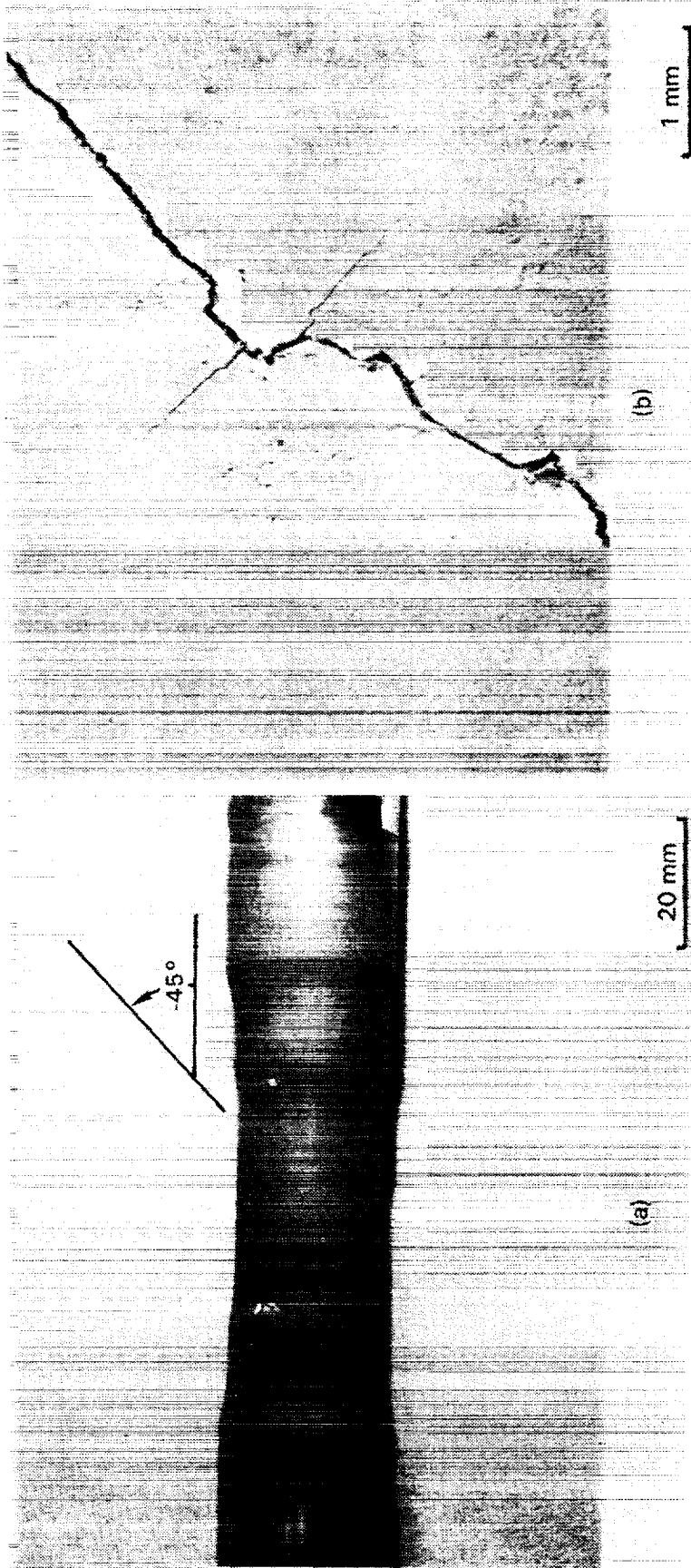
Figure 39   Multiaxial specimen #203. (a) Overall view.   (b) Higher magnification view
of suspected initiation site.

52

The fracture surfaces of specimen 203 were examined optically and by SEM. Figures 40(a) and 40(b) show the optical and SEM micrographs, respectively, of the crack initiation site of Specimen 203. The secondary crack is clearly visible in Figure 40(b). No anomalous features were evident at the initiation site.

Specimen 210 was tested in pure torsion at 871°C (1600°F), 0.804% torsional strain range and 1 CPM. Its initiation life was 5440 cycles but the test was discontinued after 5523 cycles because of the long rig time involved (92 hrs.).

Specimen 219 was tested for a total of 45,500 cycles at 871°C (1600°F) and 10 CPM using a pure torsional strain range of 0.729% . The surface replica taken after cessation of testing showed numerous small cracks (0.035 inch long maximum) oriented at ±45° to the specimen longitudinal axis throughout the gage length. Figure 41 presents micrographs of surface replicas taken during the test that showed the evolution of the longest crack. Figure 42 shows crack growth data based on crack surface length measurements from these replicas versus cyclic life. It can be seen that a small crack developed prior to 10,000 cycles but grew very slowly and did not reach the initiation size of 30 mils until 40,000 cycles. This behavior differs considerably from the previous torsional test (specimen 203) conducted at a higher strain level in which a dominant crack developed early with few secondary cracks and grew much more rapidly to failure.

Specimen 212 was tested in pure torsion at 871°C (1600°F) at 1.014% torsional strain range, and 10 CPM. Its initiation life was 2337 cycles, and the total test life 3770 cycles. These lives can be compared directly with those from Specimens 203 and 219, which were run at the same conditions but at lower strain ranges.

Comparison of pure torsion and axial loading results show that, on a maximum normal strain range basis, the pure torsion lives were essentially the same as those obtained using axial loading alone.

The initiation life of pure torsion Specimen 210 can be compared directly with those from Specimens 207 and 213, which were run at the same low frequency but with out-of-phase, tension-torsion conditions. The results from all three tests indicated that, on a maximum normal strain range basis, the slow rate (1 CPM) lives were approximately half those obtained using the fast rate (10 CPM).

4.2.3 Combined In-Phase Tension-Torsion Cycle (Proportional Loading)

4.2.3.1 538°C (1000°F)

Specimen 223 was tested for a total of 6090 cycles at 538°C (1000°F) and 10 CPM using an axial strain range of 0.509% and a torsional strain range of 0.775% in-phase. Its initiation life was 1708 cycles, with 50% tensile load drop occurring at 2880 cycles. Specimen 225 was tested at 1000°F with 0.384% axial strain range, 0.569% torsional strain range, in-phase, and 10 CPM. Its initiation life was 6164 cycles, and the total test life was 11222 cycles. These lives are in good agreement with other in-phase data, in that the in-phase tests tend to show slightly higher lives than tests run at the same total maximum normal strain range but with 90° out-of-phase loading or with axial loading alone.
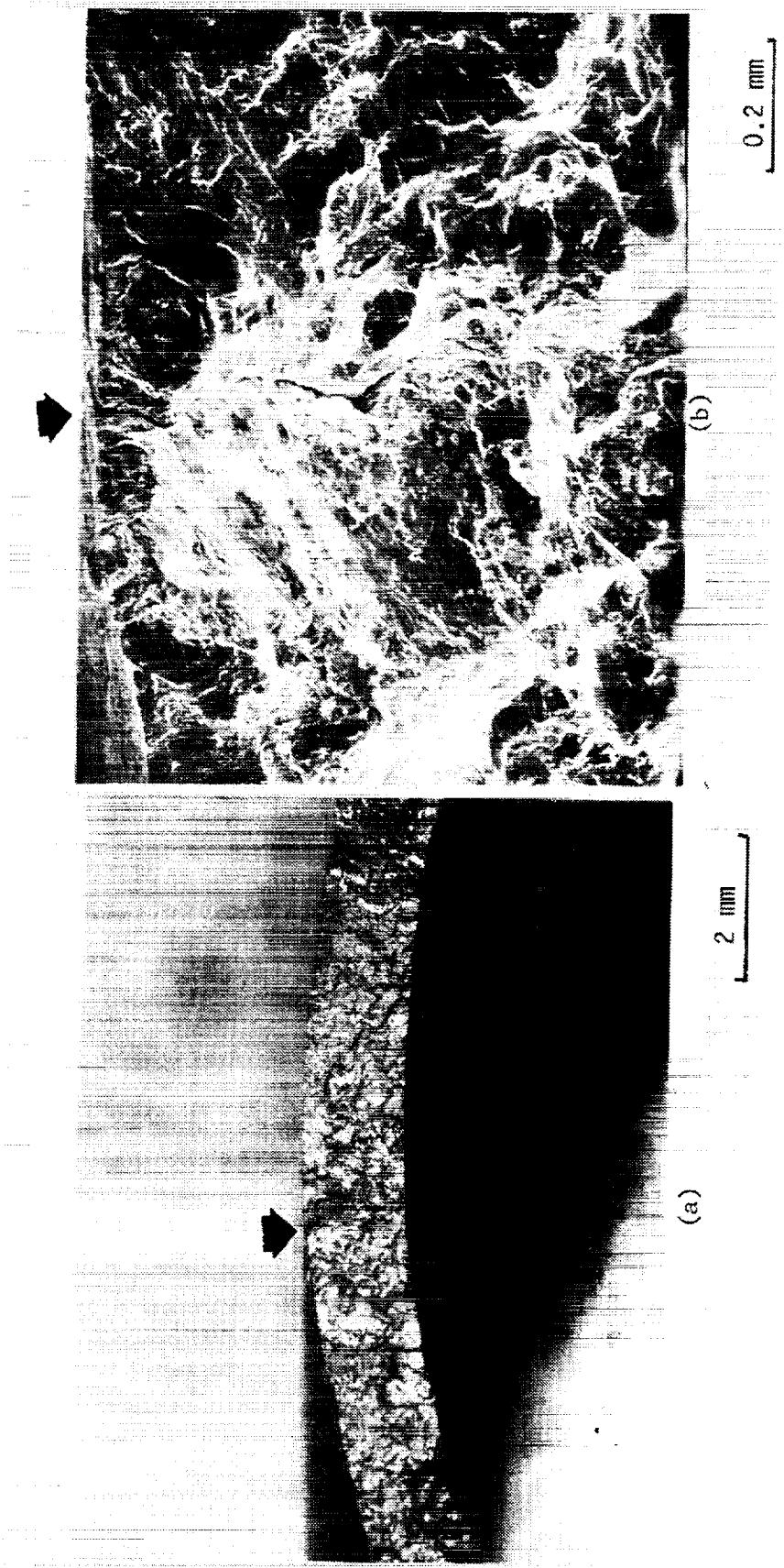
Figure 40   Multiaxial specimen 203 (torsion only).
(a) Optical and (b) SEM micrographs of initiation site showing
secondary crack perpendicular to primary crack.

54

(a)

5 MIL LONG CRACK AT 10,000 CYCLES

(b)

9 MIL LONG CRACK AT 15,539 CYCLES

(c)

12 MIL LONG CRACK AT 18,619 CYCLES

(d)

35 MIL LONG CRACK AT 45,500 CYCLES
(CHROME WAS EVAPORATED ON REPLICA
TO ENHANCE CRACK RELIEF)
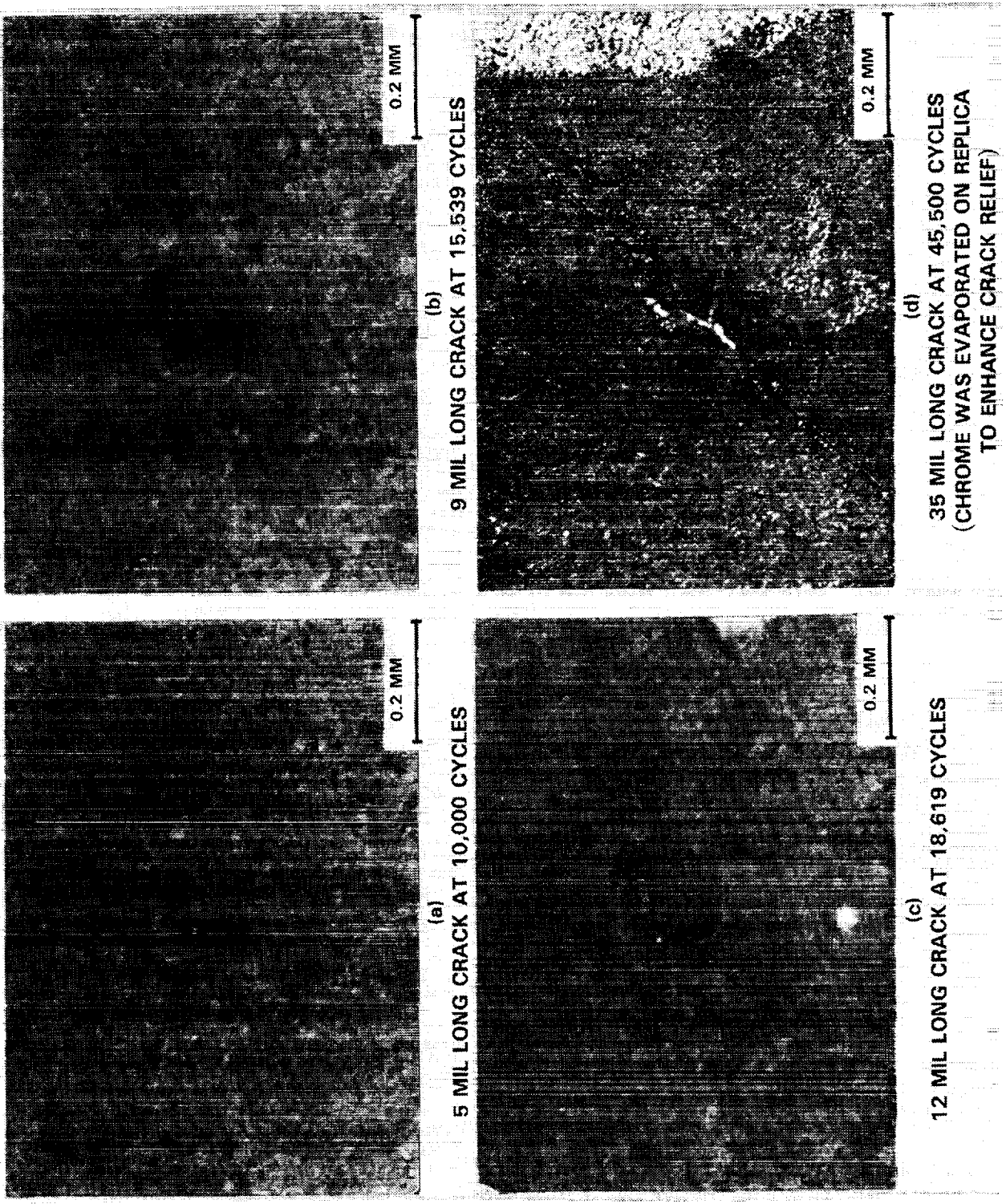
Figure 41   Micrographs of Surface Replicas of Multiaxial Specimen 219 (Torsion Only)

55
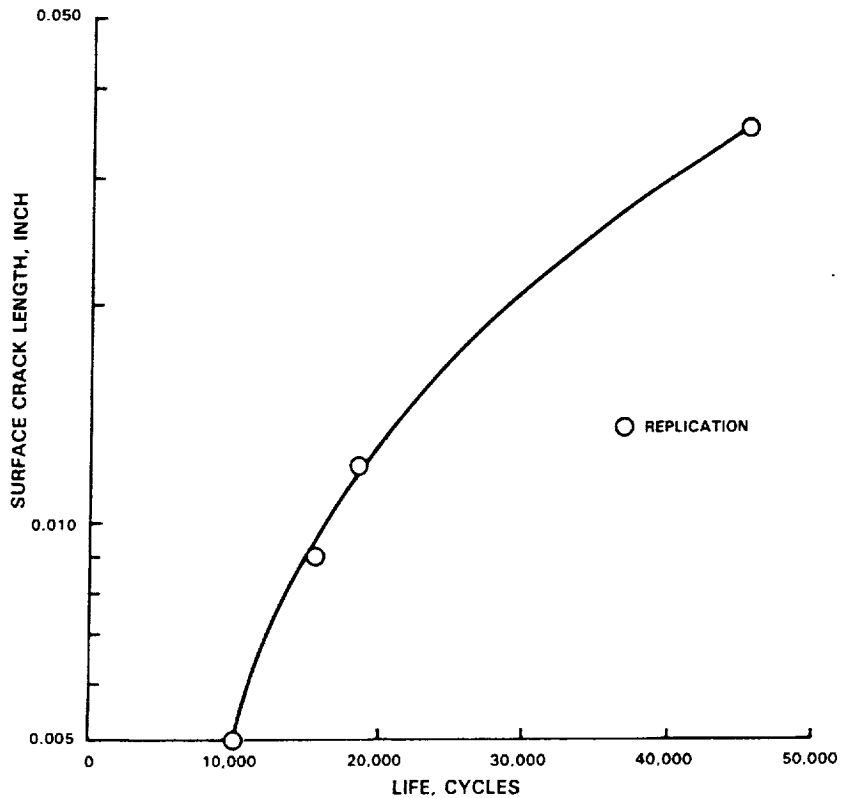
Figure 42.– Crack Growth Data for Multiaxial Specimen 219 (Torsion Only).

4.2.3.2   871°C (1600°F)

Specimen 204 was tested for a total of 1085 cycles at 871°C (1600°F) and 10 CPM with an axial strain range of 0.371% and a torsional strain range of 0.541%. This specimen had an initiation life of 350 cycles, which is very low relative to other specimens. A tantalum (Ta) rich area at the initiation site of this specimen was found during SEM examinations, and in view of the low life of this sample, this area was further analyzed by electron microprobe. A SEM micrograph and Ta x-ray map of this area are shown in Figures 43(a) and 43(b), respectively. The specimen was sectioned longitudinally through the Ta rich area as indicated by the dashed line in Figure 43(a) and the schematic diagram of Figure 44(a). A SEM micrograph of the longitudinal section at the area of the initiation site is shown in Figure 44(b). It can be seen that an oxide layer ranging in thickness from 2×10^{-3}mm to 3×10^{-2}mm was present at the fracture surface as well as at a secondary crack beneath the fracture.

X-ray energy spectroscopy results showed this oxide to be Ta rich. This type of oxide buildup suggested that the crack initiated from dross at location A instead of from a Ta rich MC carbide as was suspected earlier. The presence of dross is believed to be responsible for the unexpected low life of this sample. In order to prevent future low life tests, the remaining untested multiaxial specimens were screened for unacceptable surface and subsurface discontinuities by fluorescent penetrant, visual and x-ray inspections. No such problems were detected by these techniques in any other specimen. Therefore, specimen 204 will not be included in life correlations.

56
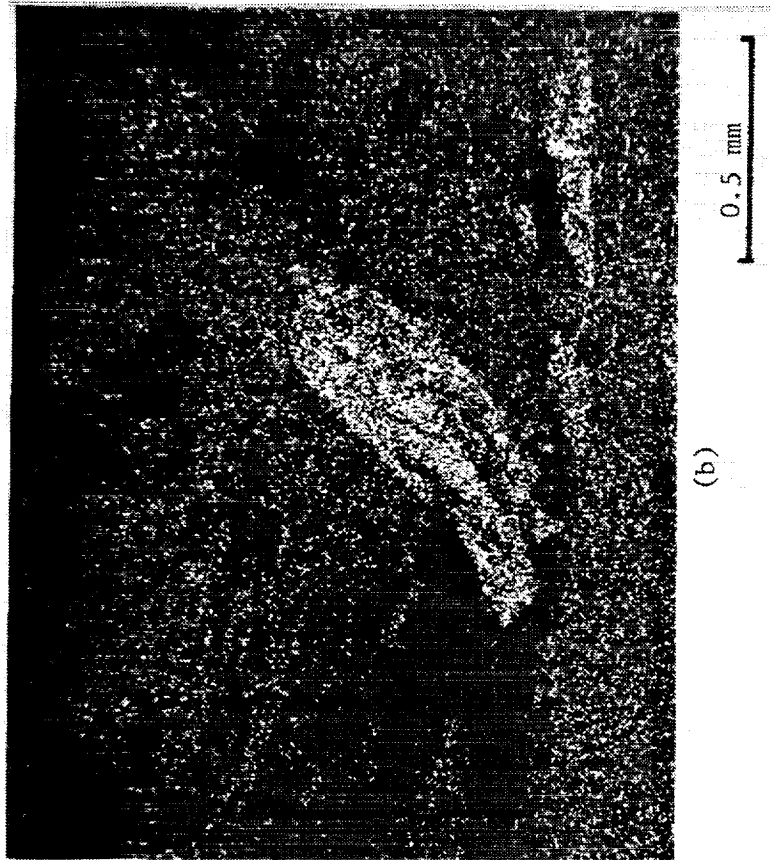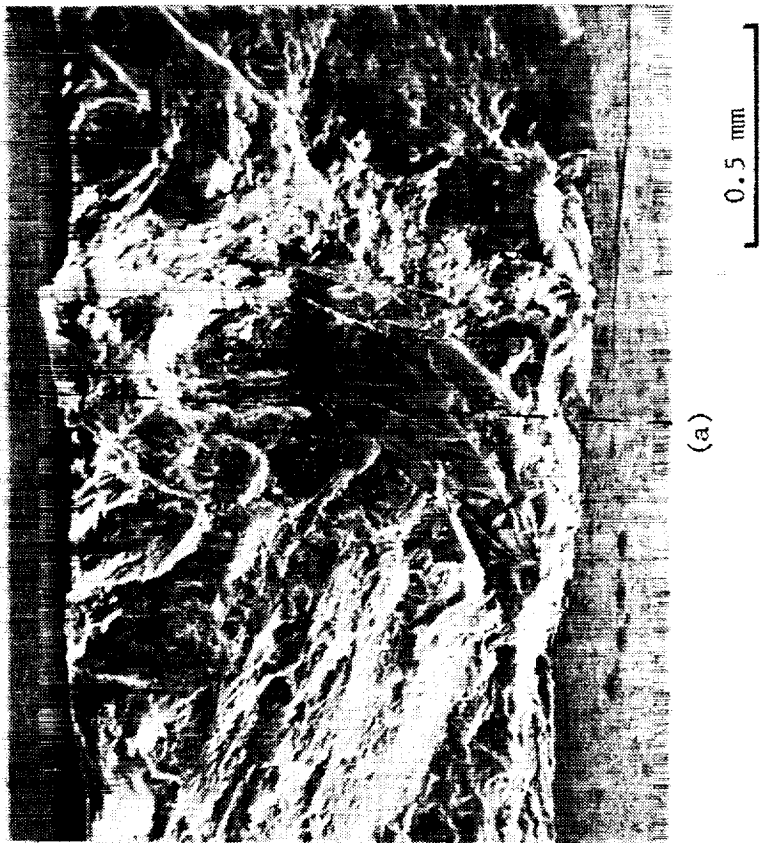
Figure 43   Initiation site of multiaxial specimen 204.

(a)   SEM micrograph showing location where specimen was sectioned longitudinally.
(b)   Ta x-ray map of initiation site.

Figure 44   Characterization of longitudinal section through
             initiation site.

             (a)   Schematic diagram showing orientation of section
                    examined by SEM.

             (b)   SEM micrograph of longitudinal section at initiation
                    site showing oxide buildup on fracture surface as well
                    as in secondary crack.

58
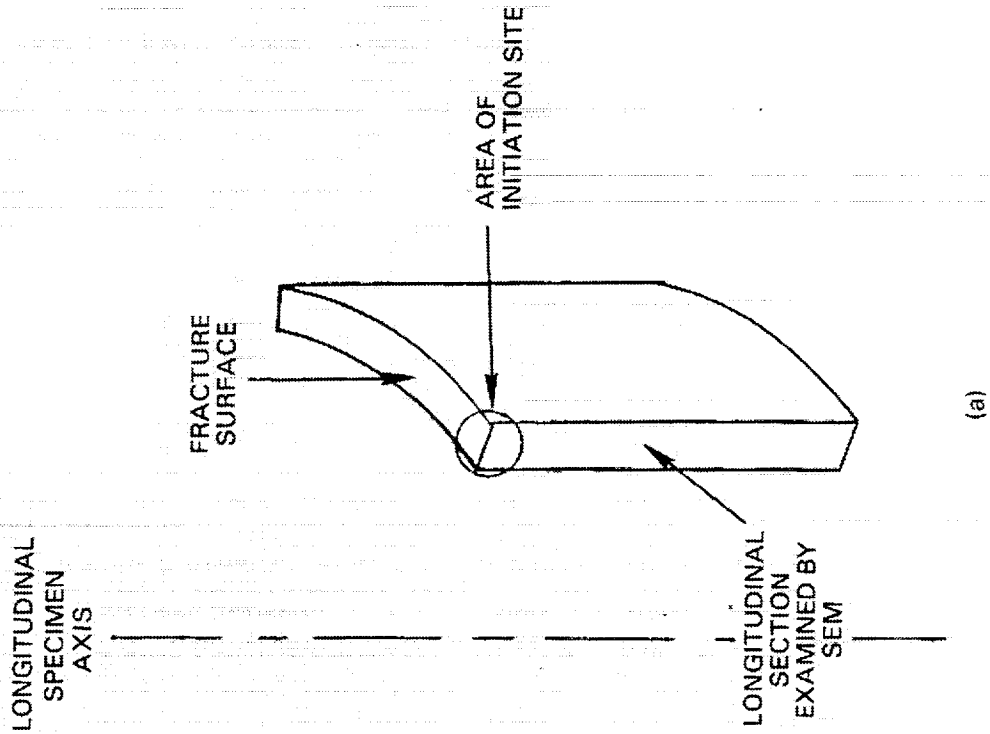
Specimen 226 was tested for a total of 9653 cycles at 871°C (1600°F) and 10 CPM using an axial strain range of 0.355% and a torsional strain range of 0.544% applied in-phase. This specimen was subjected to the same conditions used on specimen 204, whose life was severely limited by dross. The crack initiation life of 5811 cycles was much greater (16X) than that of the prior test confirming the deleterious effect of the dross. In both specimens the crack was oriented at 65° to the longitudinal axis which corresponded to the maximum normal strain plane. However, the life of specimen 226 is somewhat higher than expected based on the normal strain correlation.

Specimen 218 was tested for a total of 9801 cycles at 871°C (1600°F) and 10 CPM using an axial strain range of 0.291% and a torsional strain range of 0.439% in-phase. No surface replication was performed on this specimen; however, based on crack growth data from previously tested specimens, the crack initiation life was estimated at 6615 cycles. Optical and SEM examinations of specimen 218 showed this specimen had one crack at an angle of 65° from the longitudinal specimen axis, as indicated in Figure 45(a). The optical and SEM micrographs of Figure 45(b) and 45(c) show that there was an initiation site at the midwall of the sample as well as another possible initiation site at the specimen I.D. To determine the cause for this midwall initiation, further SEM examinations using x-ray mapping were made. Figure 46(a) is a conventional SEM image of the midwall initiation site, and Figure 46(b) is its associated x-ray map for tantalum (Ta). The Ta rich area is believed to indicate the presence of dross which may be responsible for the midwall initiation. Further work was undertaken to characterize the size of the dross; however, this initial observation indicated that the dross in Specimen 218 was probably much smaller than the dross found in specimen 204. Because of this dross related initiation, the life of specimen 218 will not be included in life prediction correlations.

Specimen 228 was tested at 871°C (1600°F), 0.307% axial strain, 0.457% torsional strain, in-phase, and 1 CPM. The test was terminated at 39,467 cycles, and its initiation life was estimated as 56000 cycles. These conditions duplicate those used for specimen 218, which cracked very early (6615 cycles initiation life) from Ta-rich dross in the middle of the wall of the gage section. Since specimen 218 had lives which were about one-eighth those from specimen 228, earlier testing on specimen 218 was discounted. As noted above, the results of this test show that there is a trend for the in-phase tests to produce lives which are slightly higher than those from tests run at the same total maximum normal strain range but with 90° out-of-phase loading or with axial loading alone.

(b)

1 mm
20X

(a)

5 mm
4X

(c)

0.5 mm
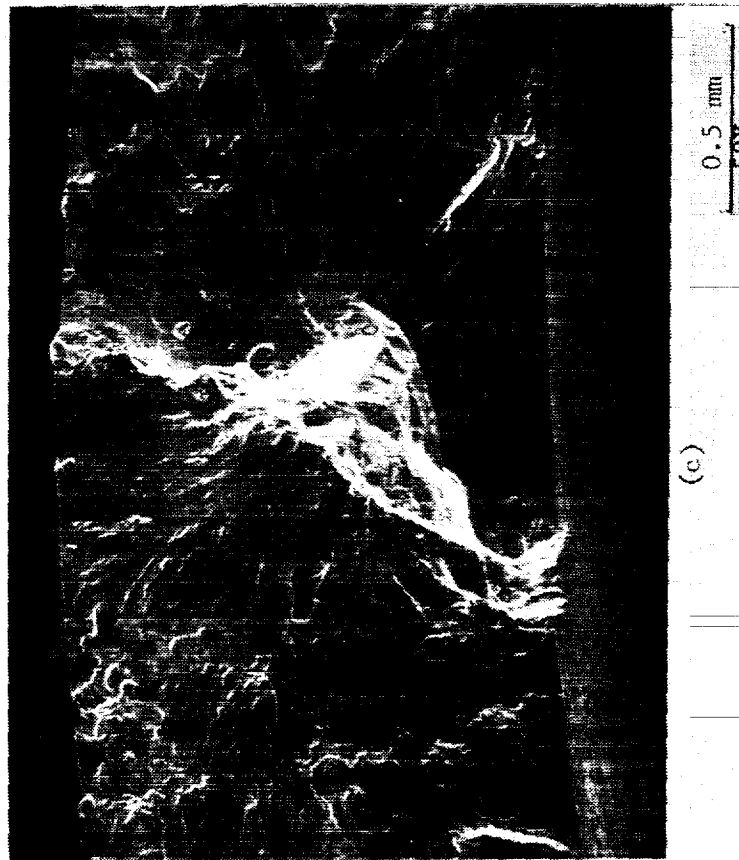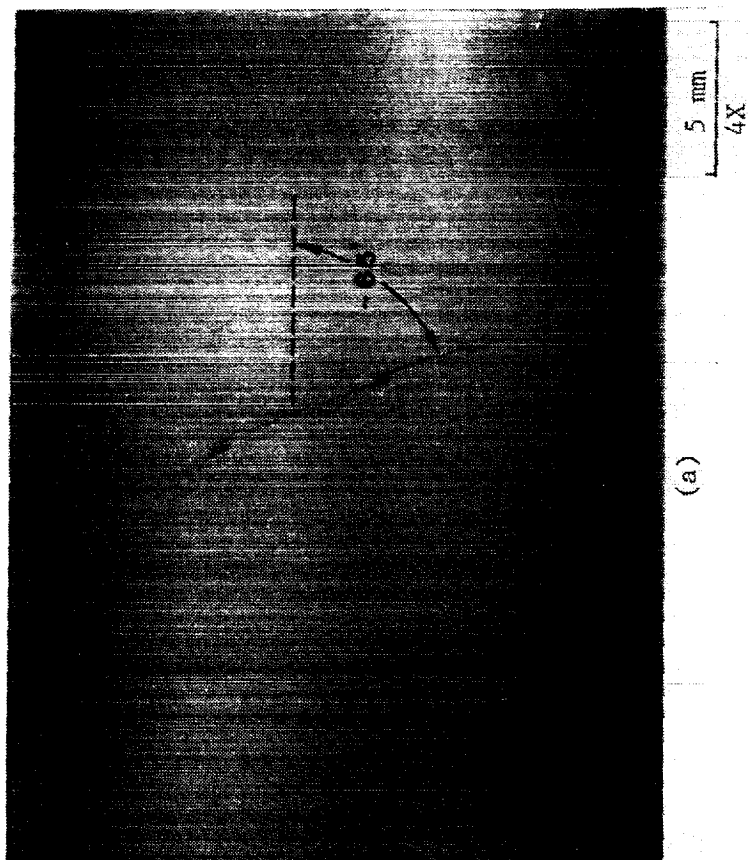
Figure 45

Multiaxial Specimen #218 (871°C (1600°F), Δε = 0.291%, Δγ = 0.439%, in-phase, 10cpm, initiation life = 6615 cycles, total test life = 9801 cycles).

(a) Optical micrograph showing main crack ∣ 65° from longitudinal specimen axis.

(b) and (c) Optical and SEM micrographs of initiation site.

(a)

$\dfrac{50 \ \mu m}{350X}$

(b)

$\dfrac{50 \ \mu m}{350X}$
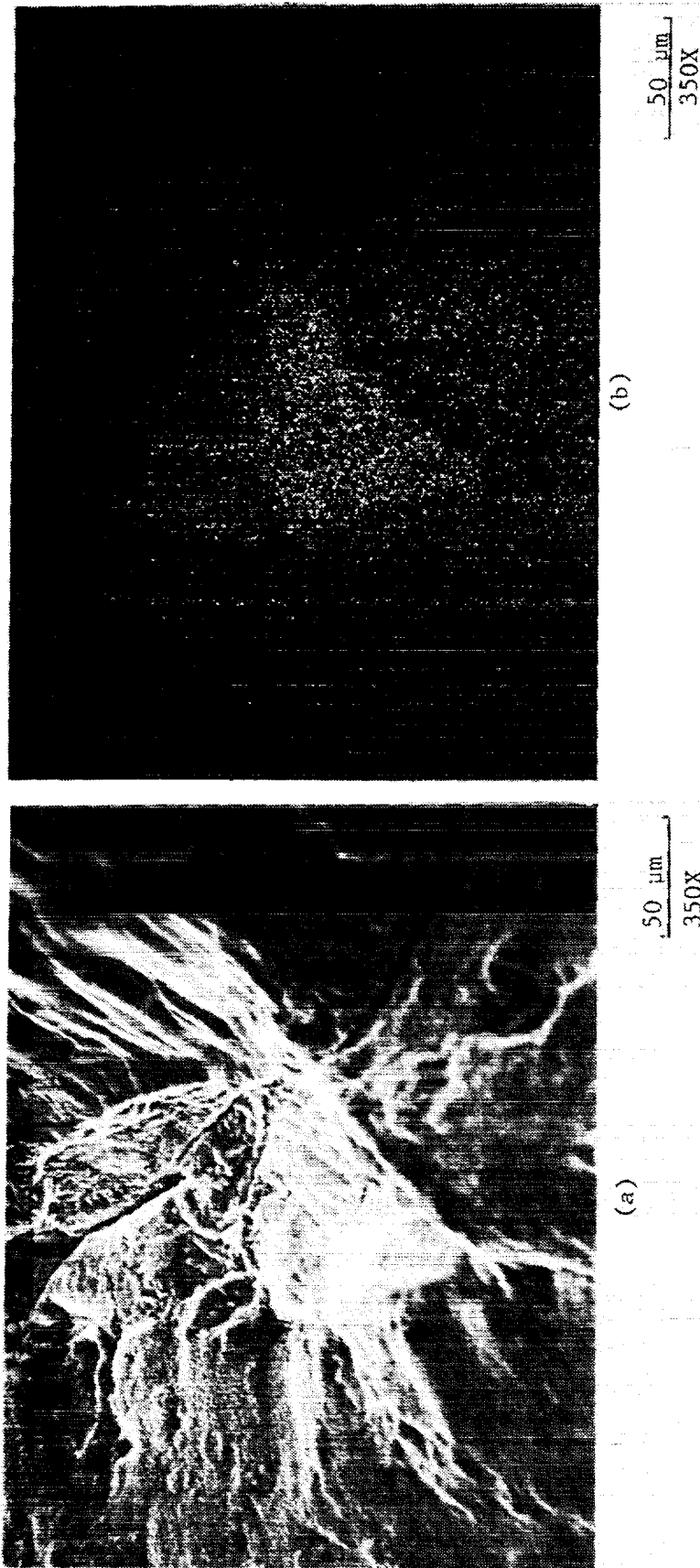
Figure 46   Multiaxial specimen #218 (538°C (1600°F), $\Delta\varepsilon$ = 0.291%, $\Delta\gamma$ = 0.439%, in-phase, 10cpm, initiation life = 6615 cycles, total test life = 9801 cycles).

(a) Conventional SEM micrograph (secondary electron image) of midwall initiation site.

(b) Ta x-ray map of same area as (a) showing possible dross.

4.2.4 Out-of-Phase Tension-Torsion (Non-Proportional)

4.2.4.1 538°C (1000°F)

Specimen 202 was tested for a total of 543 cycles at 538°C (1000°F) and 10 CPM using an axial strain range of 0.680% and a torsional strain range of 1.027% applied 90° out-of-phase. The crack initiation life was 240 cycles which was only 1/8 of the initiation life of the specimen (220) tested earlier in pure tension using the same axial strain range. As shown in Figure 47(a), the fracture surface of specimen 202 was overall perpendicular to the longitudinal specimen axis, which corresponded to the maximum normal strain plane, although sections of the crack grew at oblique angles to the specimen axis. The longest such section was near the center of the crack and was at an angle of 45° to the longitudinal specimen axis which corresponded to the maximum shear strain plane. The specimen exhibited O.D. initiation sites which originated from porosity. Figure 47(b) is a SEM micrograph of a typical initiation site showing porosity at the origin. Some of the details of the fracture surface were obscured by rubbing that occurred during testing. Comparison of the life of this test with those from similar tests indicates, however, that this test is anomalous. It will therefore not be included in life prediction correlations.

Specimen 214 was tested for a total of 9544 cycles at 538°C (1000°F) and 10 CPM using an axial strain range of 0.503% and a torsional strain range of 0.758%, applied 90° out-of-phase. The crack initiation life of 5210 cycles is 4X greater than the 871°C (1600°F) test of specimen 216 using the same strain levels. The initiation life was also consistent with simple tension and in-phase test results (specimens 201 and 225). Optical and SEM observations of specimen 214 are shown in Figure 48. As shown in Figure 48(a) this specimen had one main crack that undulated somewhat but was overall perpendicular to the longitudinal specimen axis. The optical micrograph of Figure 48(b) and the SEM micrograph of Figure 48(c) both show the occurrence of extensive rubbing of opposing fracture surface features. This rubbing action prevented observation of any initiation sites by SEM.

Specimen 206 was tested at 538°C (1000°F), 0.692% axial strain, 1.027% torsional strain range, 90° phase angle, and 10 CPM. Its initiation life was 1417 cycles, and the total test life was 2544 cycles. These conditions duplicated those used for Specimen 202, which cracked very early from a region of porosity in the gage section. Since specimen 202 had lives which were about one-sixth those of Specimen 206, the earlier test was discounted. Results of Specimen 206 also compared favorably with those from specimen 214, which was run at the same conditions but with a lower strain range. It should be noted that the lives of both of these specimens are close to those of other tests run in tension alone (specimens 220 and 201) when compared on a maximum normal strain basis.
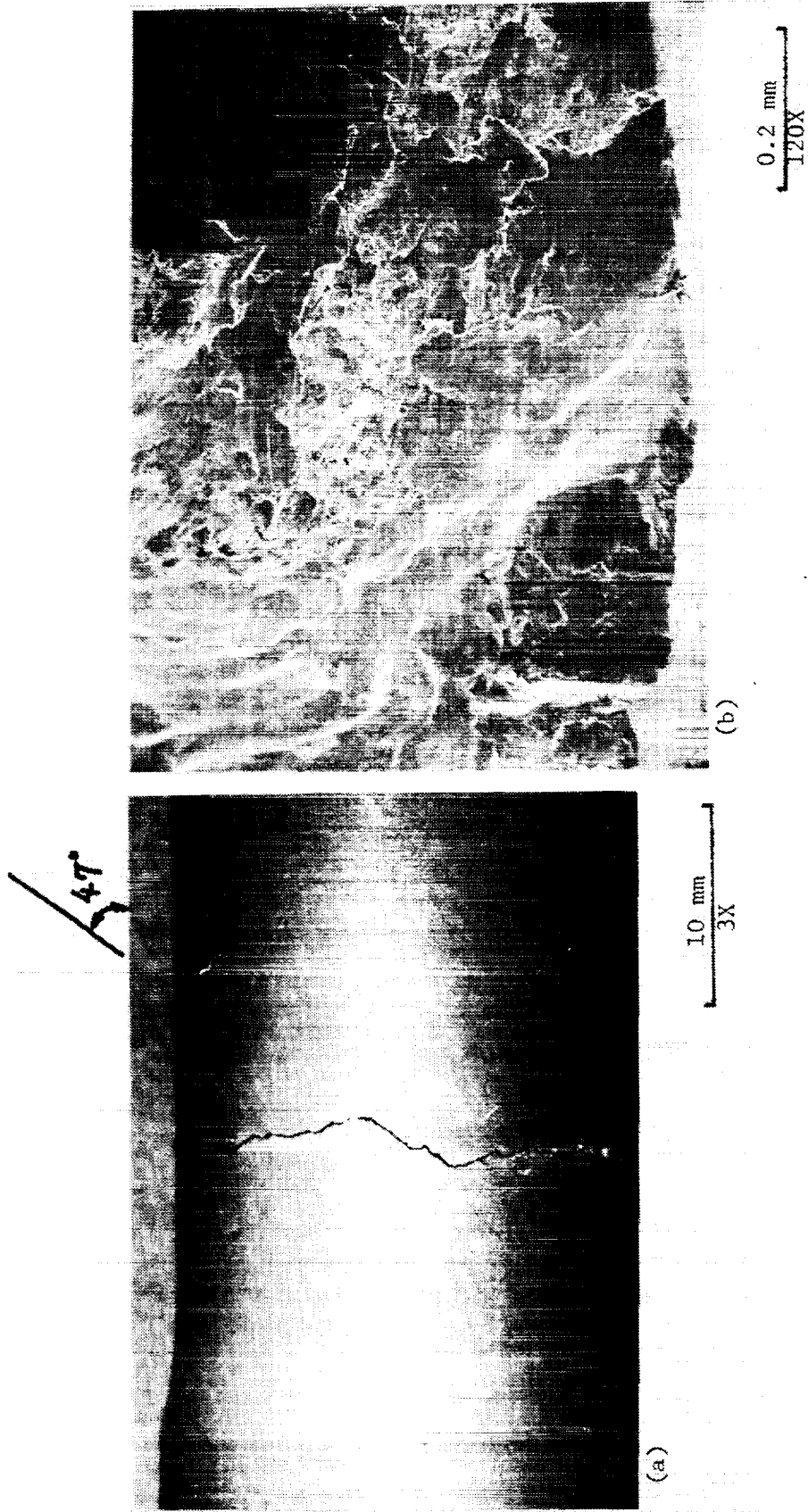
Figure 47   Multiaxial specimen 202 (538°C (1000°F), $\Delta\varepsilon_x$ = 0.680%, $\Delta\gamma$ = 1.027%, out of phase, 10 cpm, initiation life = 240 cycles).

(a) Optical micrograph showing crack overall perpendicular to longitudinal specimen axis. Sections of crack are inclined to specimen axis.

(b) SEM of typical initiation site showing porosity at origin.
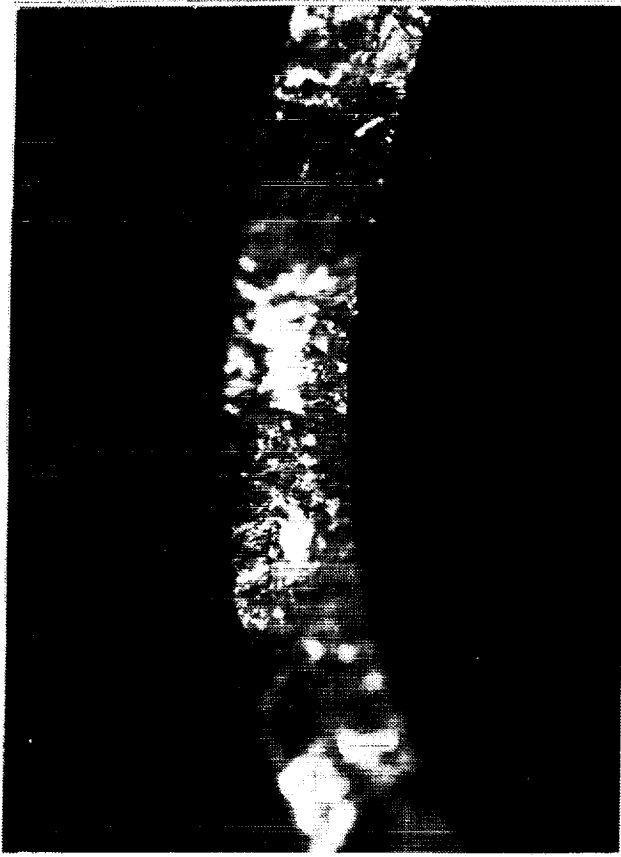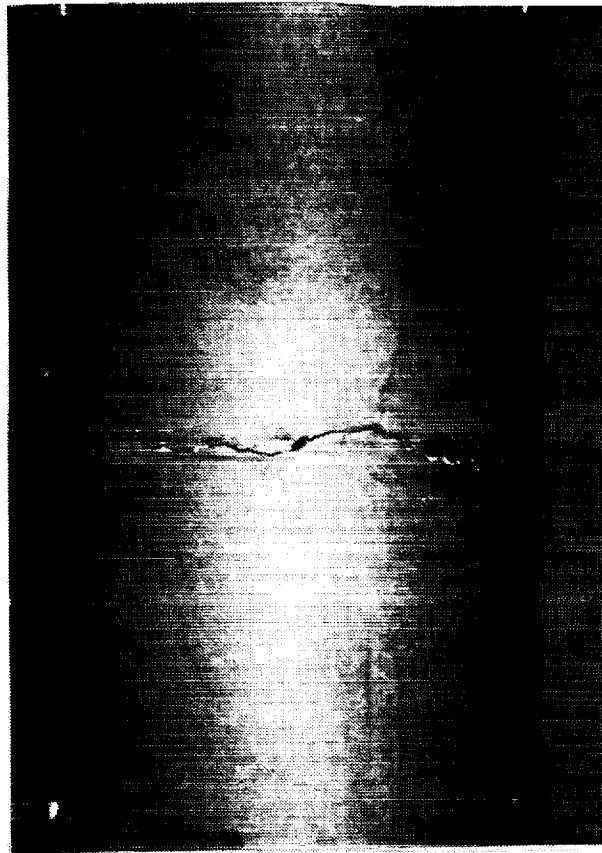
Figure 48

Multiaxial specimen 214 (538°C (1000°F), $\Delta\varepsilon = \pm 0.250\%$, $\Delta\gamma = \pm 0.375\%$, 10 cpm, 90° out of phase, initiation life = 5,210 cycles, total test life = 9,544 cycles).

(a) Optical micrograph of crack.

(b) and (c) Optical and SEM micrographs of fracture surface showing evidence of extensive rubbing. It was not possible to examine initiation sites on this sample.

Specimen 211 was tested at 538°C (1000°F), 0.504% axial strain range, 0.748% torsional strain range, 90° phase angle, and 1 CPM. Its initiation life was 1454 cycles, and the total test life was 3111 cycles. These lives can be compared directly with those from Specimen 214, which was run at the same conditions but at a 10 CPM rate. That test showed an initiation life of 5210 cycles, and it can be seen that the slow rate life is significantly lower (one-fourth). This contradicts findings from the uniaxial fatigue testing in which no rate effect was seen at this temperature.

The test conditions for specimen 215 were exactly the same as those for specimen 206 except that the frequency was 1 CPM instead of 10 CPM. Specimen 215 was tested for a total of 918 cycles at 538°C (1000°F) and 1 CPM using an axial strain range of 0.681% and a torsional strain range of 1.024% applied 90° out-of-phase. The initiation life of 486 cycles was approximately one-third the initiation life of specimen 206, once again demonstrating a frequency effect of reduced life for the lower frequency even at 538°C (1000°F).

Optical and SEM observations of specimen 215 are shown in Figure 49. This specimen had three crack segments approximately 53°, 65°, and 87° from the longitudinal specimen axis as shown in Figure 49(a). The optical micrograph of Figure 49(b) shows the occurrence of extensive rubbing of opposing fracture surface features. This rubbing action is also evident in the SEM micrograph of Figure 49(c) which prevented examination of the initiation site(s). The above observations indicated that extensive rubbing of opposing fracture surface features occurred for tests 90° out-of-phase and that examination by SEM of specimens tested under these conditions may not provide useful information.

4.2.4.2 871°C (1600°F)

Specimen 205 was tested for a total of 16,504 cycles at 871°C (1600°F) and 10 CPM using an axial strain range of 0.294% and a torsional strain range of 0.443%, applied 90° out-of-phase. The crack initiation life of 11,434 cycles appeared to be low considering the low strain ranges used for this test. Detailed metallographic investigations were therefore carried out on this specimen.

Optical and SEM observations of Specimen 205 are shown in Figure 50. This specimen had one main crack 81° from the longitudinal specimen axis, as shown in Figure 50(a). Optical examination of the fracture surface revealed that extensive rubbing of opposing fracture surface features occurred during testing which obscured the fracture surface features as shown in Figure 50(b). A SEM micrograph showing oxide buildup on the fracture surface is shown in Figure 50(c).

(b)

2 mm
10X

(a)

10 mm
3.2X

(c)

50 μm
350X
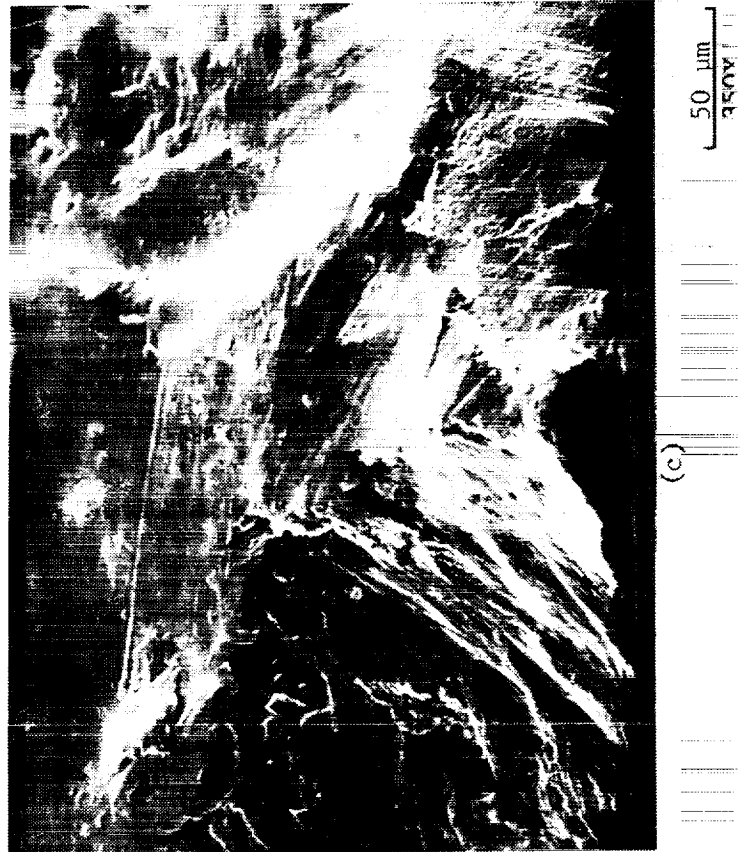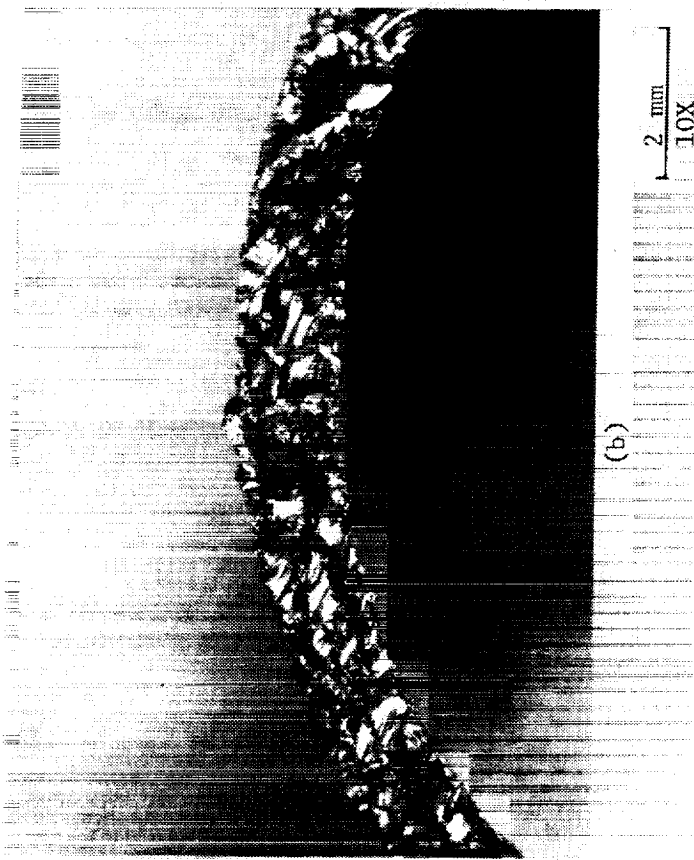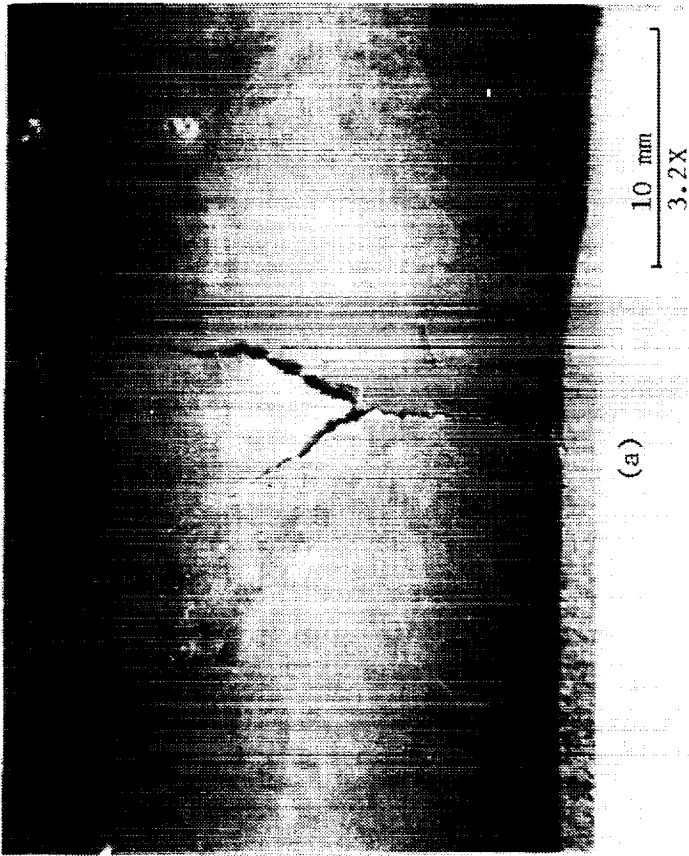
Figure 49

Multiaxial specimen 215 (538°C (1000°F),
$\Delta\varepsilon = 0.681\%$, $\Delta\gamma = 1.024\%$, 1 cpm, 90° out
of phase, initiation life = 486 cycles,
total test life = 918 cycles).

(a) Optical micrograph showing crack segments.

(b) and (c) Optical and SEM micrographs of
        fracture surface showing evidence
        of extensive rubbing. It was not
        possible to examine initiation sites
        on this sample.
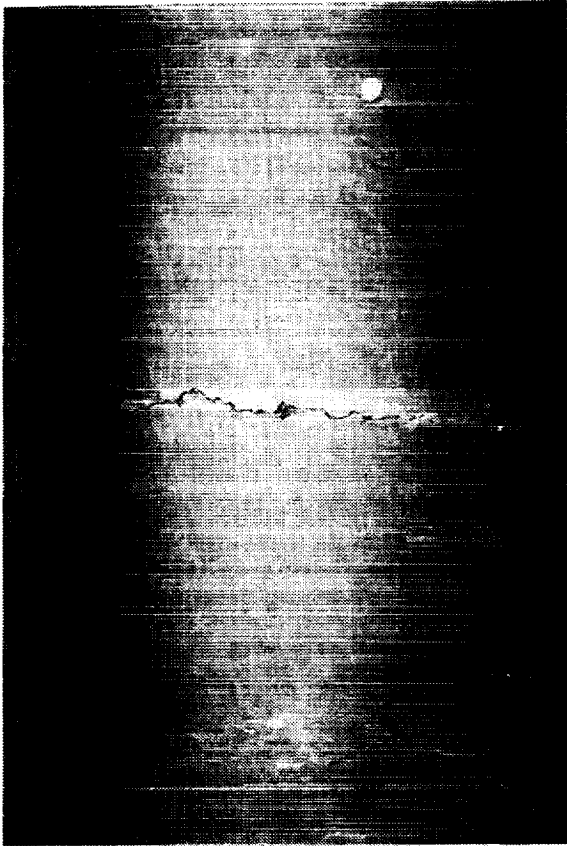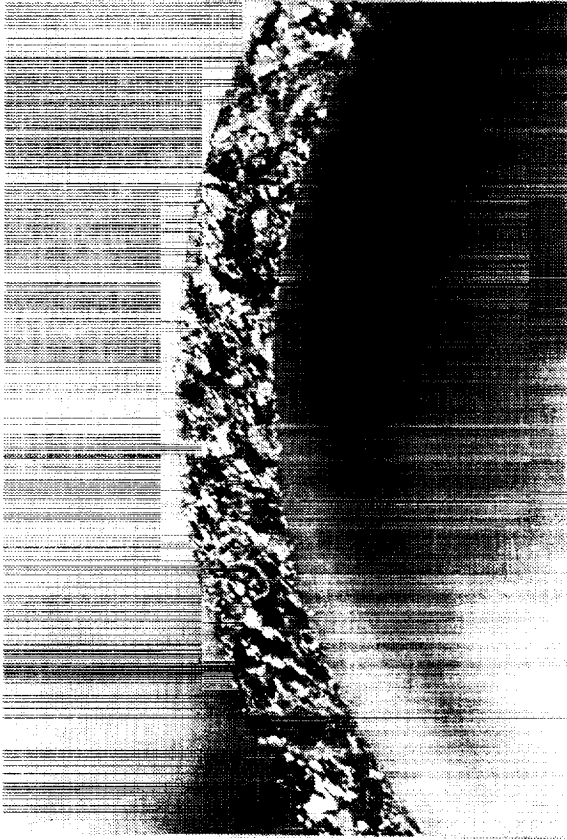
Figure 50

Multiaxial specimen 205 (871°C (1600°F),
$\Delta\epsilon = 0.294\%$, $\Delta\gamma = 0.443\%$, 10 cpm, 90° out
of phase, initiation life = 11,434 cycles,
total test life = 16,504 cycles).

(a) Optical micrograph of crack.

(b) Optical micrograph of fracture surface
    showing evidence of extensive rubbing.

(c) SEM micrograph of fracture surface showing
    area of oxide buildup.

67

During previous examinations numerous secondary cracks were noted below the major crack along specimen 205. One of these areas was spot polished and then etched in order to determine the crack path. The optical micrograph of Figure 51 shows that the secondary cracks grew transgranularly. SEM examination of the specimen revealed areas on the side of the specimen that have a rumpled appearance such as that shown in the area of the secondary crack in Figure 52 which may have been caused by the presence of dross that could affect the life of the test. The specimen was examined by microprobe which indicated that the rumpled appearance resulted from mechanical deformation of the oxide layer on the surface of the specimen. As shown in Figure 53, the rumpling effect was seen only near the fracture surface which indicated that contact of the opposing fracture surfaces resulting from out-of-phase loading deformed the side surface of the specimen near the fracture surface and caused the rumpled appearance of the oxide. This same mechanism is thought to be responsible for the rumpling around the secondary crack shown in Figure 52. Porosity was also noted as shown in Figure 54(a), which shows porosity in evidence on the side of the specimen in the vicinity of the fracture surface and Figure 54(b) which shows porosity on the fracture surface itself. The extent to which this porosity may have influenced the life of the test is difficult to determine due to the extensive rubbing of the fracture surfaces which eliminated virtually all fracture surface details. However, as with specimen 202, comparison of the life of specimen 205 with those of other tests (such as specimen 227 discussed later) shows that it is much too low. It will therefore not be included in life model correlations.

Specimen 227 was tested using a new extensometer and was run at 871°C (1600°F), 0.402% axial strain range, 0.606% torsional strain range, 90° phase angle, and 10 CPM. Its initiation life was 13,794 cycles. This life is actually longer than that of specimen 222, which was run at the same conditions, except without the torsional strain. Also, it is longer than the life of specimen 205 which was run at similar conditions but with much lower strain ranges.

Specimen 207 was tested for 834 cycles at 871°C (1600°F) and 1 CPM, using an axial strain range of 0.500% and a torsional strain range of 0.756% applied 90° out-of-phase. The crack initiation life of 327 cycles is about one-fourth of the life of specimen 216, which was tested at the same conditions except at a faster rate (10 CPM). This frequency effect was considerably greater than that noted in baseline tests at the same axial test conditions. In those tests the initiation lives of specimens tested at 1 CPM were still about 75% of the lives of those tested at 10 CPM.

Specimen No. 216 was tested for a total of 1973 cycles at 871°C (1600°F) and 10 CPM using an axial strain range of 0.494% and torsional strain range of 0.742% with the strains applied 90° out-of-phase. Comparison of the resulting initiation life of 1313 cycles with that for the uniaxial test at the same tensile strain range (1107 cycles) indicated that there was no detrimental effect due to the non-proportional loading path of this test.

0.5 mm
45X
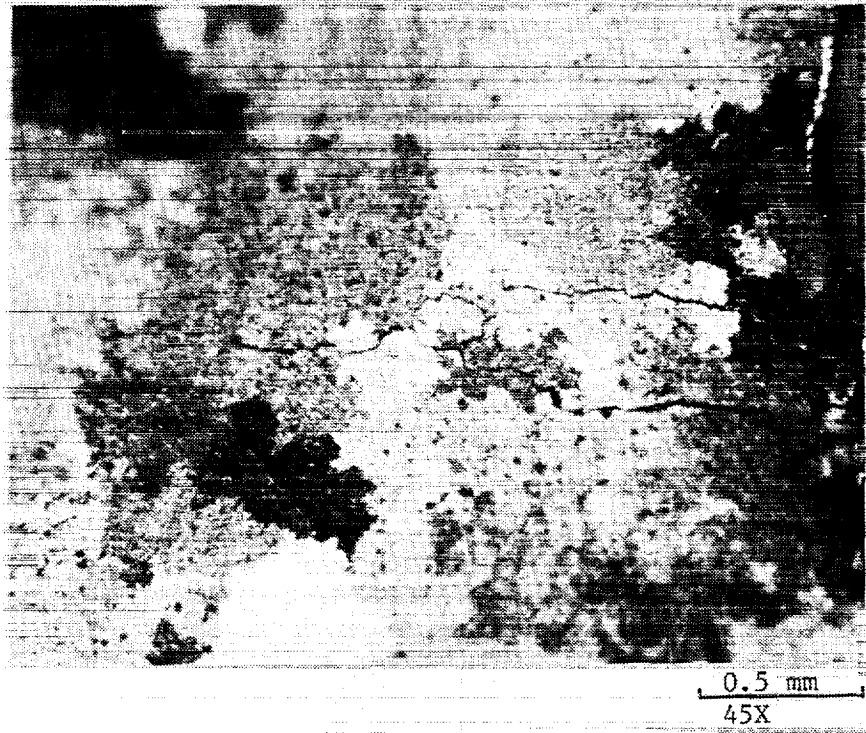
Figure 51.– Secondary Cracks on Side Surface of Multiaxial Specimen #205 871°C (1600°F), $\Delta\varepsilon$ =0.294%, $\Delta\gamma$ = 0.443%, ϕ = 90°, 10 cpm, Total Test Length = 16504 Cycles). Cracks are growing in a transgranular mode.
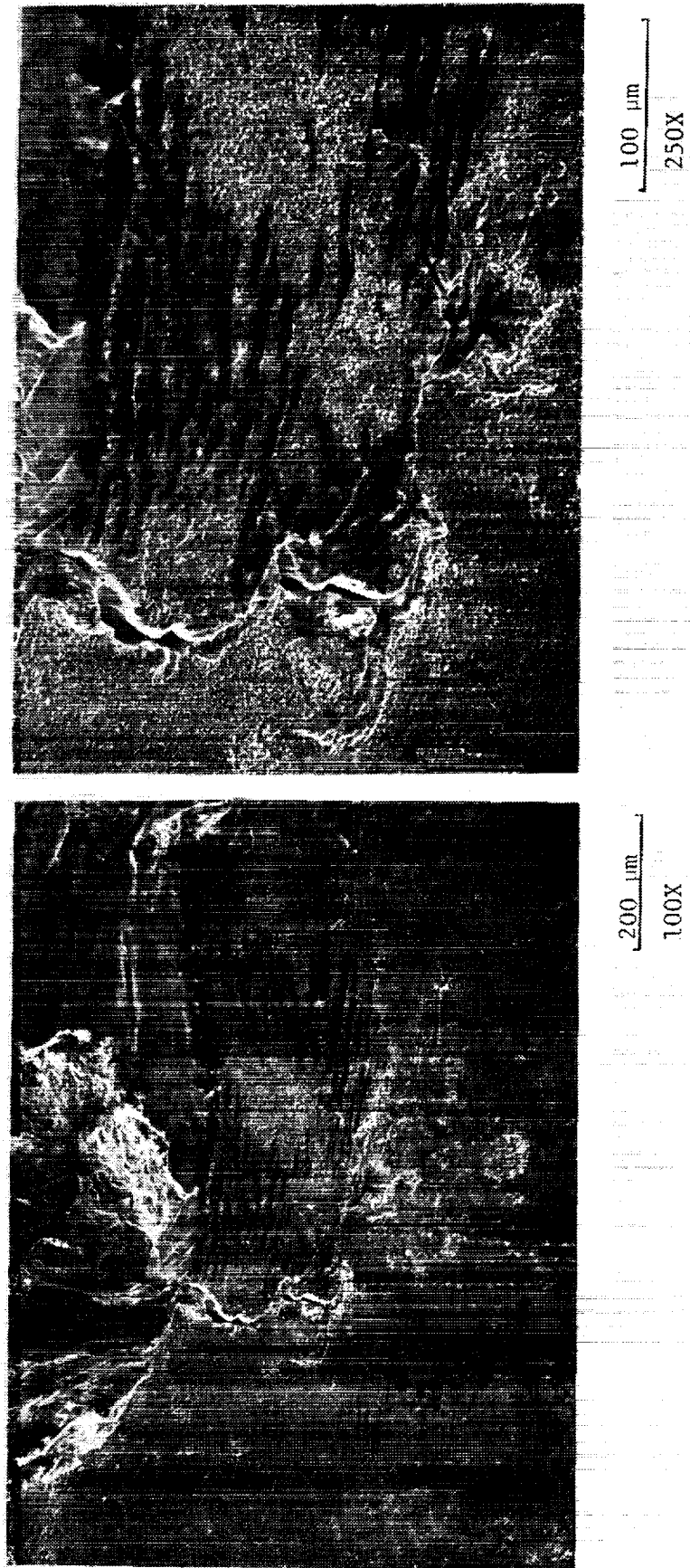
Figure 52 Multiaxial specimen #205 (871°C (1600°F), $\Delta\varepsilon = 0.294\%$, $\Delta\gamma = 0.443\%$, $\phi = 90°$, 10 cpm, total test length = 16504 cycles). SEM micrographs of side of specimen showing rumpled appearance of surface in area of secondary crack.

Figure 53   SEM micrographs of side of multiaxial specimen #205 showing rumpling occurs only in the vicinity of the fracture surface.
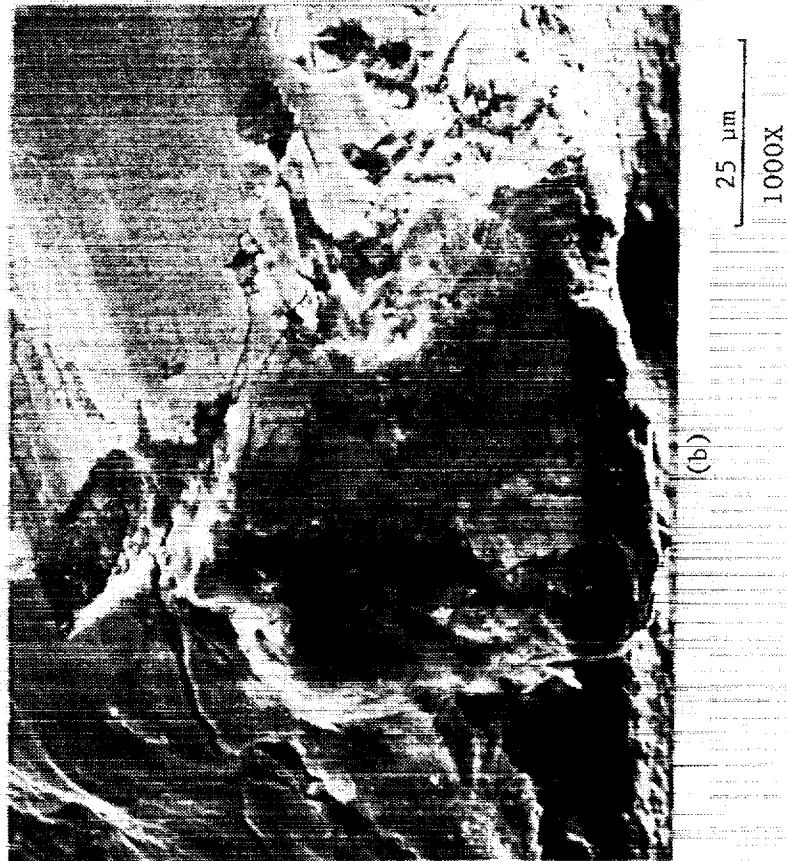
Figure 54   SEM micrographs of multiaxial specimen #205 showing evidence of porosity.

(a)   Porosity found on side of specimen, near fracture surface.

(b)   Porosity found on fracture surface of specimen. Smooth area around porosity is the result of rubbing.

72

A suspected initiation site, shown in Figure 55, was sectioned out for characterization by SEM. Replicas showed that three separate cracks grew simultaneously perpendicular to the longitudinal specimen axis, then linked up by means of crack segments roughly parallel to the specimen axis. Optical micrographs of two adjacent crack segments are shown in Figure 56. The out-of-phase loading caused extensive rubbing of the opposing fracture surfaces which obscured most fracture surface details and therefore no SEM observations were made on this sample.

Specimen 213 was tested at 871°C (1600°F), 0.442% axial strain range, 0.663% torsional strain range, 90° phase angle, and 1 CPM. Its initiation life was 1911 cycles, and the total test life was 4682 cycles. These results agreed with those from specimen 207, since the lives of both specimens were many times lower than those of comparable tests run at 10 CPM (specimens 216 and 227).

4.2.5 Dislocation Observations in Multiaxial Specimens

TEM examinations were made of four multiaxial specimens to document the dislocation structures that arise during various types of loading conditions. These examinations were usually performed on foils taken from longitudinal sections. Specimens tested in pure tension at 871°C (1600°F), pure torsion at 538°C and 871°C (1000°F and 1600°F), and tension-torsion 90° out-of-phase at 871°C (1600°F) were chosen for study.

The dislocation structure of specimen 217 [871°C (1600°F)], axial strain = ±0.250%, pure tension, 10CPM) after 2442 cycles was examined using TEM foils taken from both longitudinal and transverse sections of the gage section. This was done in order to determine if there was an orientation effect on the appearance of the dislocation structure. The dislocation structure of specimen 217 as seen in longitudinal and transverse foils is shown in Figures 57 and 58, respectively. The dislocation density appears higher in the transverse section than in the longitudinal section, since the transverse foil could be taken closer to the fracture surface than was possible for the longitudinal foil (0.10 in. vs. 0.25 in.). However, other than the dislocation density, no significant difference was found between the two orientations.

The typical dislocation structure of specimen 221 [538°C (1000°F), torsional strain = ±0.675%, pure torsion 10 CPM] after 2332 cycles is shown in Figure 59. Extensive dislocation tangles were present in the matrix surrounding the γ' particles and straight dislocation segments were seen cutting through γ' particles. This structure was markedly different from that observed in a pure torsional specimen tested at 871°C (1600°F) (specimen 203, torsional strain = ±0.404%, 10CPM) which had networks of short dislocation segments, roughly parallel to one another, enveloping γ' particles at the γ/γ' interface with the γ' particles themselves being relatively free of dislocations as shown in Figure 60. The difference in dislocation structure in specimens tested at 538°C (1000°F) and 871°C (1600°F) is an apparent result of the inability of the dislocations to cross slip at the lower temperature. This caused the dislocations to pile up at the γ/γ' interface and to also cut through γ' particles as stresses built up.

LONGITUDINAL
SPECIMEN AXIS
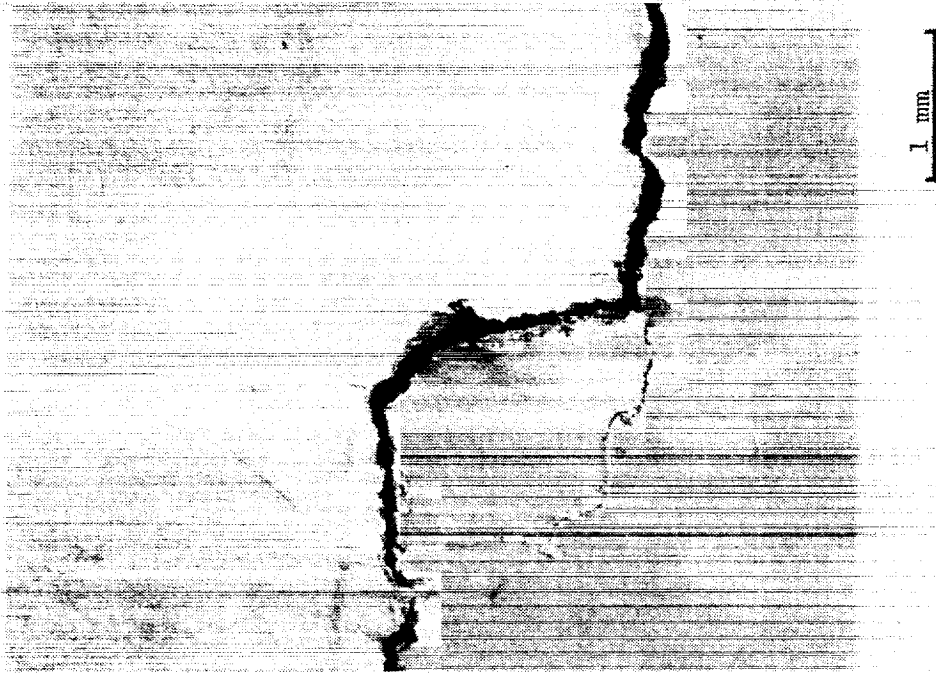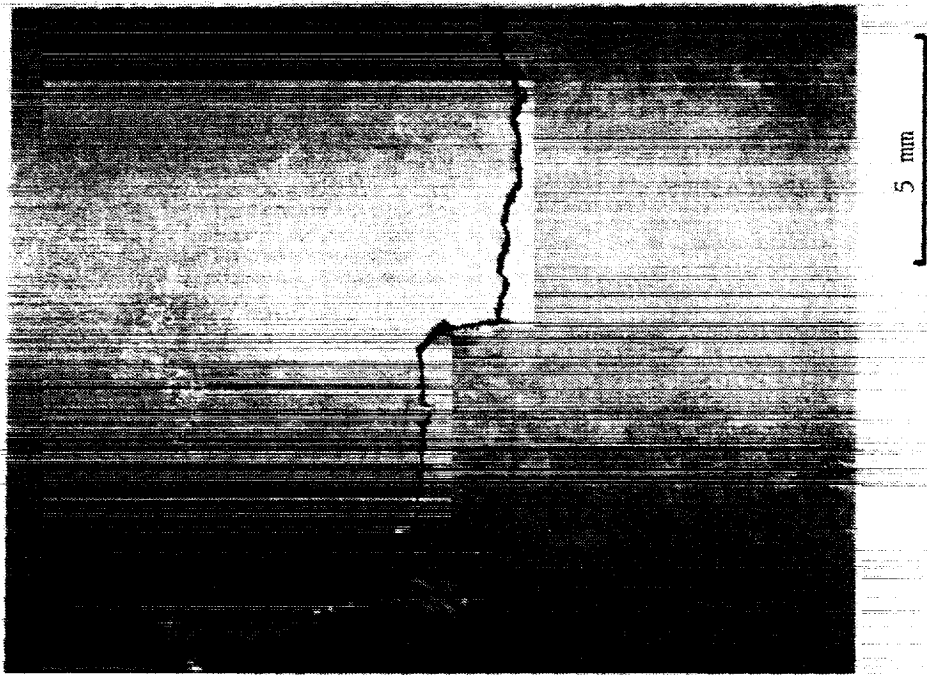
Figure 55   Multiaxial specimen 216 (0.494% axial strain range, 0.742% torsional strain range, out of phase ∅ = 90°, 1973 cycles), suspected initiation site.
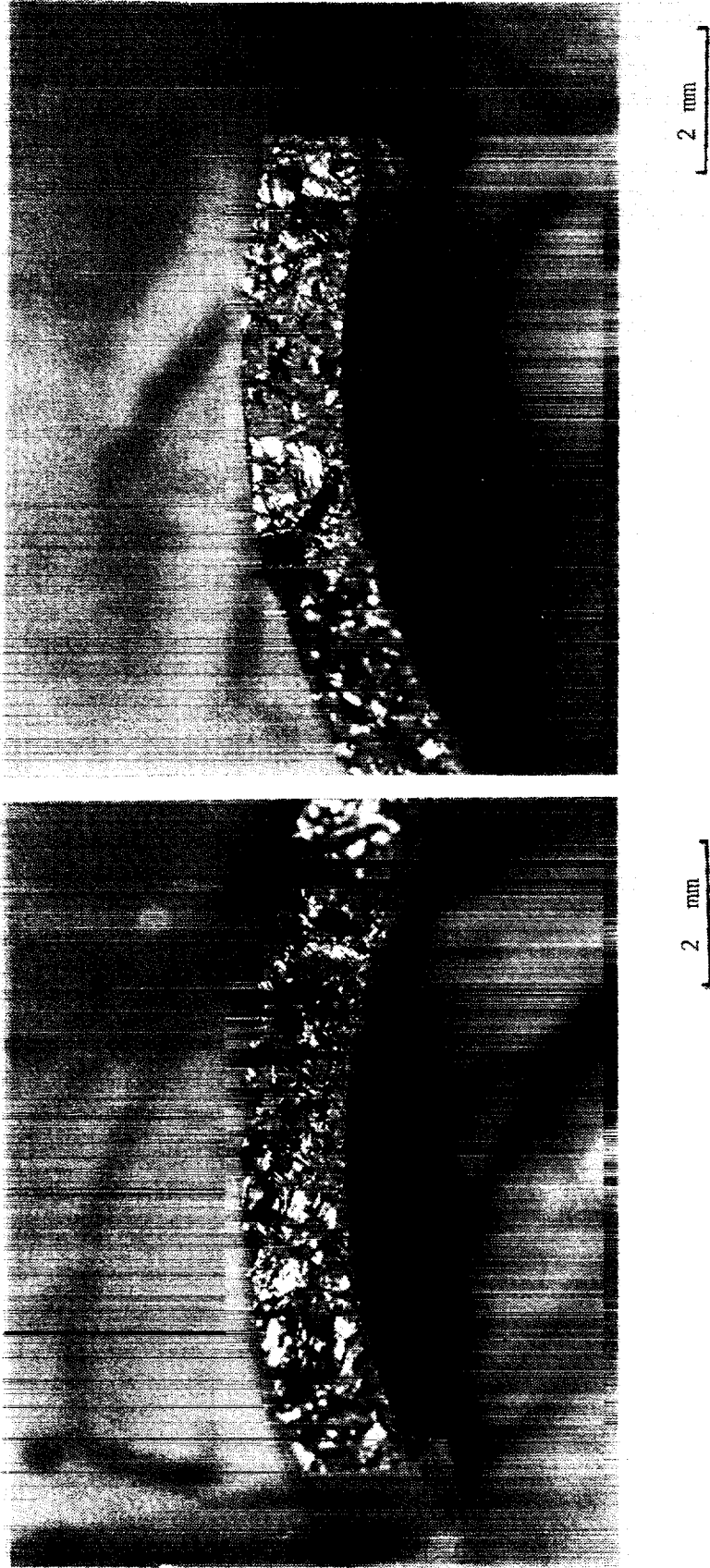
Figure 56   Multiaxial specimen #216 (0.494% axial strain range, 0.742% torsional strain range, 90° out of phase, 1973 cycles). Optical micrographs showing extensive rubbing of fracture surface features.

75
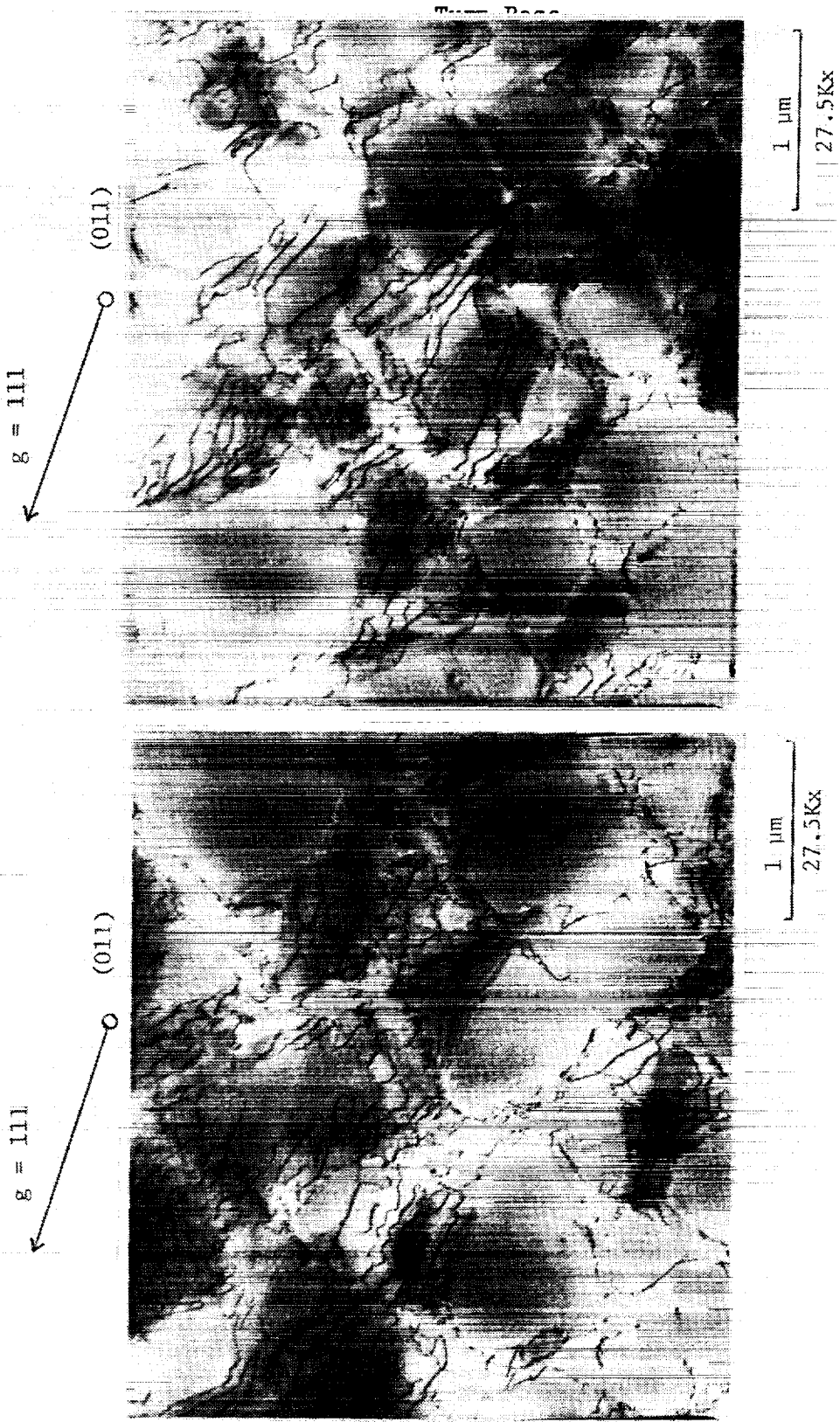
Figure 57   Multiaxial specimen 217 (871°C (1600°F), $\Delta\epsilon = \pm0.250$, $\Delta\gamma = 0$, 10 cpm, initiation life = 1107 cycles, total test life = 2442 cycles). Dislocation structure of foil taken from longitudinal section of sample ∤ 0.250" from fracture surface.
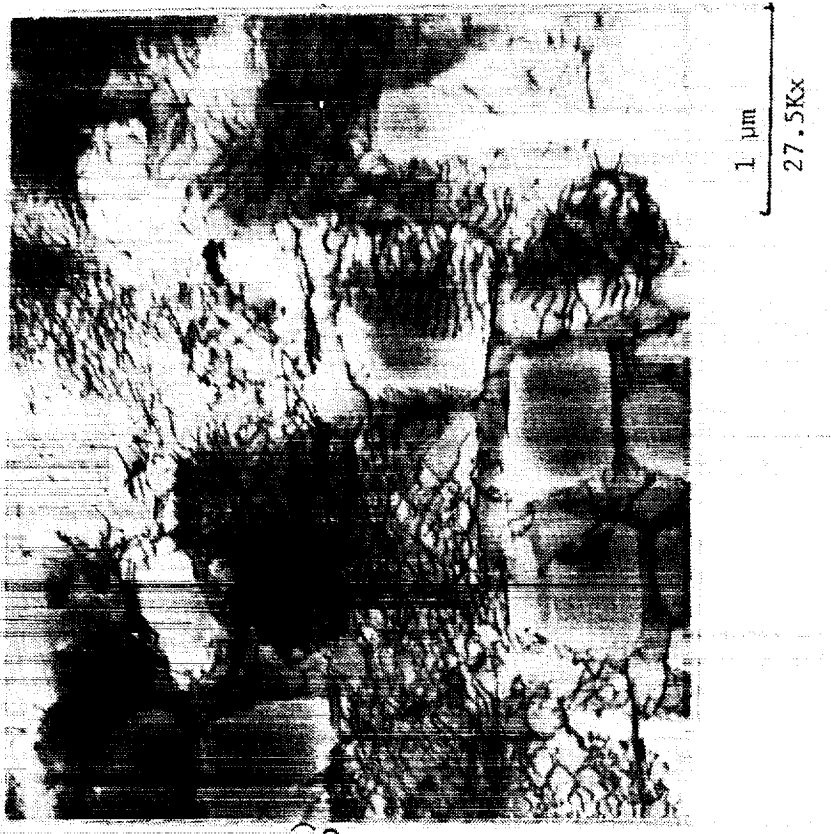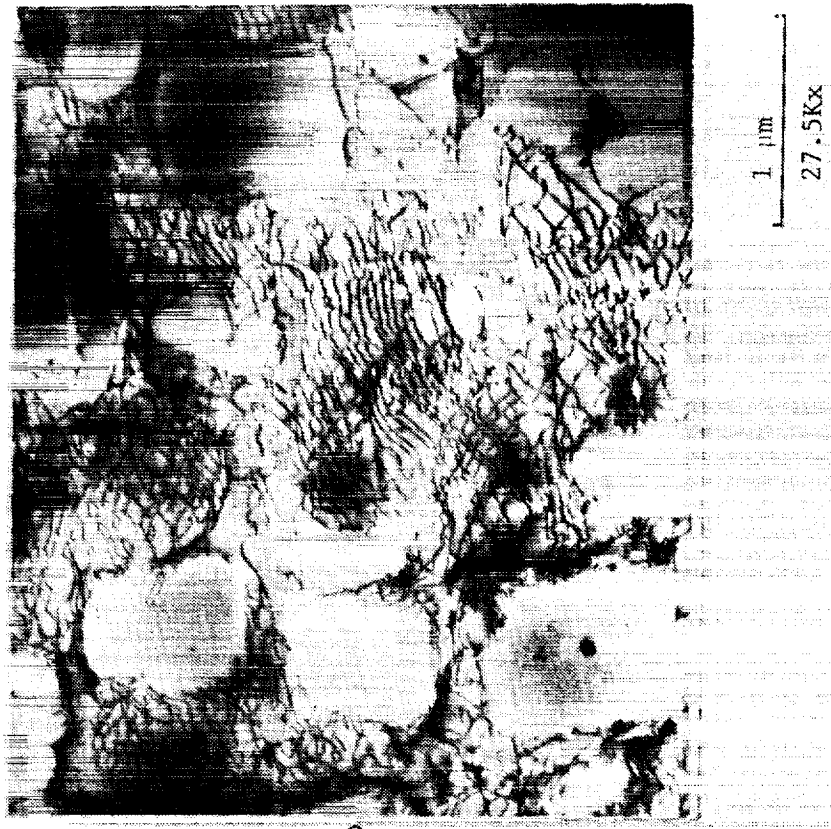
Figure 58   Multiaxial specimen 217 (871°C (1600°F), Δε = ± 0.250, Δγ = 0, 10 cpm, initiation life = 1107 cycles, total test life = 2442 cycles). Dislocation structure of foil taken from transverse section of sample ↓0.1" from fracture surface.
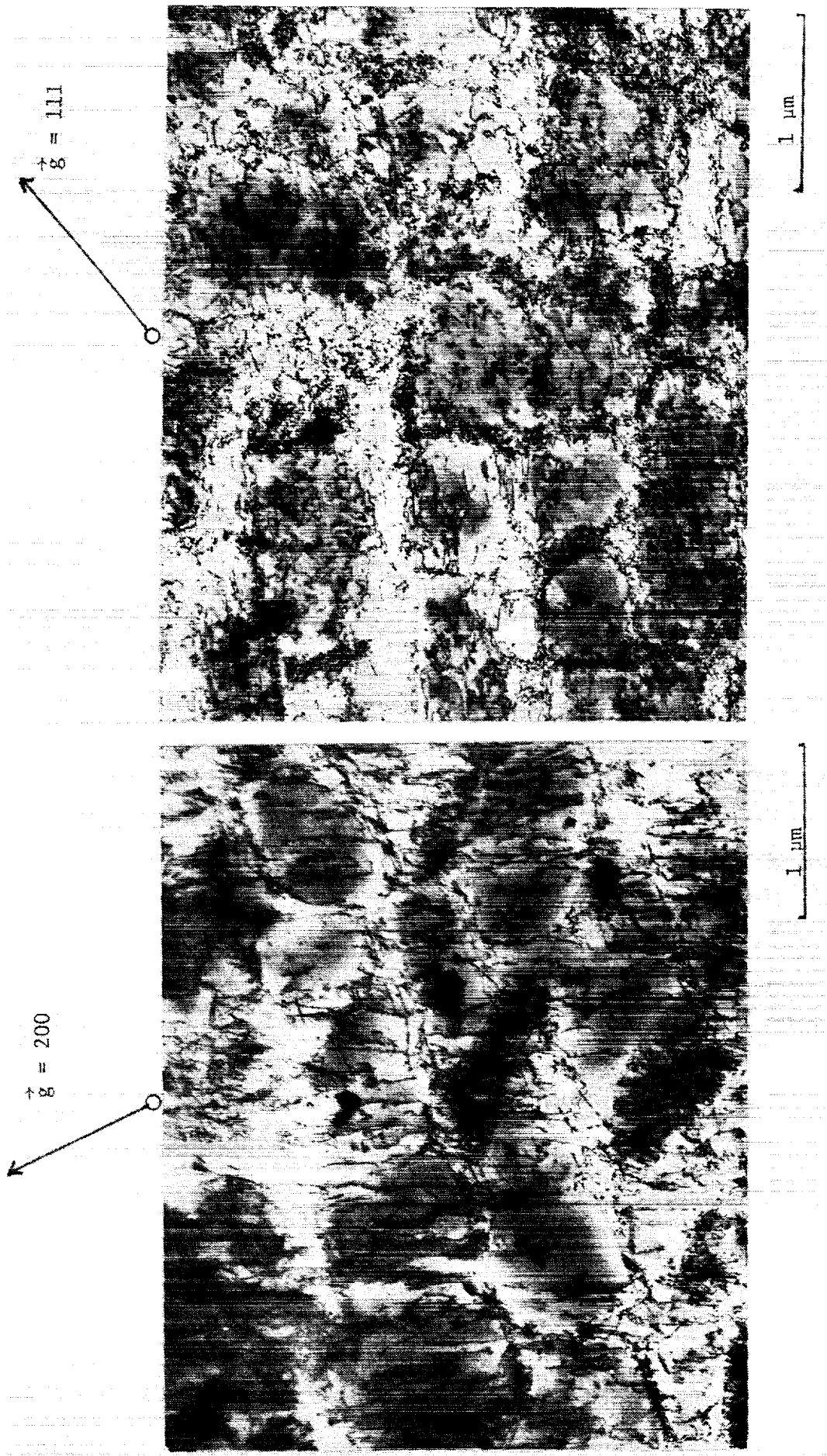
Figure 59   Multiaxial specimen 221 (pure torsion, $\Delta\gamma = 1.362\%$, $538°C$ ($1000°F$), life = 2332 cycles). TEM showing extensive dislocation tangles in γ matrix around γ_1' particles and straight dislocation segments cutting through γ' particles.
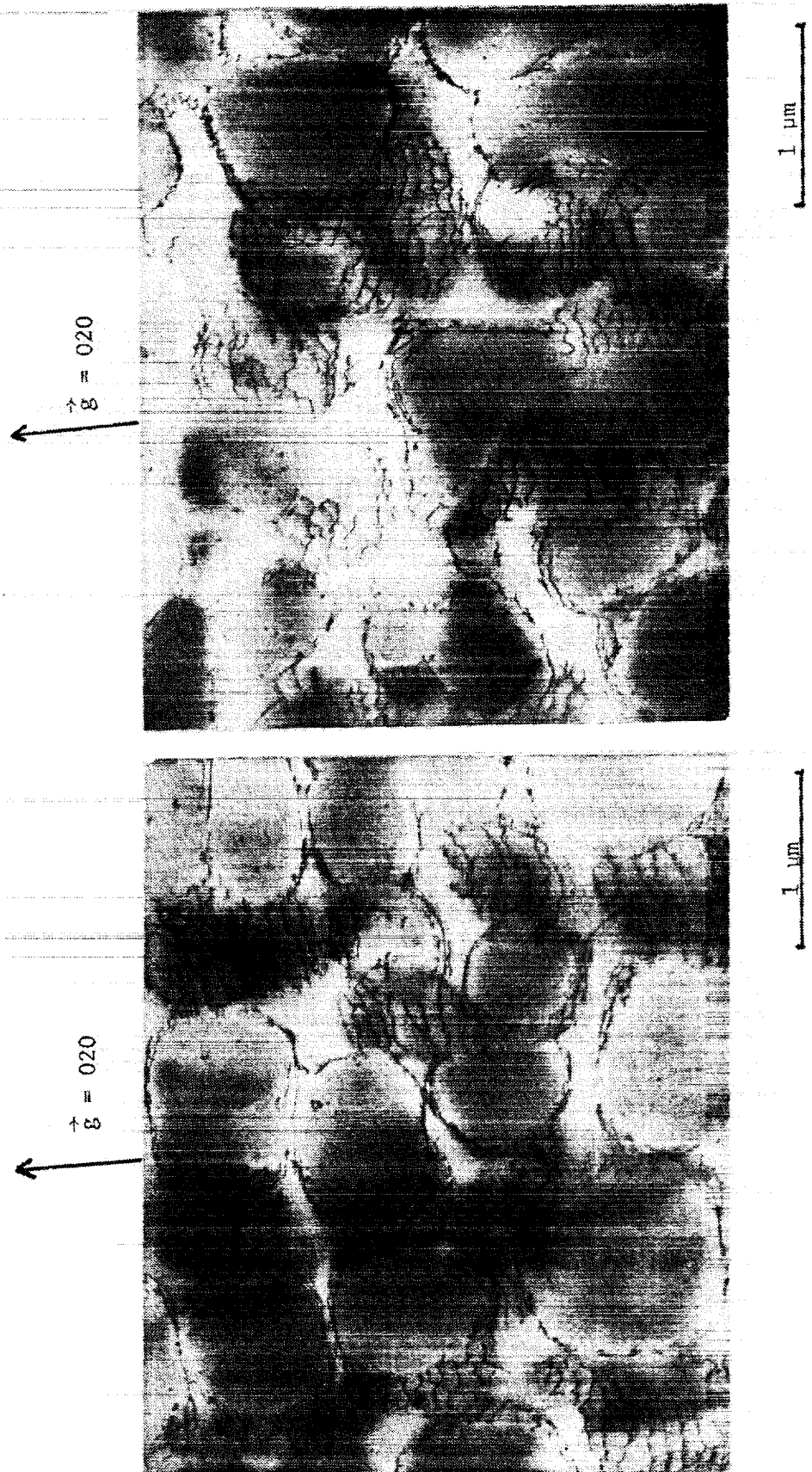
Figure 60   Multiaxial specimen #203 dislocation structure after pure torsion
            testing (torsional strain range of 0.805% for 11,224 cycles).

TEM examinations performed on specimen 216 [871°C (1600°F), axial strain = ±0.250%, torsional strain = ±0.375%, 90° out-of-phase, 10 CPM] reveal dislocation structures as shown in Figure 61 which are similar to those previously observed in the pure torsion specimen 203 and the in-phase, tension-torsion specimen 204 [871°C (1600°F), axial strain = ±0.185%, torsional strain = ±0.260%, in-phase, 10 CPM] consisting of wavy dislocation segments that were roughly parallel to one another surrounding γ' particles.

4.3 Task IX - Environmental Attack Model

The environmental creep-fatigue test program consists of 27 tests utilizing B1900+Hf solid smooth baseline fatigue test specimens. The initial screening tests were conducted in three different environments: lab air, high pressure oxygen (same partial pressure as encountered in high pressure turbines), and high purity argon. The remaining tests will use the environment which produces the largest effect and will examine sequence effects to support development of an advanced life model which can account for the observed life trends.

During this reporting period, a total of eight initial screening tests in lab air and 75 psia oxygen were completed at baseline conditions at both 871 and 982°C (1600 and 1800°F). In general, the higher oxygen partial pressures caused lower specimen lives, with initiation life being more influenced than propagation life. However, the argon screening tests produced inconclusive data, due in part to mechanical problems (air/water leaks). Another factor may be that the type of oxide scale which forms in very low partial pressures of oxygen may be more porous than the oxide which forms at higher pressures. The detailed data for these tests is found in Appendix C. The test matrix covering the tests conducted during this reporting period is shown in Table VII.

TABLE VII
ENVIRONMENTAL SCREENING TESTS

	Test Matrix and Results								
Conditions	Lab Air			Shop Air			60 Psi O_2		
	Spec.	N_i	N_f	Spec.	N_i	N_f	Spec.	N_i	N_f
871°C (1600°F), ±.25%, slow[1]	124D Base[2]	1350 929	5632 2773	123A	560[4]	1443	111C	674	2245
982°C(1800°F), ±.20%, slow	123B	1320	2493				111D 112A	559 460	1216 1000
982°C(1800°F), ±.20%, Fast[1]	124B	1560	4464				112C	924	2641e[3]

[1]"Slow" = 1.67×10^{-4} sec^{-1}; "Fast": = 1.67×10^{-3} sec^{-1}
[2]"Base" = median of baseline test results
[3]Life estimated from replica data; failed prematurely at 958 cycles
[4]Low test results believed to be caused by contaminated atmosphere
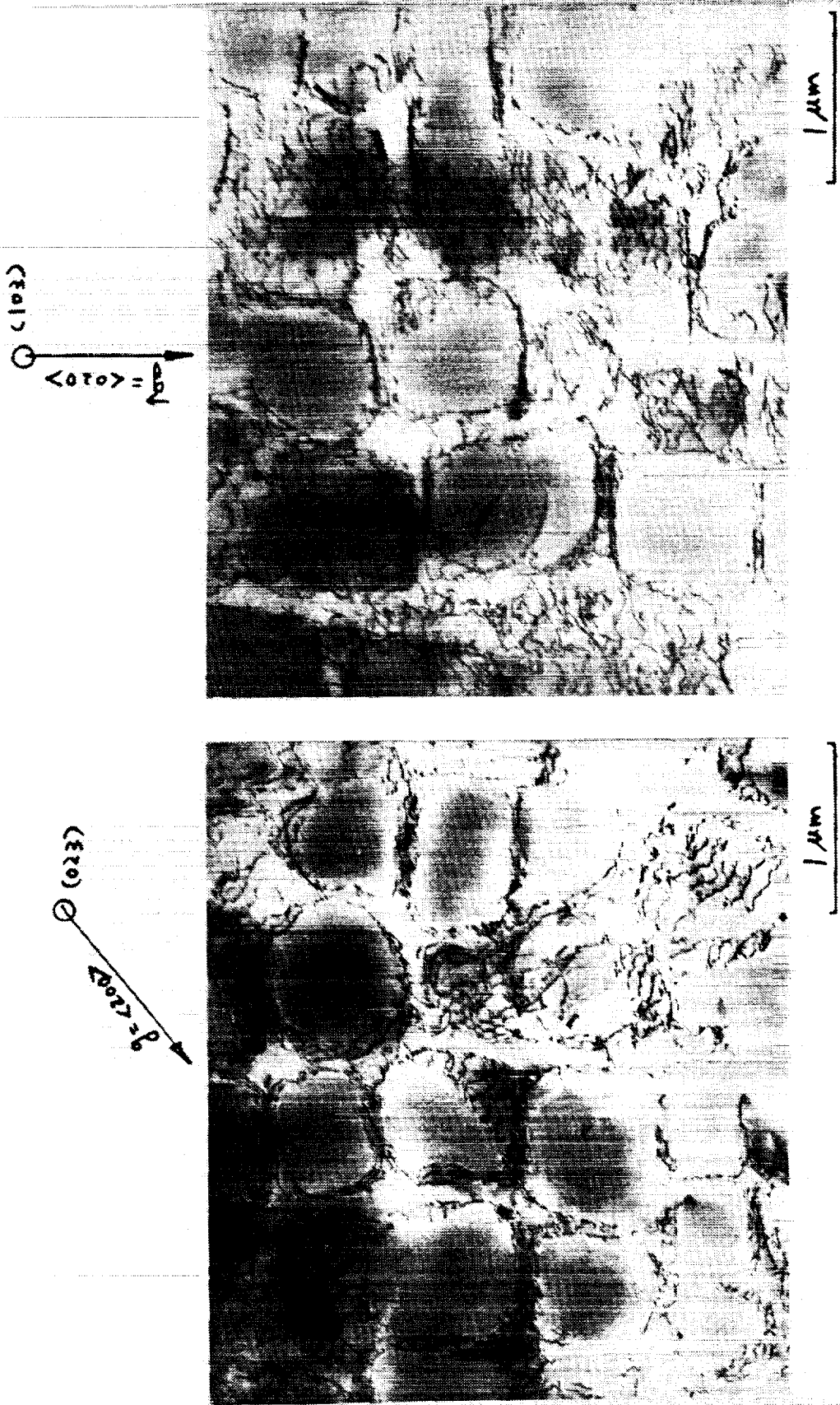
Figure 61   Multiaxial specimen 216 Dislocation Structure After 90° Out-of-Phase
Tension-Torsion Testing (871°C (1600°F), $\Delta\epsilon$ = 0.494%, $\Delta\gamma$ = 0.742%
90° Out-of-Phase, 10CPM, Initiation Life = 1313 Cycles, Total Test
Life = 1973 Cycles).

81

4.3.1 Baseline Lab Screening Tests

Three tests were run in laboratory air with the pressure chamber open. One duplicated the low strain rate, 871°C (1600°F) test conditions from the base program, whereas the other two tests were run at low strain, 982°C (1800°F) conditions which had not been run before.

Specimen 124D was tested in laboratory air at 871°C (1600°F) and 1.0 CPM using a strain range of ±0.25%; its lives were 1350 and 5632 cycles which were significantly higher than the lives of Specimen 123A which was tested in shop air at these conditions.

Specimen 123B was tested in laboratory air at 982°F (1800°F) and 1.25 CPM using a strain range of ±0.20%; its initiation and separation lives were 1320 and 2493 cycles, respectively. The initiation life appeared to be consistent with baseline testing at the same temperature and strain rate but using a higher strain range.

Specimen 124B was tested in laboratory air at 982°C (1800°F) and 12.5 CPM using a strain range of ±0.20%; its initiation and separation lives were 1560 and 4464 cycles, respectively. Compared to Specimen 123B, the initiation life increased by a factor of 1.2 while the propagation life increased by a factor of 2.5. These results indicated that the environment may affect crack propagation more than initiation at these conditions.

4.3.2 Shop Air Testing

Specimen 123A was tested at 871°C (1600°F) and 1 CPM using a strain range of ±0.25%. In order to check out the operation of the environmental rig apparatus when subjected to a working pressure, an environment of +5 psi shop air (regular compressed air used by the manufacturing shop) was used in this test, resulting in initiation and separation lives of 560 and 1443 cycles, respectively. This life is marginal when compared to baseline test specimens which indicates that the shop air environment might have had an adverse effect. It is probable that contaminants were present in the shop air which accelerated the environmental attack during this test.

4.3.3 High Pressure Oxygen Testing

Four high-pressure oxygen screening tests were completed. For these tests, the chamber was first evacuated and then filled with oxygen to 60 psig (75 psia). This simulated the highest partial pressure of oxygen seen by modern hot section components.

Specimen 111C was tested at 871°C (1600°F), 0.5% strain range, R=-1, and 1 CPM, and had initiation and separation lives of 674 and 2245 cycles, respectively. This was about half the lives of typical specimens tested at these conditions in lab air during the baseline testing. Interestingly, they were slightly higher than the lives of Specimen 123A, which was tested at these same conditions but in 5 psig of shop air. This provides additional evidence that contaminants were present in the shop air which accelerated the environmental attack during that test.

Specimen 111D was tested at 982°C (1800°F), 0.4% strain range, R=-1, and 1.25 CPM, and its initiation and separation lives were 559 and 1216 cycles, respectively. As with specimen 111C, this was about half the lives of typical specimens tested at these conditions in lab air during the baseline testing. Some problems were encountered with the extensometry during this test, resulting in slight overloads on three occasions. Another specimen (112A) was tested at these same conditions to verify these results. Its lives were 460 and 1000 cycles, which were slightly lower than the lives of 111D. This indicated that the problems encountered with the extensometry during the test of 111D did not significantly lower its life.

Specimen 112C was tested at 982°C (1800°F), 0.4% strain range, R=-1, and 12.5 CPM, which were the same conditions used for the previous test (112A), except at a faster rate. The initiation life of 112C was 924 cycles, which was double the life of the specimens tested at the slower rate. Specimen 112C failed at 958 cycles from a crack which developed at one of the extensometer contact points. By comparing the data from similar specimen tests, it was estimated that the separation life of this specimen would have been 2641 cycles if it had not failed prematurely. This life also doubles that of the slower strain rate tests.

4.3.4 Purified Argon Testing

Several trial runs of the environmental chamber with an argon atmosphere were made. For these tests the specimen was heated to 982°C (1800°F) for several hours with no load to see how well this arrangement prevented oxidation of the specimen surface. The argon was continuously processed to an indicated level of $1x10^{-7}$ ppm oxygen. However, it was found that a few drops of water leaked into the chamber from the water lines needed to cool the extensometer and other hardware inside the chamber. These apparently provided enough free oxygen in the immediate vicinity of the specimen to cause a bluish tint to the surface. After these leaks were repaired, the temperature exposure caused only a slight straw color on the specimen surface. Several techniques were evaluated to eliminate completely all such oxidation effects during actual specimen testing in the argon atmosphere. Actual testing in this environment will be covered during the final contract reporting period.

4.4 Task X – Protective Coating Models

Since protective coatings are frequently used on components made from cast superalloys to resist oxidation and corrosion, a practical life prediction system must be able to account for the effects of such coatings. To provide a basis for understanding those effects under isothermal conditions, a total of 8 overlay coated (PWA 286) specimen tests have been completed at 871°C (1600°F) and 982°C (1800°F). A matrix of these tests is given in Table VIII, with most of the conditions being identical to base program tests to provide direct comparisons. These tests also serve as complements to the overlay coated TMF tests described under Section 4.0. A detailed listing of the test data generated under this task is found in Appendix D.

TABLE VIII
COATED PWA 1455 ISOTHERMAL TEST MATRIX

Coating Type: PWA 286 Overlay; 0.13 mm. (0.005 in.) Nominal Thickness

Temp (°C(°F))	(in/in)	R	Fast Rate[1]			Slow Rate[1]			Tensile Hold		
			Spec	N_i	N_f	Spec	N_i	N_f	Spec	N_i	N_f
871(1600)	0.005	0	117A	3799	4041	118C	2349	3262	118D	1618	3794e[2]
982(1800)	0.004	-1	118B	3857	6429	118A	3409	3830			
982(1800)	0.005	-1				117D	643	643[3]			
982(1800)	0.005	0				117B	1780	2000			
982(1800)	0.008	-1	117C	395	420						

Notes: 1. "Fast: = $1.67 \times 10^{-3} sec^{-1}$; "slow" = $0.83 \times 10^{-4} sec^{-1}$, 871°C (1600°F); $1.67 \times 10^{-4} sec^{-1}$, 982°C/1800°F
2. 60 sec. hold at max strain; specimen failed at 2147 cycles under extensometry rods.
3. Specimen failed under extensometer rods; no cracks visible in gage section.

Specimen 117A was tested at 871°C (1600°F), 0.5% strain range, R=0, and 10 CPM; its lives were 3799 and 4041 cycles. This separation life was essentially the same as the median separation life of uncoated specimens tested at these conditions during the base program, but the initiation life as determined by surface replication was approximately 3X higher. This apparent rapid propagation indicated that the failure actually initiated in the substrate under the coating, and the crack growth monitored by surface replication reflected the growth of coating cracks only. Optical and SEM micrographs of the fracture surface of Specimen 117A are shown in Figure 62. It can be seen that the crack initiated at porosity in the base material beneath the coating and that crack initiation and growth in the base material could occur before the crack would be visible through the coating. This agrees with the crack propagation behavior as determined by surface replicas. The actual initiation life of this specimen may be lower than surface replica results indicate.

Specimen 117B was tested at 982°C (1800°F), 0.5% strain range, R=0; its lives were 178 and 2000 cycles. Since the median lives of baseline specimens tested at the same conditions were 115 and 820 cycles, the initiation life of this coated specimen is somewhat higher and the separation life dramatically higher than those of the uncoated baseline testing. Apparently oxidation was a very important factor in the initiation life of this alloy at 1800°F and this strain level. This specimen was checked for subsurface initiation by both optical microscopy and SEM. Typical micrographs are shown in Figure 63. The exact location of the initiation site is unclear and it is unknown if subsurface crack initiation occurred.

(a)

0.5 mm
64X

(b)

100 μm
150X

Figure 62   Specimen 117A 871°C (1600°F), $\Delta\epsilon = 0.5\%$, R = 0, 10 cpm, initiation
Life = 3799 cycles, separation life = 4041 cycles).
(a) Optical and (b) SEM micrographs showing crack origin at
porosity in the base material.
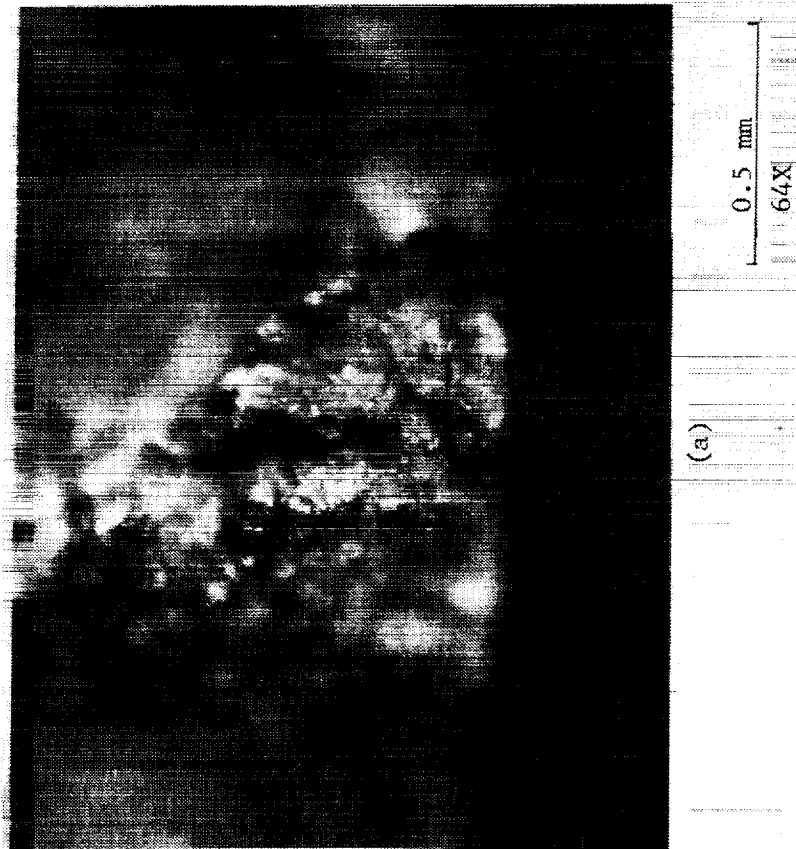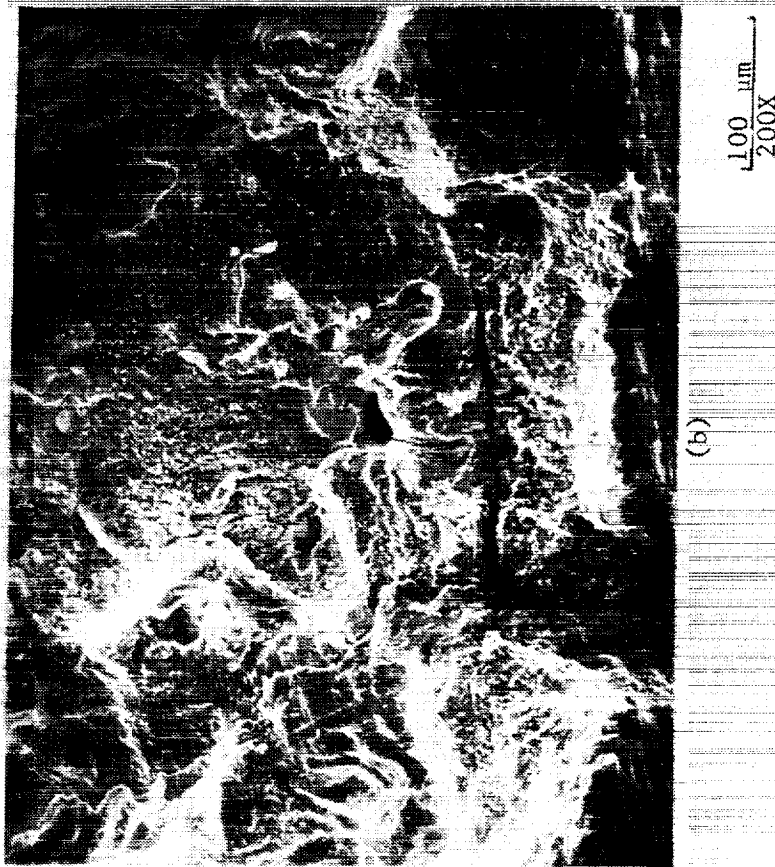
Figure 63   Specimen 117C 982°C (1800°F), Δε = 0.8%, R = -1, 6.25 cpm, initiation life = 395 cycles, separation life = 420 cycles).

The next coated specimen (117C) was also tested at 982°C (1800°F), but at a higher cyclic rate (6.25 CPM) and at a high, fully reversed strain range (±0.4%). Its initiation and separation lives were 395 and 420 cycles, respectively. Since the median lives of baseline specimens tested at the same conditions were 56 and 278 cycles, the initiation life of 117C was about 7X than those of the uncoated baseline testing, while the separation life is only about 1.5X higher. As expected, this shows a slightly reduced sensitivity to coating than was seen on the slow rate, low strain test at 1800°F. The faster cyclic rate increased the proportion of damage caused by fatigue and reduced the amount caused by oxidation. Optical and SEM examinations were made of the fracture surface of Specimen 117C and are shown in Figure 64. The crack initiated at porosity in the base material. It is possible that subsurface crack growth occurred before being visible at the coating surface although indications of this are not as clear as they are for Specimen 117A.

Specimen 117D was tested at 982°C (1800°F), 0.5% strain range, R=-1 and 1 CPM. Unfortunately, it developed cracks under the extensometer contact points and was discontinued at 643 cycles with a 10% load drop. No cracks were visible in the specimen gage section by this time. Even so, this life was more than double the initiation life seen with uncoated specimens at these conditions.

Specimen 118A was tested at 982°C (1800°F), 0.4% strain range, R=-1, and 1.25 CPM; its lives were 3409 and 3830 cycles. This initiation life was much higher than expected from the uncoated baseline tests, even though no specimens were run at these exact conditions. The propagation life was quite short as was expected for a slow rate, 982°C (1800°F) test. Since these results indicated a strong effect of the environment on initiation, these same conditions were used for testing under Task IX.

Specimen 118B was tested at 982°C (1800°F), 0.4% strain range, R=-1 and 8 CPM; its lives were 3857 and 6429 cycles. This initiation life was approximately the same as seen with specimen 118A which used the same conditions except with a slower rate (1.25 CPM). This indicated that this life was not significantly affected by time, primarily due to the coating. However, the propagation life was much longer than seen during the test at the slow rate (2600 vs. 420 cycles). It was interesting to note that the time of the propagation from 0.03 in. to separation was nearly identical for the two tests (5.4 vs. 5.6 hr.). These results indicated the influence of the environment on propagation as well as on initiation which must be considered when evaluating life prediction models for coated materials.

Specimen 118C was tested at 871°C (1600°F), 0.5% strain range, R=0, and 0.5 CPM; its lives were 2349 and 3262 cycles. This initiation life was approximately 4X higher than seen during the baseline testing at the same conditions, while the separation life was about 2X higher. However, the propagation life was about the same (roughly 1000 cycles) for both types of tests. These results suggested that, at these conditions, environment was a greater influence on initiation than on propagation. It was also possible that the crack in this specimen actually initiated in the substrate and not in the coating and therefore replica data is overestimating the initiation life.

(a)

(b)

0.5 mm
64X

0.5 mm
50X
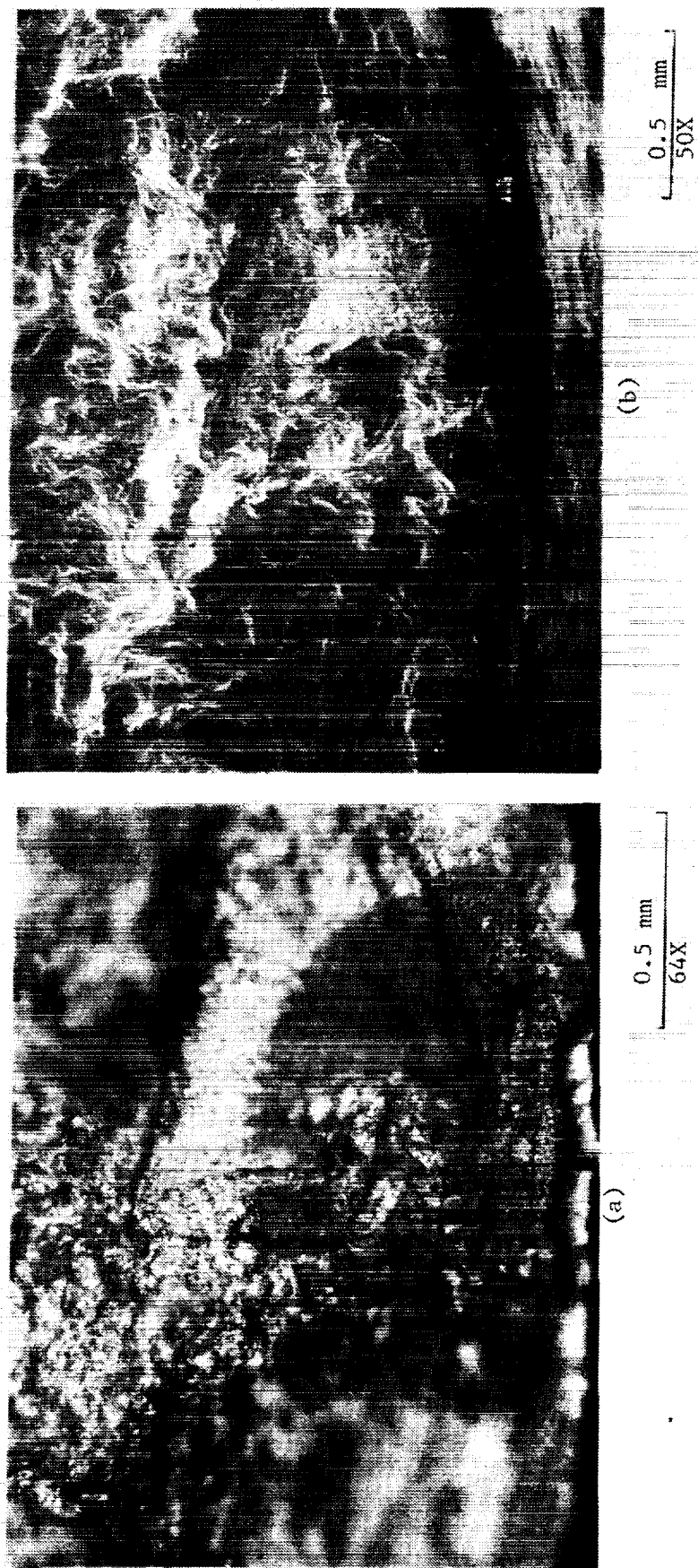
Figure 64   Specimen 117B 982°C (1700°F), Δε = 0.5%, R = 0, 1 cpm, initiation
Life = 1780 cycles, separation life = 2000 cycles).
(a) Optical and (b) SEM micrographs of initiation site.

88

Specimen 118D was tested at 871°C (1600°F), 0.5% strain range, R=0, with a one minute hold at +0.5% strain. The uncoated specimens run at these same conditions experienced intergranular fracture and low initiation lives (median life 220 cycles). However, the initiation life observed on the surface of this coated specimen was 1618 cycles, more than 7X higher. The specimen failed at 2147 cycles under one of the extensometer rod contact points, with the gage section crack being 0.040 in. at that time. Typical propagation data from other tests indicated that the separation would have been 3794 cycles if the specimen had not failed prematurely. This indicated that the propagation life from 0.030 in. to separation would have been similar to what was observed during the uncoated verification tests.

4.5 Task XI - Cyclic Mean Stress Model

A total of 25 controlled mean stress tests are planned for this task. Five of these tests under TMF conditions have been completed and are reported in this interim report; the detailed test data is given in Appendix E. The remaining 20 tests are under isothermal conditions and will be conducted using special mean stress-strain range control software available at the University of Rhode Island.

The major conclusions from this testing are as follows:

1. Mean stress was shown to have a dramatic effect on TMF life. A moderately tensile mean stress reduced the initiation life, whereas a slight compressive mean stress actually caused crack growth to slow down and eventually stop.

2. The results cannot be accounted for by linear summation of creep and fatigue damage. Total damage sums were only 0.25 for some tests (instead of 1.0 as expected from linear damage accumulation theory).

Specimen 109C was tested under load control at 30±50 ksi, 538-871°C (1000-1600°F), with in-phase temperature cycling. Based on previous creep and TMF tests, these conditions were expected to yield a typical stress rupture life of 1700 cycles and a typical TMF initiation life of 5800 cycles. However, the actual separation life was only 227 cycles, with a large increment of inelastic strain being accumulated during each cycle. Initially, it was thought that specimen 109C actually failed by ratchetting rather than by creep or fatigue. However Figure 65 shows a plot of the mean strain history of this specimen, and it can be seen that the strain increment per cycle was not really constant. The form of the curve is actually rather typical of high strain rate creep tests.

Specimen 110D was tested at the same conditions used for specimen 109C, except with 10±50 ksi; its lives were 1914 and 2454 cycles. Figure 65 shows the mean strain history for this specimen as well as for the higher mean stress test (109C), and its behavior was also typical of creep tests. Note that the lives of both of these specimens were much lower than what would be expected from standard strain controlled TMF testing at the same strain range.

Fixed conditions: 538-871°C (1000-1600°F),

in-phase, 100 ksi stress range
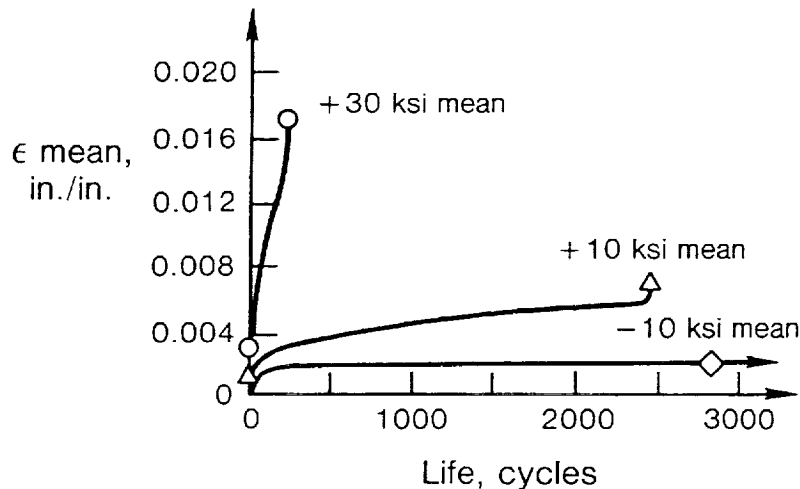
Figure 65.- Mean Strain Histories for Load Controlled TMF Tests.

Detailed TEM examinations of TMF specimens 109C and 110D were conducted to determine if there was some difference in their dislocation structure, perhaps caused by a measure of ratchetting in the higher mean stress test. Typical dislocation structures of 109C and 110D are shown in Figures 66 and 67, respectively. Both have dislocations in the γ matrix and encasing γ' particles at the γ/γ' interface. No significant features were seen in the dislocation structure of 109C that would distinguish it from that of 110D. Based on these observations it did not appear that there was a dislocation structure associated with the ratchetting phenomenon. It was noted that there appeared to be more dislocations cutting through γ' particles in 109C and that the extent of dislocation buildup in 109C was approximately the same as that of 110D despite the order of magnitude lower number of cycles on 109C. This was a reflection of the higher mean stress level applied to 109C.

Specimen 111B was tested at -10±50 ksi, 538-871°C (1000-1600°F), with in-phase temperature cycling. The crack grew to 0.030 in. by 5611 cycles, but the growth slowed considerably beyond that point. By 16,503 cycles, the crack was still only 0.071 in. long, and the rate of growth was very small. The test was terminated at this point to examine the crack by breaking open the specimen. The mean strain history for this specimen is also shown in Figure 65.

Specimen 114B was tested at 538-871°C (1000-1600°F), 90 ksi stress range +15 ksi mean stress, with in-phase strain-temperature cycling; its initiation life was 5765 cycles, which is close to the life to 1% creep at these conditions. This indicated that the strain cycling had little effect on the creep life. The separation life was 7062 cycles which showed about the same propagation life as for other TMF tests at similar conditions.

Specimen 112B was tested at 538-871°C (1000-1600°F), 100 ksi stress range, -10 ksi mean stress, with out-of-phase strain-temperature cycling. The initiation life was 2684 cycles, which indicated that there was very little effect of creep on this test, since this was essentially the same as the predicted life due to strain cycling alone. The test was stopped at 7062 cycles with a 0.145 in. crack, which was similar to the behavior of strain controlled tests conducted at similar conditions.
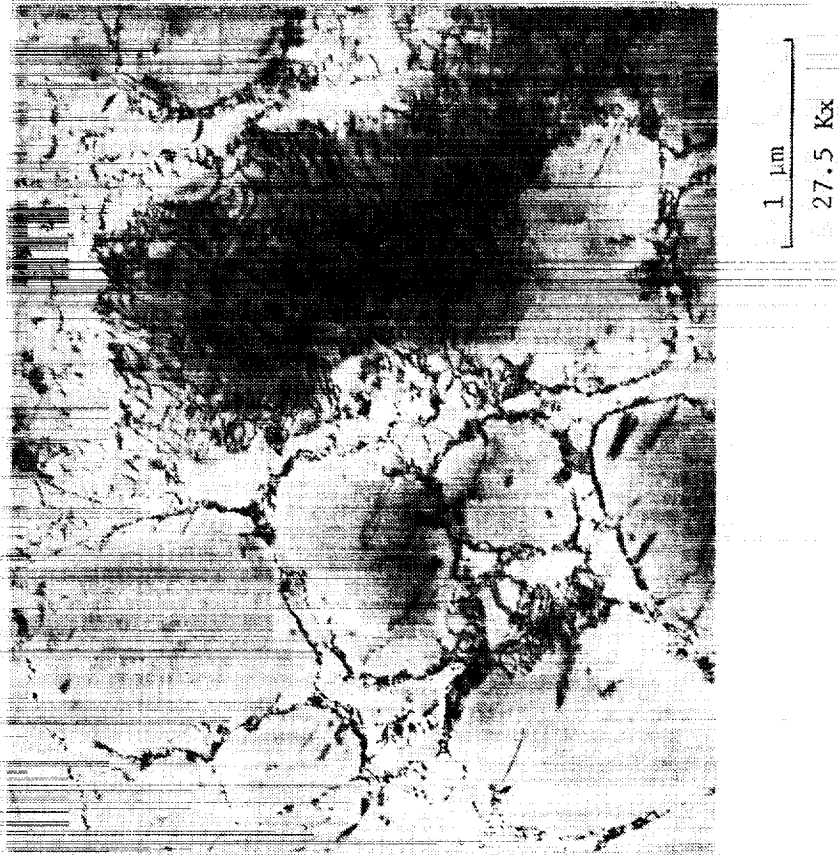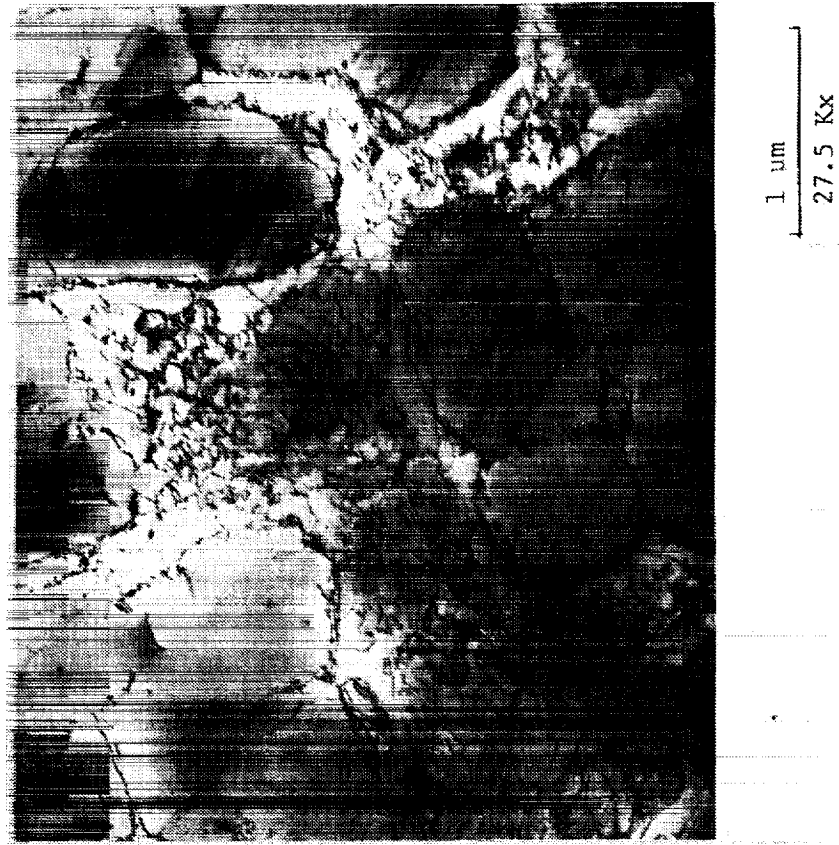
Figure 66   Load controlled TMF specimen 109C (538-871°C (1000-1600°F)), σ_{max} = 80 Ksi, σ_{min} = -20 Ksi, Cycle II, 1 cpm, 229 cycles). Typical dislocation structure showing dislocations in γ matrix and encasing γ' particles at the γ/γ' interface. More dislocations cut through γ' particles than in 110D and this is a reflection of the high mean stress applied to 109C. However, no distinct features can be identified that can be associated with ratcheting.
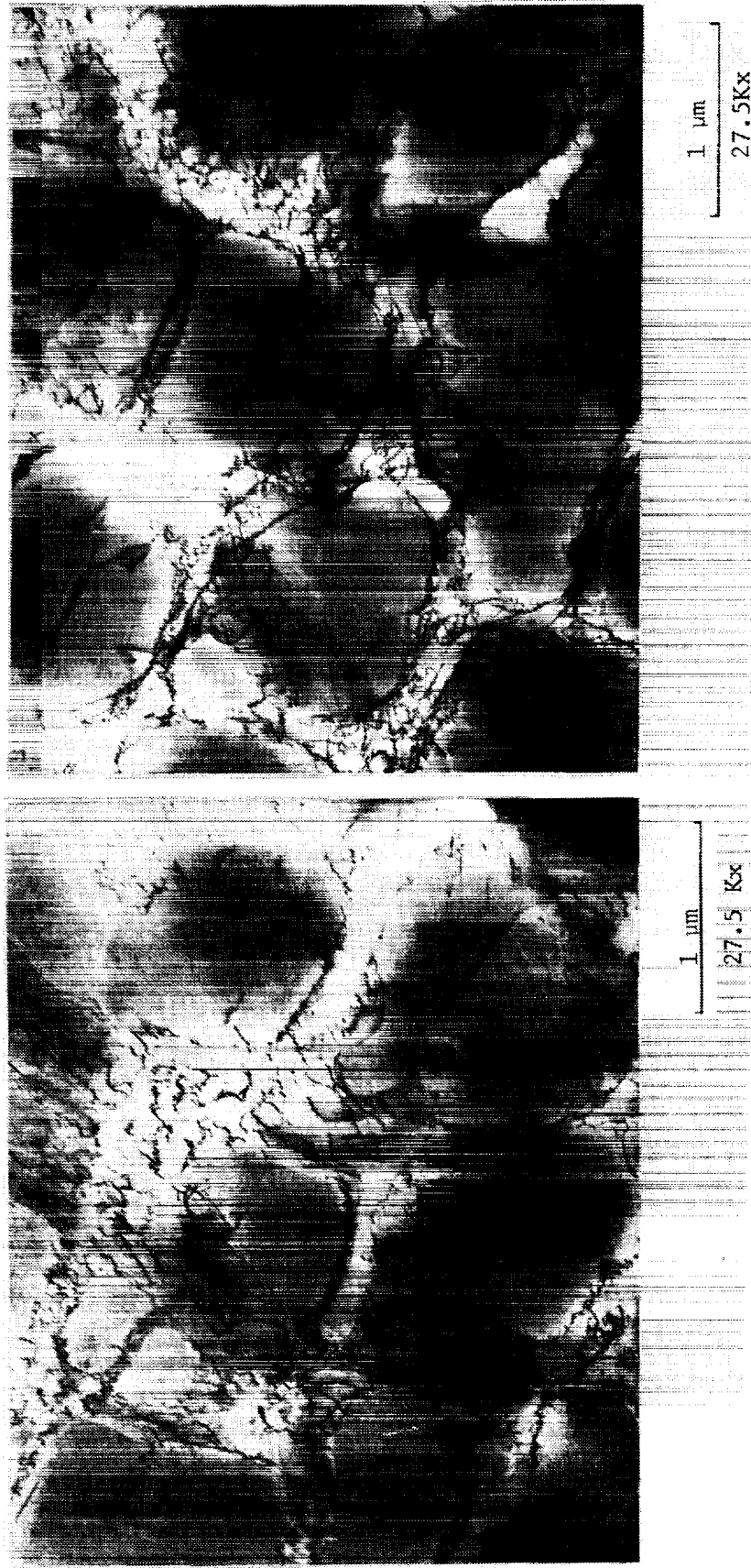
Figure 67   Load controlled TMF specimen 110D (538-871°C (1000-1600°F)), σ_{max} = 60 Ksi, σ_{min} = -40 Ksi, Cycle II, 1 cpm, 2454 cycles). Typical dislocation structure showing dislocations in γ matrix and encasing γ' particles at the γ/γ' interface.

4.6 Task XII – Final Verification and Evaluation of the Alternative Material/Protective Coating System/Component Combination

In order to verify the general applicability of the life prediction models developed under this contract, additional testing is planned for an alternative material. Since cast B1900+Hf was used for the baseline testing, wrought INCO 718 was chosen as the alternative alloy. During this reporting period, initial monotonic and fatigue tests were completed; details of the fatigue tests are found in Appendix F.

4.6.1 Monotonic Testing

Three notched (Kt=3.8) stress rupture specimens were tested during this reporting period. The first test was specimen 427, which was tested at 649°C (1200°F) and 110 ksi for 120 hours. Comparison with published smooth data at similar conditions indicates good notched strength. The second test, specimen 428, was conducted at 732°C (1350°F) and 40 ksi stress. The test was discontinued after more than 1500 hours at these conditions. Finally, the third specimen, 429, was run at 732°C (1350°F) and 50 ksi stress for a total of 621 hours. Taken together, these tests demonstrate very good notched rupture strength for this material at high temperatures.

4.6.2 Isothermal Fatigue Testing

Four isothermal fatigue specimen tests were completed during this reporting period. Preference was given to high temperature, slow rate tests due to rig availability. Specimen 718-1 was tested at 732°C (1350°F), 0.8% strain range, R=-1 and 1 CPM; its lives were 1339 and 2939 cycles. The specimen displayed significant cyclic softening at these conditions, with a reduction in stress range from 167 ksi at cycle 1 to 136 ksi at 1500 cycles. Specimen 718-2 was tested at the same conditions except with 0.65% strain range; its lives were 4719 and 6506 cycles. Specimen 718-3 was tested at 649°C (1200°F), 0.8% strain range, R=-1, and 1 CPM; its initiation life was 2122 cycles, which was higher than the life of the specimen at the higher temperature. However, its separation life was 2868 cycles, which is slightly lower than the 2939 cycles seen during the higher temperature test. Finally, specimen 718-4 was tested at 649°C (1200°F), 0.65% strain range, R=-1, and 1 CPM, and its lives were 11,066 and 13,332 cycles.

The microstructures of specimens 718-1 and 718-2 are shown in Figures 68(a) and 68(b), respectively. These micrographs are from the center of the specimens in the gage section. Both specimens show more of the fine needle shaped δ phase along grain boundaries as compared to the material in the as-received condition. The amount of δ phase appears greater in 718-2.

C-2
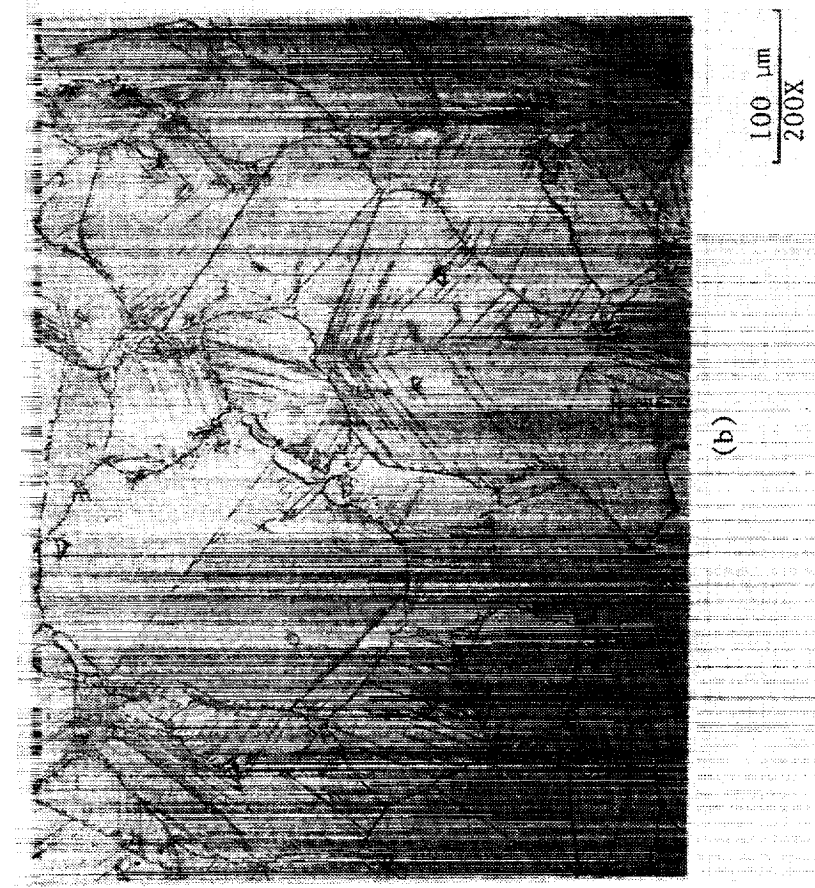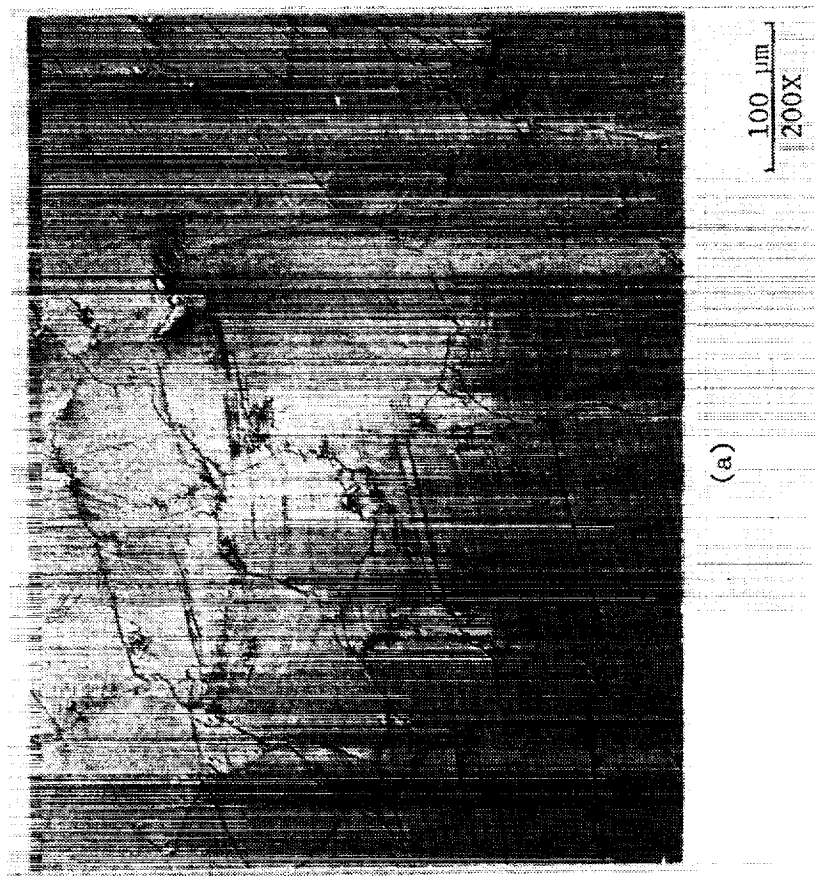
Figure 68   Optical micrographs in IN 718 alternate material specimens after testing.

(a)   Specimen 718-1 (732°C (1350°F), isothermal, ε_{max} = 0.4%, ε_{min} = -0.4%, 1 cpm, test length = 2939 cycles.

(b)   Specimen 718-2 (732°C (1350°F), isothermal, ε_{min} = + 0.325%, ε_{min} = -0.325%, 1 cpm, test length = 6506 cycles).

94

Optical examinations were made of the fracture surfaces of specimens 718-1 and 718-2. Figure 69 shows the fracture surface of 718-1, with multiple initiation sites as indicated by the arrows. The overall fracture surface appearance was indicative of a mixture of predominantly transgranular with some intergranular crack growth except in the immediate vicinity of the initiation sites where the fracture had a faceted appearance. Optical micrographs of 718-2 are shown in Figure 70, again with multiple initiation sites indicated by the arrows. Optically the fracture surface was similar to that of 718-1, with transgranular crack growth at the initiation sites and a mixture of predominately transgranular growth with some intergranular crack growth overall. SEM examinations were also completed on 718-1. The primary initiation site is shown in Figure 71(a). Based on the appearance of the fracture surface, the crack propagated 1 mm in a transgranular mode before changing to mixed mode growth. A higher magnification view of the initiation site is shown in Figure 71(b).

These early results suggest that the particular rolled-ring AMS 5663 forging used to produce these specimens has excellent creep resistance as well as good fatigue capability. Of particular interest is the pronounced cyclic softening noted during the fatigue testing at 732°C (1350°F). It is possible that some modification to the form of the CDA model will be necessary to account for this.
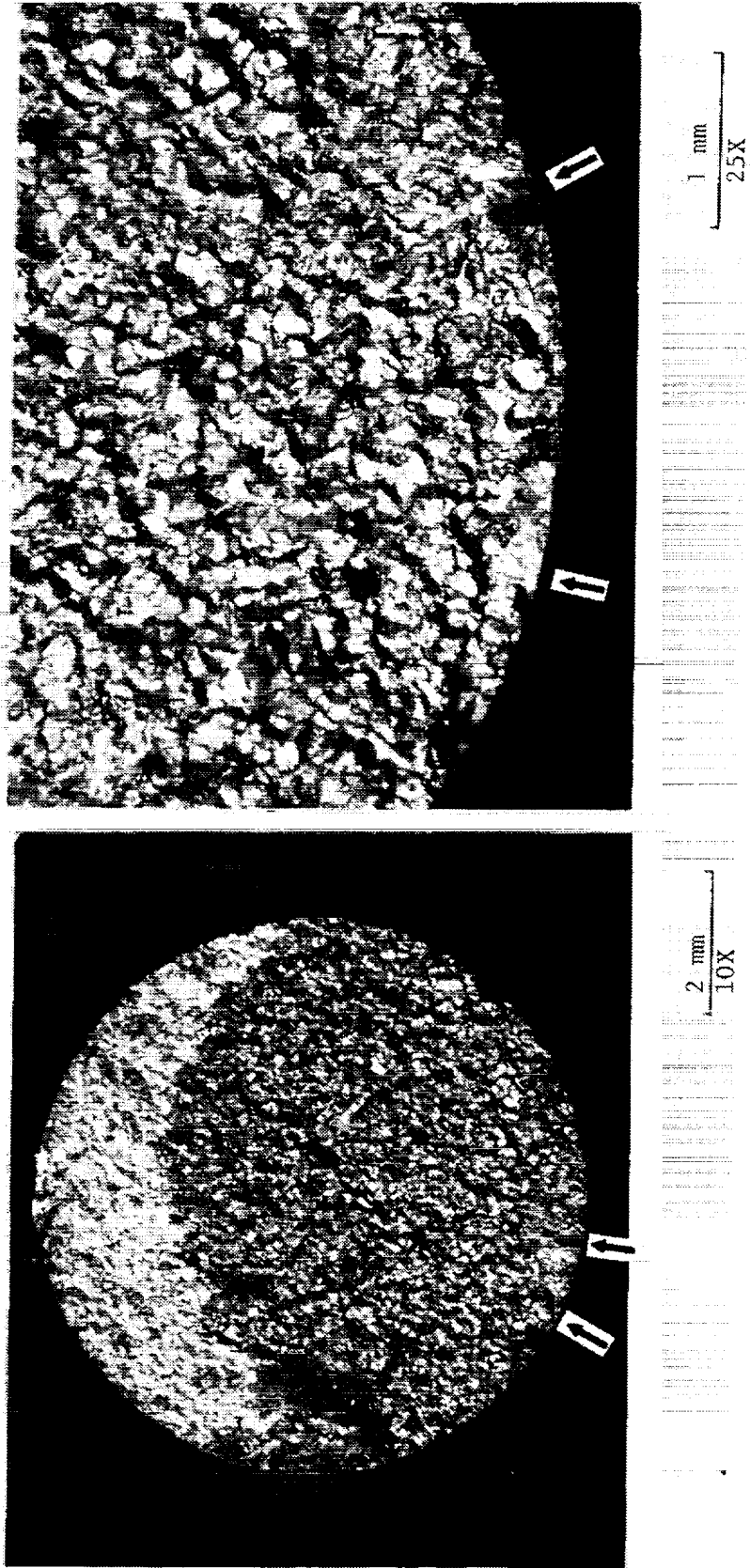
Figure 69   Optical micrograph of specimen 718-1 (732°C (1350°F), isothermal
ϵ_{max} = 0.4%, ϵ_{min} = -0.4%, 1 cpm, test length = 2939 cycles).
Initiation sites are indicated by arrows.
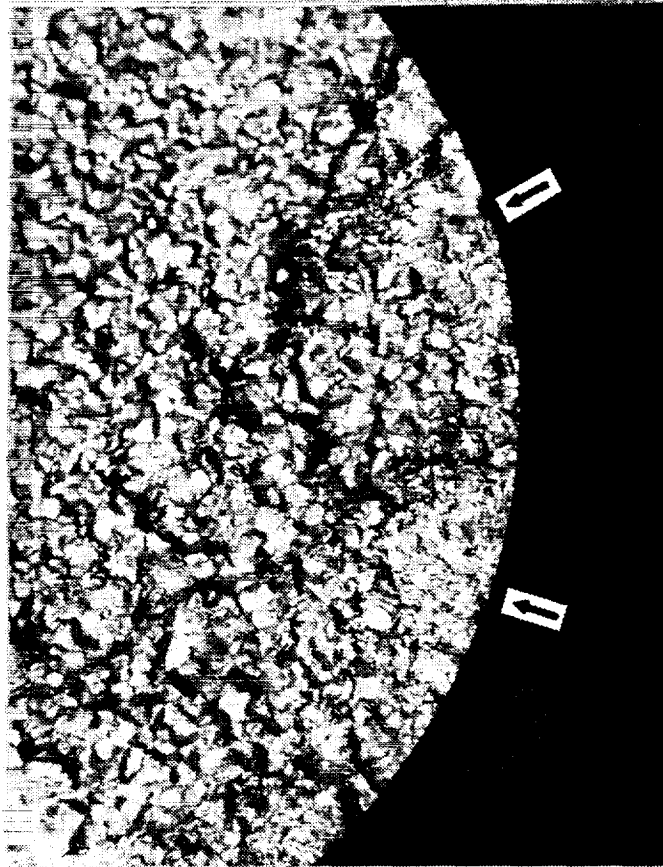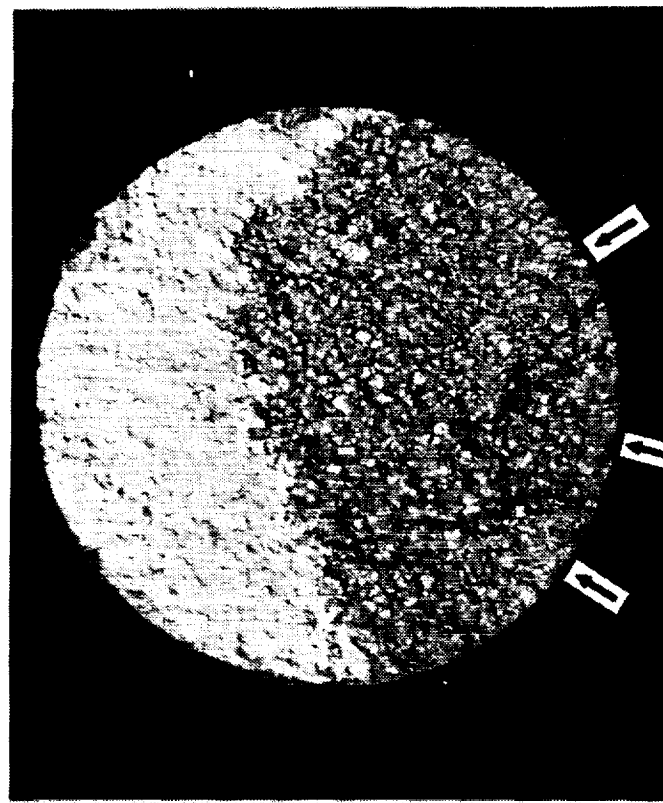
Figure 70   Optical micrographs of specimen 718-2 (732°C (1350°F), isothermal, ε_{max} = 0.325%, ε_{min} = -0.325%, 1 cpm, test length = 6506 cycles). Initiation sites are indicated by arrows.
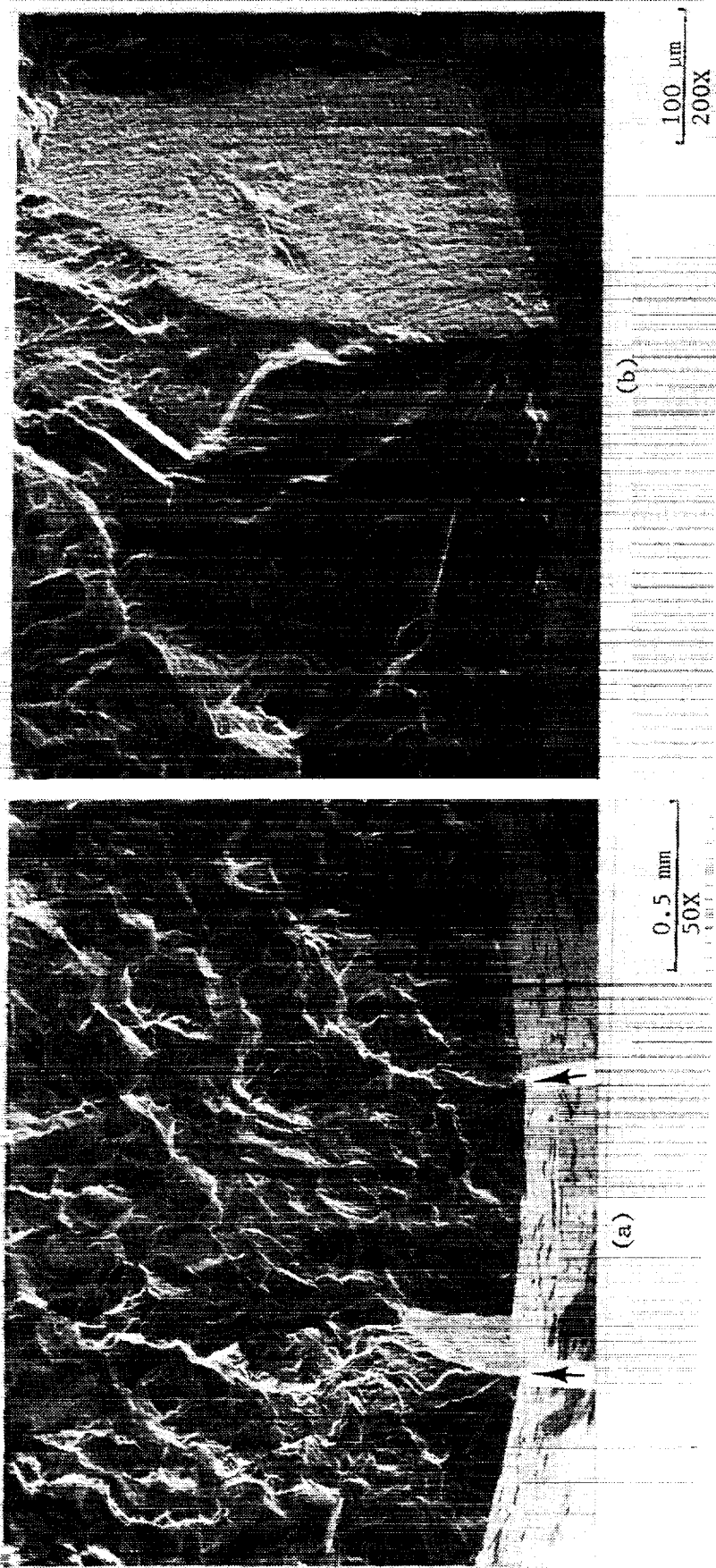
Figure 71   SEM micrographs of fracture surface of specimen 718-1.   Initiation
             sites are indicated by arrows.

        (a) Primary initiation site located at left arrow, smaller
             initiation occurred at right arrow. Crack appears to
             propogate in a transgranular mode for ∤ 1 mm before changing
             to mixed mode growth.

        (b) Higher magnification of (a) showing primary initiation site.

5.1 TMF Data Trends and Life Prediction Modeling

In order to discern the effects of the variables investigated under TMF conditions for coated PWA 1455 material, the results of this testing must be compared with those from the uncoated tests reported in the previous interim report (Nelson et al, 1986). For the in-phase and out-of-phase tests, Figure 72 shows a plot of initiation life vs. total mechanical strain range, along with median life lines from uncoated TMF tests at the same conditions. Note that the coated data lie approximately 2X higher in life than the uncoated data, indicating that for these conditions, the coatings reduced the damage done by mechanisms such as oxidation. It is known, however, that the reverse is often true: coatings can themselves reduce the life under certain TMF strain cycles. This was the case with the "LC dogleg" cycle test run with an overlay coated specimen. This particular cycle caused a high tensile strain to occur in the coating and therefore resulted in early coating cracking. Figure 73 shows that the initiation life of this specimen was somewhat lower than the lives of coated specimens tested with out-of-phase cycles. In fact, the initiation life of this specimen was lower than what had been observed for uncoated specimens using the "LC dogleg" cycle. This once again serves to emphasize the need to understand and model the actual damage mechanisms active under TMF conditions. Simple data correlations based on only certain cycle types may not always give conservative predictions.
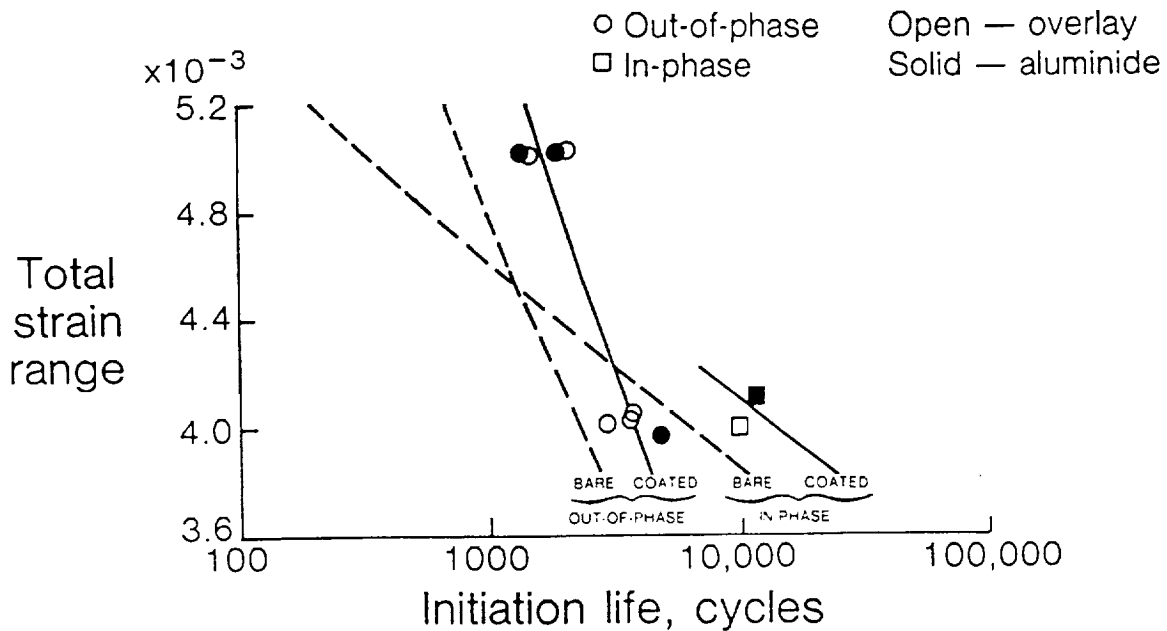
Figure 72.- Coating Effects for In-Phase and Out-of-Phase TMF Testing.
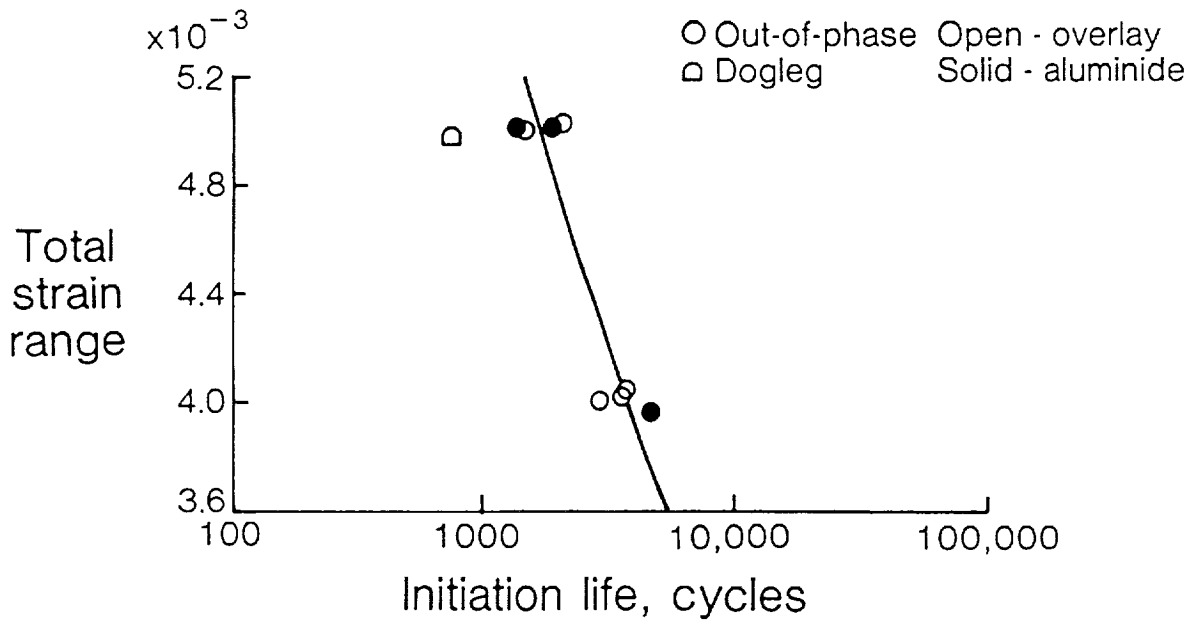
Figure 73.– Dogleg Cycle Path Effect for Coated Specimens.

Perhaps the most interesting results obtained during this task are those from the elliptical cycle tests. As mentioned earlier, these were designed to give insight into the behavior of actual engine components which experience strain-temperature cycles similar to these. Figure 74 shows a plot of the elliptical test results for the coated specimens relative to the median lives from the out-of-phase coated tests. Clearly there is approximately a 5X initiation life difference between the two types of elliptical cycles. Note that life predictions methods based solely on the extremes of a cycle will not be able to predict this behavior, since they cannot distinguish between CW and CCW cycles.
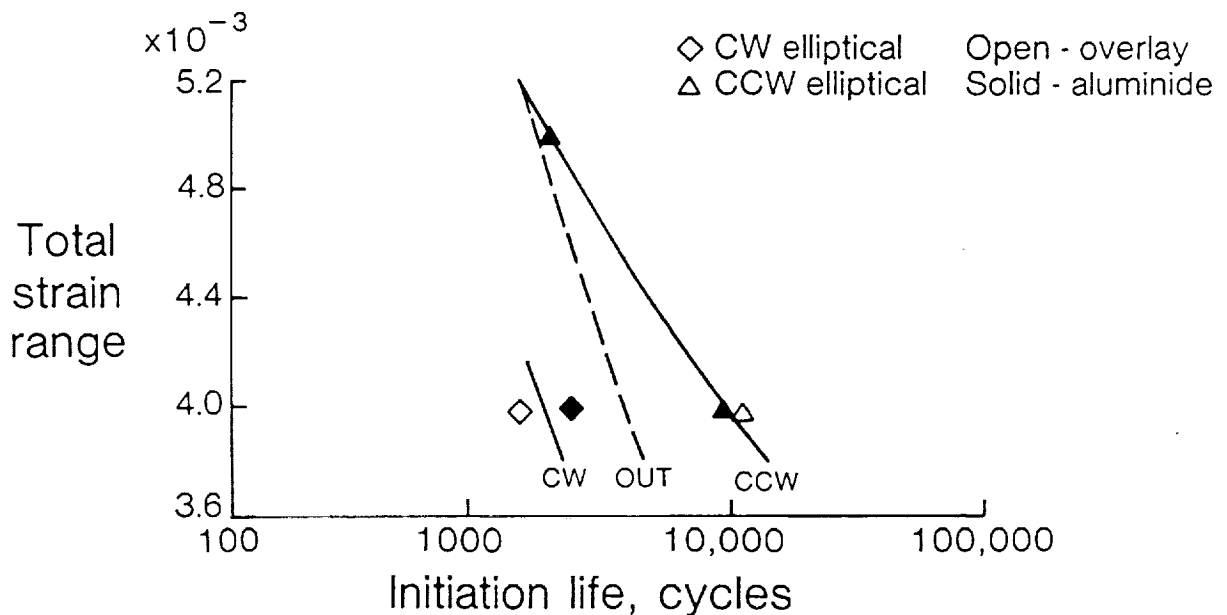
Figure 74.– Elliptical Cycle Path Effects.

100

The results of strain hold tests for both coated and uncoated specimens are shown in Figure 75 relative to data from continuously cycled TMF tests. Note that the hold time causes a large debit for both the coated and the uncoated specimens, but that the coating still gives approximately the same life increase over the uncoated material no matter which cycle was used. This information helps to quantify the level of environmental interaction under these cycle conditions.
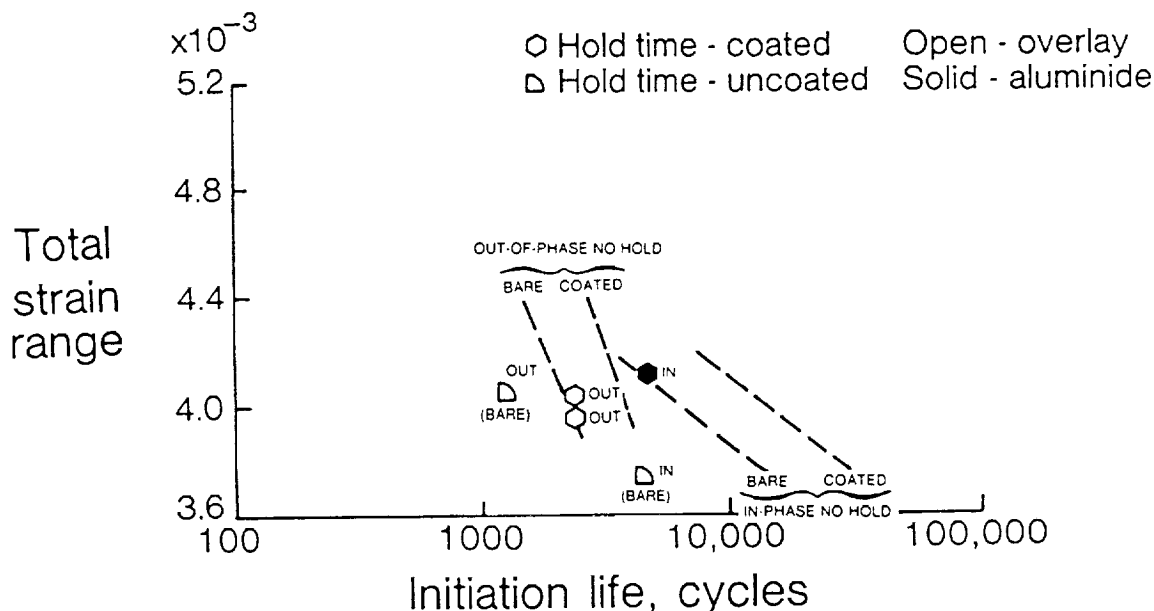
Figure 75.- Effect of Hold Time at Maximum Cycle Temperature.

Figure 76 shows the results of the four coated specimens which were run at a higher temperature range 538-982°C (1000-1800°F) to determine if trends seen at the baseline temperature range would still hold true. It is clear that all the data are shifted lower in life than the median data from the lower temperature range. However, note that the life increase for an elliptical cycle relative to an out-of-phase cycle is still present.

Several new techniques were evaluated during the period of this report to enhance the ability of the basic Cyclic Damage Accumulation (CDA) life model to predict TMF initiation life. These include the following:

1. Modified integration techniques for cycle-by-cycle calculation of damage under TMF conditions.

2. Prediction of inelastic strain ratios using viscoplastic constitutive equations.

3. Use of the general purpose optimization program ADS (Vanderplaats et al, 1983) for determination of life model coefficients.

4. Evaluation of alternative equations for the CDA time-independent damage term.

Work will continue on these methods during the remaining part of the optional program, and those which are ultimately incorporated into the CDA model will be discussed in detail in the final report.
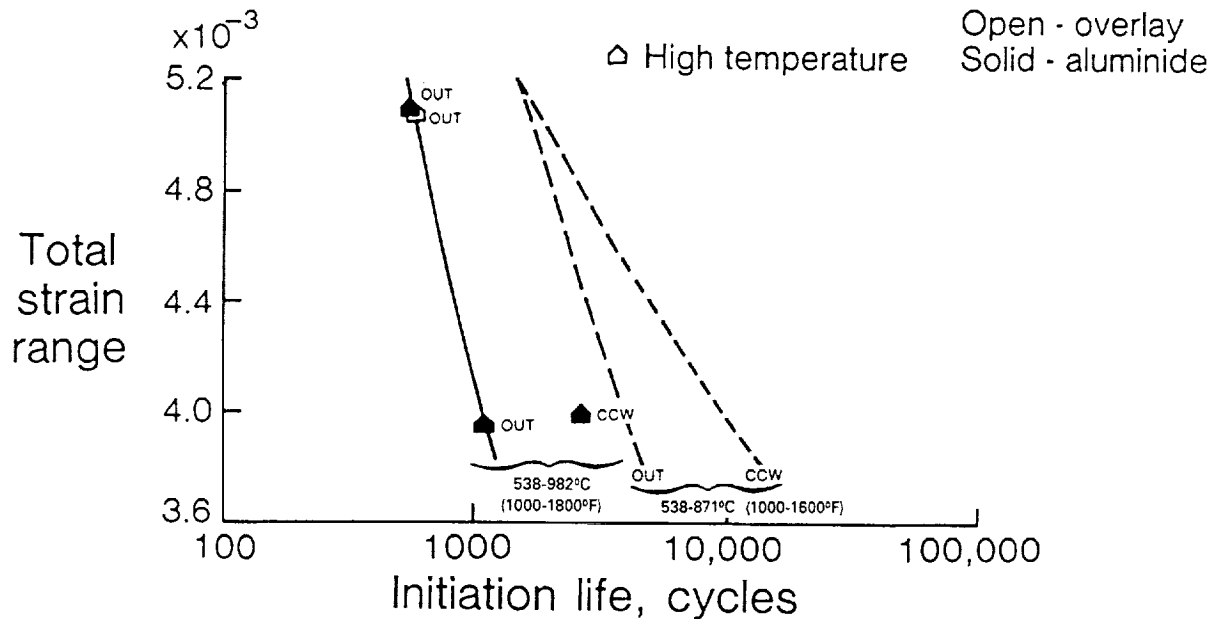
Figure 76.- Effect of Temperature Range.

5.2 Multiaxial Data Correlations

Evaluation of various multiaxial life prediction parameters has continued,
with maximum principal strain range still giving the best correlation and this
also agrees with the experimentally observed crack directions. Plots based on
this parameter are shown in Figure 77 for the 538°C (1000°F) data and Figure
78 for the 871°C (1600°F) data. Most of the results fall in line using this
parameter, with the low strain rate tests being lower than the fast rate
tests. Of particular interest is the effect of frequency seen at 538°C
(1000°F), which was not observed at all during the baseline uniaxial tests.
The in-phase data at 871°C (1600°F) also is not well predicted using this
parameter alone. Various revisions to the CDA model are being considered to
improve the accuracy of the predictions for these tests, but the final
selection of the form of the model will be made after the evaluation of the
INCO 718 multiaxial data is completed during Task XII.

5.3 Selection of Environmental Models

The majority of the effort under this task was performed earlier and was
reported in CR-179550. The earlier work surveyed and screened environmental
candidate models and developed a method to evaluate test specimens. This led
to selection of a candidate life prediction model for environmental effects
during this period. The model has the potential to predict the environmental
(oxidation) effects on the cyclic creep-fatigue life of superalloys. The
initial form of the model consists of a modification of the time dependent
damage term of the Cyclic Damage Accumulation (CDA) life model to account for
the faster accumulation of damage in an oxidizing environment. It has been
observed that preferential oxidation of surface connected MC carbides can
enhance the initiation of cracks in cast Ni-base alloys. This infers that
direct penetration of oxygen results in time dependent damage.

102
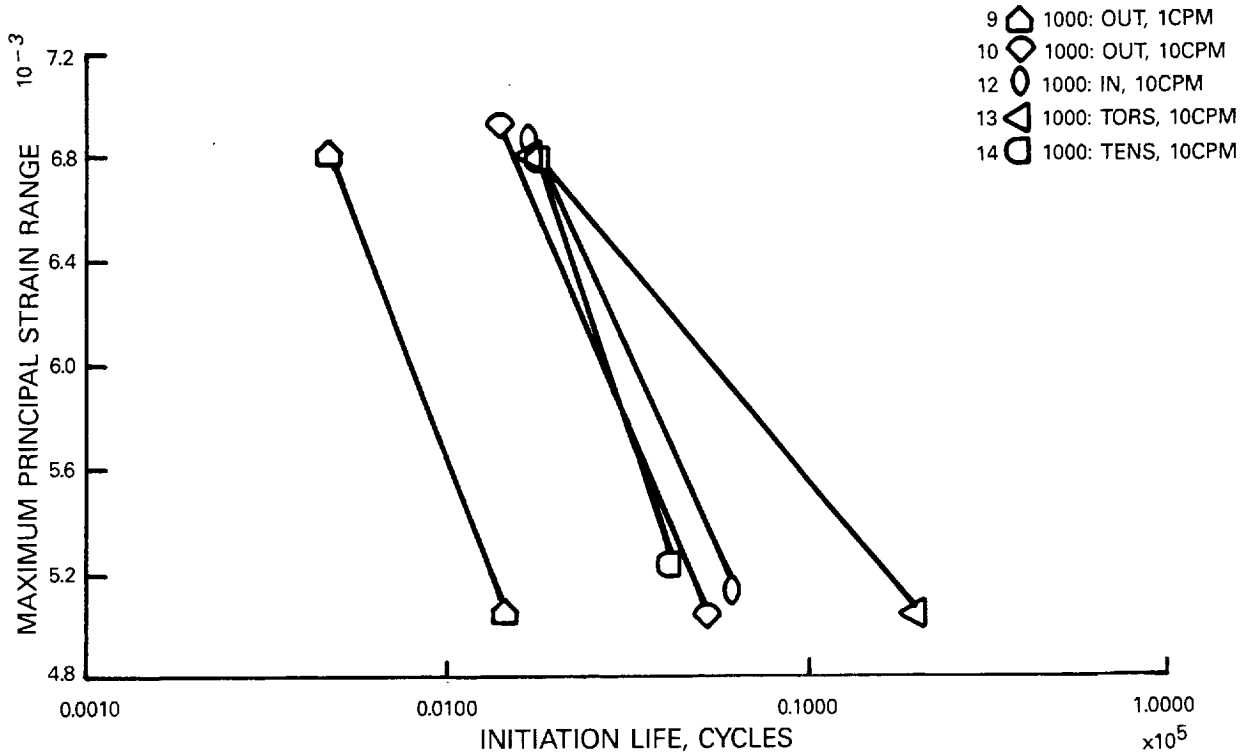
Figure 77.– PWA 1455 Multiaxial Test Data – 538°C (1000°F).
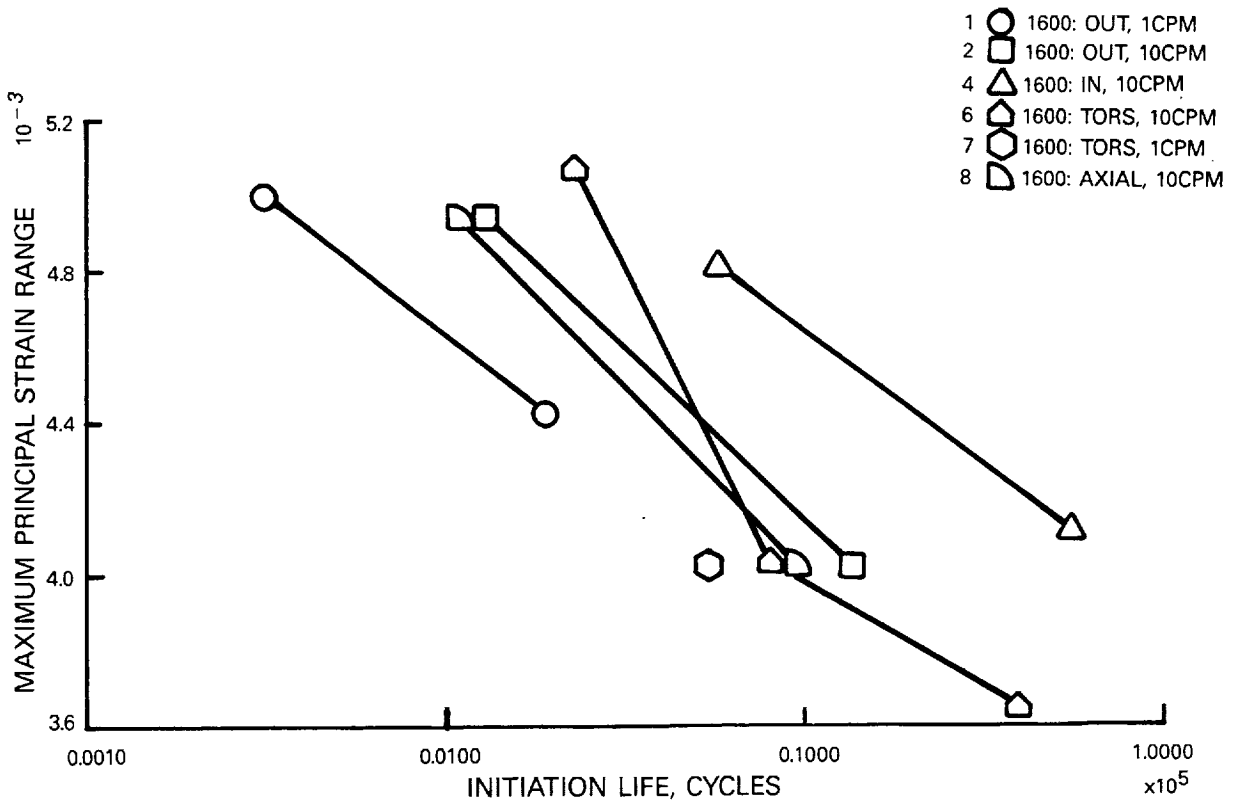
Figure 78.– PWA 1455 Multiaxial Test Data – 871°F (1600°F).

103

The kinetics of preferential oxidation of MC carbides can be described as a diffusion process with a time dependence (oxidation t^n with n = 1/4) and an Arrhenius temperature dependence (K = A exp(-Q/RT)). At longer times under static conditions, there is a saturation of the process. However it is expected that there will be an acceleration of carbide oxidation with cyclic stressing and possibly with increased partial pressure of oxygen. A schematic of these relationships is shown in Figure 79. Since the reference damage rate (dD/dN_{REF}) is established for the given temperature, temperature is not a variable.

An oxidation damage factor (fox) which modifies the time dependent damage rate is a function of depth of oxygen penetration (lo_2) as shown in Figure 80. Depth of oxygen penetration and consequently damage factors can be determined for the new and reference conditions. Multiplying the time dependent damage term in the CDA life model by the ratio (fox/fox_{REF}) accounts for the different accumulation of oxidation damage.

The revised time dependent damage rate is:

$$\left(\frac{dD}{dN}\right) = \left(\frac{dD}{dN}\right)_{REF}\left[\left(\frac{\Delta\sigma_{REF}}{\Delta\sigma}\right)\left(\frac{\sigma_T}{\sigma_{T,REF}}\right)\right]^{B'}\left[\left(\frac{t}{t_{REF}}\right)^{C'} - 1\right]\left(\frac{f_{OX}}{f_{OX,REF}}\right) \qquad (7)$$

It is expected that this initial form of the model will be subject to further revision as more data becomes available from the environmental testing (Task IX).

5.4 Effects of Coating on Isothermal Specimens

These specimens showed initiation lives as determined by replica data which were 2X-7X higher than the lives of uncoated specimens run at similar conditions. In some cases, the replica data may be overestimating the initiation lives due to subsurface cracking. This was the case for several specimens and is a result of the high ductility of the PWA 286 coating at the temperatures used for this test. It is also possible that the effect of oxidation was significantly reduced by the coating, so long as the ductility of the coating was not exceeded. However, other test conditions are known to result in early coating cracking and hence a lower life for a coated specimen relative to an uncoated one. Situations such as these clearly require a life model with at least two different modes of damage to capture correctly both coating and substrate initiation lives. The coating life model being developed under a companion HOST contract (Swanson et al, 1987) is being integrated with the CDA model to accomplish this capability. The environmental model developed under Task IX will be used to increase the life of the substrate in the presence of uncracked coatings. The detailed form of this model will be discussed in the final report.

104

ℓ_{O2}
(depth of oxygen penetration)

σ_t, P_{O2}

Temp = constant

t (time)
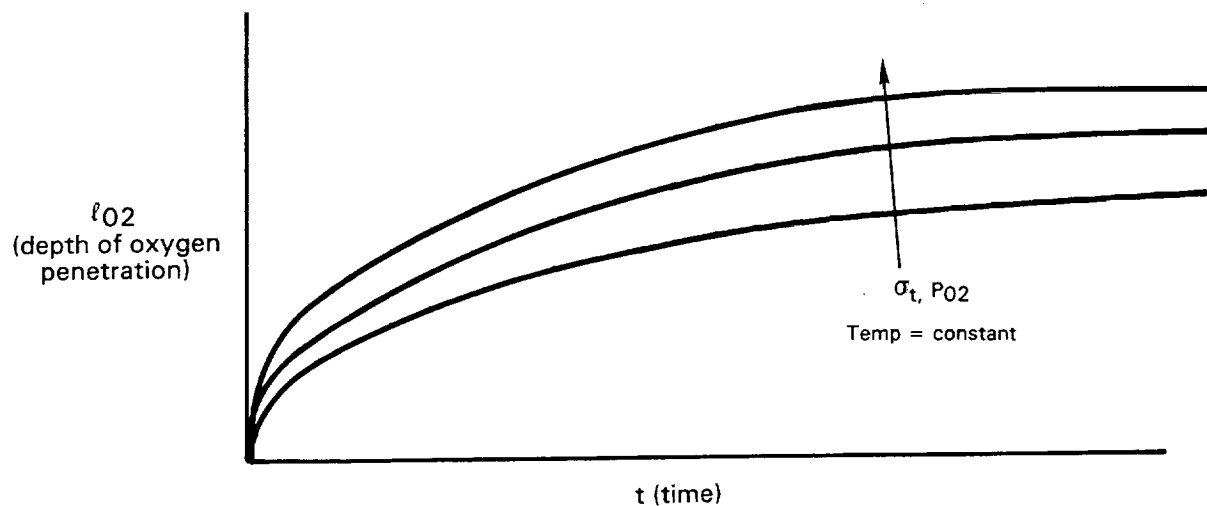
Figure 79.- Schematic Showing Depth of Oxygen Penetration to be a Function of Time, Stress and Partial Pressure of Oxygen at Constant Temperature.

f_{ox}
(Oxidation damage) factor

ℓ_{O2} (depth of oxygen penetration)
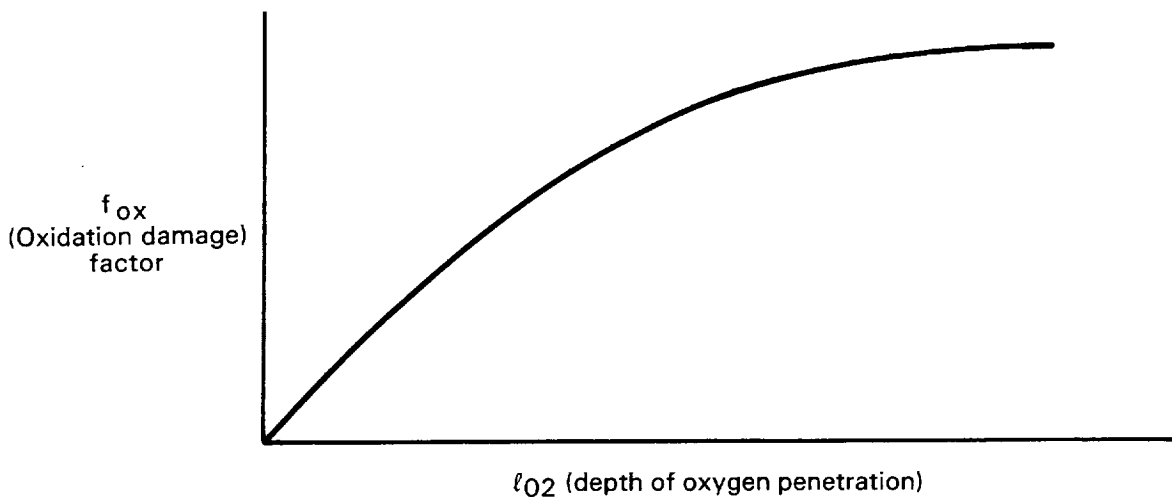
Figure 80.- Schematic showing Possible Relationship Between Damage Factor and Depth of Oxygen Penetration.

5.5 Creep-Fatigue Interaction During Mean Stress TMF Testing

A common practice for prediction of life under creep-fatigue conditions is linear summation of creep and fatigue damage fractions. An interaction plot based on this model is shown in Figure 81 for the three back-to-back in-phase TMF tests completed under this task. Note that the assumption of linear damage summation does not hold for these tests; predicted lives for the high mean stress tests would be approximately 3X too high. Preliminary review of data from the isothermal tests being conducted at URI shows similar trends. This indicates that non-linear interactions will be needed for accurate life predictions of this data. Revisions to the CDA life prediction model are underway to account for this and will be discussed in detail in the final report.

105

Fixed conditions: 538-871°C (1000-1600°F), in-phase, 100 ksi stress range
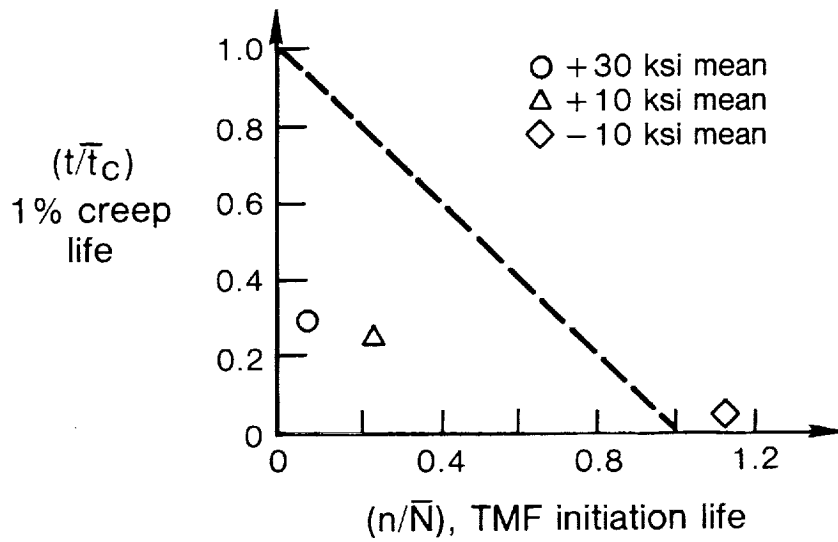
Figure 81.- Interaction Diagram for Load Controlled TMF Tests.

SECTION 6.0
CONCLUSIONS

This report covers the activity under NASA Contract NAS3-23288, "Creep Fatigue
Life Prediction for Engine Hot Section Materials (Isotropic)", for the period
from October 1985 through April 1987. During this time, a series of high
temperature, strain controlled fatigue tests were completed to study the
effects of complex loadings such as thermomechanical fatigue, multiaxial
loading, reactive environments, and imposed mean stresses. Most of these tests
used the cast nickel-base superalloy B1900+Hf (with and without coatings) as a
baseline alloy. A small number of alternate alloy tests were run using wrought
INCO 718.

Under Task V, Thermal-Mechanical Cycling Model, a total of 25 thermomechanical
fatigue (TMF) tests were completed (12 specimens with PWA 286 overlay coating,
11 specimens with PWA 273 diffusion coating, and 2 uncoated specimens).
Various revisions and enhancements to the CDA life prediction model were
studied for TMF life prediction. The major conclusions which resulted from
this effort were as follows:

1. Strain range and cycle type were both shown to be significant factors in
   determining coated TMF life. As with the uncoated TMF tests, the phase
   angle between strain and temperature for elliptical cycle tests
   (clockwise vs. counterclockwise) was also very important, especially at
   low strain ranges.

2. For the conditions used in this task, the presence of the coatings in
   general increased the specimen lives by 2-5X. This is in contrast to most
   actual service conditions, in which the coating will crack prematurely
   when exposed to high local strains. This was confirmed by judicious
   selection of a cycle type which resulted in high coating strains and
   hence lower life than an uncoated specimen.

Under Task VI, Multiaxial Stress State Model, a total of 26 strain controlled
multiaxial fatigue tests were completed during this period. The major
conclusions which resulted were as follows:

1. Strain range and cycle type were both shown to be significant factors in
   determining multiaxial life. The phase angle between axial strain and
   torsional strain was also important, although frequently there was little
   interaction between the two.

2. A strong frequency effect was noted at both 538°C (1000°F) and 871°C
   (1600°F), whereas such an effect was seen during simple tension baseline
   tests only at the higher temperature.

3. Unusual levels of dross and/or porosity were found to have caused
   premature cracking in four of the tests. This was no doubt caused by the
   casting process used to create the bars for these specimens. The grain
   size and gamma prime site were found to be comparable to those of the
   uniaxial specimens. The specimen wall thickness contains approximately
   two grains and therefore elastic anisotropy effects may be more important
   in the case of the multiaxial specimens than for the uniaxial specimens.

4. Out-of-phase loading caused extensive rubbing of the opposing fracture surfaces which obscured mot of the fracture surface details.

5. The best parameter used thus far for multiaxial life prediction for the PWA 1455 data is maximum principal strain range which agrees with experimentally observed crack directions.

Under Task VIII, Screening of Potential Environmental and Protective Coating Models, a model was selected and approved for further study and development. This consists of a damage term which modifies the time-dependent term of the CDA as a function of time, temperature, and oxygen partial pressure.

Under Task IX, Environmental Attack Model, a total of 8 screening specimen tests were completed using moderate pressure oxygen (75 psia, which is the partial pressure of oxygen in the engine operation), lab air, and purified argon. In general, the higher oxygen partial pressures caused lower specimen lives, with initiation life being more influenced than propagation life. However, the argon screening tests produced inconclusive data, due in part to mechanical problems (air/water leaks). Another factor may be that the type of oxide scale which forms in very low partial pressures of oxygen may be more porous than the oxide which forms at higher pressures.

Under Task X, Protective Coatings Models, a total of 8 strain controlled isothermal fatigue tests were completed. The important conclusions from this activity were as follows:

1. For the conditions tested, initiation lives of these coated specimens were significantly higher than the lives of uncoated specimens run at the same conditions. This may be due to the tendency for replica data to overestimate initiation life when subsurface cracking occurs. It is also possible that the coating reduced the influence of the environment on the PWA 1455 substrate.

2. For several specimens, the failure origin was in the substrate, not in the coating itself. This is due to the high ductility of this coating at the high temperatures used for these tests.

A multi-mode damage model is being incorporated into the CDA framework to allow accurate prediction of these results from Tasks IX and X. The substrate initiation will be handled as though it is taking place in an inert environment. The coating initiation will be calculated separately.

Under Task XI, Cyclic Mean Stress Model, a total of 5 load controlled TMF tests were completed. These tests were run at various mean stresses to provide an understanding of what mean stress means in the context of varying temperature. The major conclusions from this testing are as follows:

1. Mean stress was shown to have a dramatic effect on TMF life. A modest tensile mean stress cut the initiation life by more than 90%, whereas a slightly compressive mean stress actually caused crack growth to slow down and eventually stop.

2. The results are not well explained by linear summation of creep and fatigue damage. Total damage sums were only 0.25 for some tests (instead of 1.0).

A method has been developed at the University of Rhode Island to permit a test to be conducted with independent control of both strain range and mean stress. This has been checked out and will be used for the remaining isothermal mean stress tests.

Under Task XII, Final Verification and Evaluation of Alternative Material/Protection Coating System/Component Combination, a rolled ring forging of AMS 5663 (INCO 718) was obtained and specimens were machined and prepared for use (including electropolishing). A total of 4 isothermal fatigue tests and 3 notched stress rupture tests were completed.

APPENDICES A – F

APPENDIX A-1

B1900+HF TMF TEST RESULTS

OUT-OF-PHASE CYCLES, 538-871°C (1000-1600°F)

Specimen Identification		120A	120B	119A	113A	114A	115C	112D	116C
Type of Specimen		MERL 44C	MERL 44C	MERL 44C	MERL 73C	MERL 73C	MERL 73C	MERL 73C	MERL 73C
Coating Type		Overlay	Overlay	Overlay	Overlay	Aluminide	Aluminide	Overlay	Aluminide
Test Conditions:									
Cycle Type		OUT	OUT	OUT	OUT	OUT	OUT	OUT	OUT
Temperature Range	(°C)	538-871	538-871	538-871	538-871	538-871	538-871	538-871	538-871
"	(°F)	1000-1600	1000-1600	1000-1600	1000-1600	1000-1600	1000-1600	1000-1600	1000-1600
Strain Range		0.004110	0.004000	0.005020	0.005020	0.003968	0.005025	0.004050	0.005024
Strain R-Ratio (min/max)		-1.003	-0.993	-1.017	-1.001	-1.007	-1.008	-56.431	-74.366
Strain Rate	(1/sec)	1.40E-04	1.30E-04	1.70E-04	1.70E-04	1.32E-04	1.67E-04	1.35E-04	1.67E-04
Frequency	(cyc/min)	1.000	1.000	1.000	1.000	1.000	1.000	1.000	1.000
Tension Hold	(sec)	0.000	0.000	0.000	0.000	0.000	0.000	0.000	0.000
Compression Hold	(sec)	0.000	0.000	0.000	0.000	0.000	0.000	0.000	0.000
Stress-Strain Response:									
Stress Range, Init	(Mpa)	728.1	722.3	894.0	859.0	683.6	804.5	673.7	843.1
"	(psi)	105597.0	104752.0	129659.0	124584.0	99144.5	116677.0	97712.9	122279.0
Stress Range, Nf/2	(Mpa)	706.5	737.1	865.6	932.1	687.9	795.5	732.5	809.9
"	(psi)	102461.0	106910.0	125541.0	135179.0	99771.6	115367.0	106230.0	117458.0
Mean Stress, Init	(Mpa)	56.8	70.8	46.0	44.2	21.3	36.4	-172.9	-158.5
"	(psi)	8243.9	10270.2	6670.0	6412.0	3087.1	5280.1	-25076.6	-22986.8
Mean Stress, Nf/2	(Mpa)	152.4	171.4	138.1	167.6	78.4	91.7	87.6	41.6
"	(psi)	22095.9	24859.3	20035.8	24312.7	11368.7	13293.1	12704.7	6039.3
Inel Stn Rng, Init		0.000509	0.000021	0.000033	0.000080	0.000199	0.000162	0.000026	0.000045
Inel Stn Rng, Nf/2		0.000479	0.000062	0.000020	0.000120	0.000255	0.000156	0.000070	0.000046
Life Results:									
Initiation	(cycles)	3700.[1]	2938.	2073.[2]	1495.	4753.	1881.	3661.	1359.
5% Load Drop	(cycles)	5249.[1]	3658.	3046.[2]	1849.	7568.	2596.	5035.	2689.
10% Load Drop	(cycles)	5361.[1]	3803.	3110.[2]	1888.	7854.	2639.	5094.	3485.
50% Load Drop	(cycles)	5584.[1]	4452.	3240.[2]	1967.	8195.	2687.	5319.	3997.

Notes: 1. Specimen 120A failed from ID at 4033 cycles; load drop lives estimated.

2. Specimen 119A failed from ID at 2570 cycles; load drop lives estimated.

110

B1900+HF TMF TEST RESULTS

CYCLE PATH EFFECTS, 538-871°C (1000-1600°F)

Specimen Identification	120D	114D	113D	115B	119C	114C	115D	113C
Type of Specimen	MERL 44C	MERL 73C	MERL 73C	MERL 73C	MERL 44C	MERL 73C	MERL 73C	MERL 73C
Coating Type	Overlay	Aluminide	Overlay	Aluminide	Overlay	Aluminide	Aluminide	Overlay
Test Conditions:								
Cycle Type	IN	IN	CW	CW	CCW	CCW	CCW	LC Dogleg
Temperature Range (°C)	538-871	538-871	538-871	538-871	538-871	538-871	538-871	538-871
" (°F)	1000-1600	1000-1600	1000-1600	1000-1600	1000-1600	1000-1600	1000-1600	1000-1600
Strain Range	0.004060	0.004117	0.003979	0.003982	0.003965	0.003967	0.004977	0.004976
Strain R-Ratio (min/max)	-1.012	-1.006	-1.008	-1.025	-1.012	-0.997	-0.997	-1.035
Strain Rate (1/sec)	1.40E-04	1.37E-04	1.33E-04	1.33E-04	1.32E-04	1.32E-04	1.66E-04	1.66E-04
Frequency (cyc/min)	1.000	1.000	1.000	1.000	1.000	1.000	1.000	1.000
Tension Hold (sec)	0.000	0.000	0.000	0.000	0.000	0.000	0.000	0.000
Compression Hold (sec)	0.000	0.000	0.000	0.000	0.000	0.000	0.000	0.000
Stress-Strain Response:								
Stress Range, Init (Mpa)	628.3	707.8	712.7	721.3	707.3	697.0	833.4	928.3
" (psi)	91130.6	102657.0	103371.0	104612.0	102586.0	101093.0	120873.0	134630.0
Stress Range, Nf/2 (Mpa)	680.2	740.5	717.5	708.0	716.6	673.0	806.1	915.8
" (psi)	98652.6	107402.0	104058.0	102688.0	103931.0	97605.9	116917.0	132817.0
Mean Stress, Init (Mpa)	-72.2	-61.0	38.1	30.3	-4.7	27.5	-12.8	65.8
" (psi)	-10470.8	-8849.7	5520.7	4397.8	-683.1	3985.2	-1860.9	9546.4
Mean Stress, Nf/2 (Mpa)	-32.7	-83.3	170.4	136.0	88.1	95.1	-21.0	150.5
" (psi)	-4739.6	-12088.4	24711.4	19720.1	12781.6	13796.2	-3045.0	21826.6
Inel Stn Rng, Init	0.000006	0.000233	0.000129	0.000151	0.000080	0.000072	0.000102	0.000147
Inel Stn Rng, Nf/2	0.000048	0.000125	0.000280	0.000036	0.000042	0.000148	0.000021	0.000132
Life Results:								
Initiation (cycles)	10012.	11712.	1450.	2339.	11125.	9270.	1946.	742.
5% Load Drop (cycles)	15686.[1]	24103.	4157.	3957.	15215.	15695.	3334.	1734.
10% Load Drop (cycles)	16020.[1]	25060.	4228.	4055.	15514.	15785.	3406.	1791.
50% Load Drop (cycles)	16687.	26028.	4394.	4253.	16123.	15982.	3538.	1856.

Note: 1. Crack growth essentially zero at 14,497 cycles and 0.053 in. length; specimen was uploaded to +/-0.25% for the remainder of the test.

APPENDIX A-3

B1900+HF TMF TEST RESULTS

HOLD TIME EFFECTS, 538-871°C (1000-1600°F)

	120C	113B	116A	123D	124A
Specimen Identification					
Type of Specimen	MERL 44C	MERL 73C	MERL 73C	MERL 73C	MERL 73C
Coating Type	Overlay	Overlay	Aluminide	Bare	Bare
Test Conditions:					
Cycle Type	OUT+HOLD	OUT+HOLD	IN+HOLD	OUT+HOLD	IN+HOLD
Temperature Range (°C)	538-871	538-871	538-871	538-871	538-871
" (°F)	1000-1600	1000-1600	1000-1600	1000-1600	1000-1600
Strain Range	0.004103	0.004080	0.004118	0.004143	0.003740
Strain R-Ratio (min/max)	-0.978	-1.116	-1.036	-0.984	-0.932
Strain Rate (1/sec)	5.47E-05	5.00E-05	5.49E-05	5.52E-05	5.00E-05
Frequency (cyc/min)	0.400	0.400	0.400	0.400	0.400
Tension Hold (sec)	0.000	0.000	60.000	0.000	60.000
Compression Hold (sec)	60.000	60.000	0.000	60.000	0.000
Stress-Strain Response:					
Stress Range, Init (Mpa)	669.9	707.8	729.5	719.3	635.6
" (psi)	97157.3	102656.0	105797.0	104327.0	92185.2
Stress Range, Nf/2 (Mpa)	691.7	756.2	762.0	669.0	661.9
" (psi)	100326.0	109675.0	110517.0	97027.3	96002.3
Mean Stress, Init (Mpa)	45.3	34.8	-74.2	78.5	-50.2
" (psi)	6567.7	5054.3	-10765.6	11387.7	-7280.3
Mean Stress, Nf/2 (Mpa)	154.8	123.1	-166.0	157.8	-108.8
" (psi)	22454.0	17848.1	-24076.6	22889.5	-15786.3
Inel Stn Rng, Init	0.000043	0.000057	0.000014	0.000089	0.000007
Inel Stn Rng, Nf/2	0.000090	0.000073	0.000036	0.000084	0.000029
Hold Sts Rlx, Init (Mpa)	+6.7	+6.8	-2.5	+19.2	-6.2
" (psi)	+970.0	+980.0	-360.0	+2780.0	-900.0
Hold Sts Rlx, Nf/2 (Mpa)	+5.0	0.0	0.0	+1.9	0.0
" (psi)	+730.0	0.0	0.0	+270.0	0.0
Life Results:					
Initiation (cycles)	2338.	2364.	4659.	1237.	4411.
5% Load Drop (cycles)	2910.	3174.	10799.	2305.	12451.
10% Load Drop (cycles)	3033.	3242.	10878.	2445.	12500.
50% Load Drop (cycles)	3270.	3377.	11092.	2689.	12602.

112

APPENDIX A-4

B1900+HF TMF TEST RESULTS

TEMPERATURE RANGE EFFECTS, 538-982°C (1000-1800°F)

	119B	115A	116D	116B
Specimen Identification	119B	115A	116D	116B
Type of Specimen	MERL 44C	MERL 73C	MERL 73C	MERL 73C
Coating Type	Overlay	Aluminide	Aluminide	Aluminide
Test Conditions:				
Cycle Type	OUT	OUT	OUT	CCW
Temperature Range (°C)	538-982	538-982	538-982	538-982
" (°F)	1000-1800	1000-1800	1000-1800	1000-1800
Strain Range	0.005091	0.005100	0.003939	0.003990
Strain R-Ratio (min/max)	-1.006	-1.017	-1.022	-1.008
Strain Rate (1/sec)	1.70E-04	1.70E-04	1.31E-04	1.30E-04
Frequency (cyc/min)	1.000	1.000	1.000	1.000
Tension Hold (sec)	0.000	0.000	0.000	0.000
Compression Hold (sec)	0.000	0.000	0.000	0.000
Stress-Strain Response:				
Stress Range, Init (Mpa)	835.0	834.9	646.2	626.6
" (psi)	121098.0	121086.0	93724.0	90884.4
Stress Range, Nf/2 (Mpa)	842.3	833.6	647.4	608.5
" (psi)	122155.0	120904.0	93896.6	88249.0
Mean Stress, Init (Mpa)	146.4	131.4	69.1	21.8
" (psi)	21230.8	19064.4	10026.8	3157.4
Mean Stress, Nf/2 (Mpa)	203.3	174.7	142.4	123.1
" (psi)	29488.0	25343.3	20647.5	17858.3
Inel Stn Rng, Init	0.000157	0.000284	0.000064	0.000075
Inel Stn Rng, Nf/2	0.000014	0.000124	0.000099	0.000039
Life Results:				
Initiation (cycles)	577.	537.[1]	1105.	2622.[2]
5% Load Drop (cycles)	655.	589.[1]	1460.	2662.[2]
10% Load Drop (cycles)	674.	608.[1]	1483.	2676.[2]
50% Load Drop (cycles)	731.	647.[1]	1535.	2703.[2]

Notes: 1. Specimen 115A failed from ID.

2. Specimen 116B may have initiated on the ID or in the substrate.

B1900+HF MULTIAXIAL TESTS

TENSION ONLY, FAST RATE

Specimen Identification		201	220	222	217
Type of Specimen		Fig. 14C	Fig. 14C	Fig. 14C	Fig. 14C

Test Conditions:

Temperature	(°C)	538.	538.	871.	871.
"	(°F)	1000.	1000.	1600.	1600.
Axial Strain Range		0.005230	0.006790	0.004020	0.004940
Axial Strain R-Ratio (min/max)		-0.999	-0.999	-0.998	-0.999
Axial Strain Rate (1/sec)		1.74E-03	2.26E-03	1.34E-03	1.65E-03
Torsional Strain Range		0.000000	0.000000	0.000000	0.000000
Torsional Strain R-Ratio (min/max)		0.000	0.000	0.000	0.000
Torsional Strain Rate (1/sec)		0.00E+00	0.00E+00	0.00E+00	0.00E+00
Strain Ratio (torsional/axial)		0.000	0.000	0.000	0.000
Strain Phase Angle (degrees)		0.000	0.000	0.000	0.000
Frequency (cyc/min)		10.000	10.000	10.000	10.000

Axial Stress-Strain Response:

Stress Range, Init	(Mpa)	888.2	1121.4	565.3	682.7
" " "	(psi)	128823.0	162646.0	81989.9	99007.9
Stress Range, Nf/2	(Mpa)	882.9	1134.3	552.9	681.8
" " "	(psi)	128046.0	164512.0	80194.2	98881.2
Mean Stress, Init	(Mpa)	-6.9	-7.0	-4.5	-6.7
" " "	(psi)	-1004.5	-1008.0	-647.0	-971.0
Mean Stress, Nf/2	(Mpa)	3.0	-2.8	3.7	103.2
" " "	(psi)	437.2	-410.3	534.2	14962.5
Inel Stn Rng, Init		0.000018	0.000056	0.000067	0.000070
Inel Stn Rng, Nf/2		0.000018	0.000016	0.000136	0.000019

Torsional Stress-Strain Response:

Stress Range, Init	(Mpa)	0.0	0.0	0.0	0.0
" " "	(psi)	0.0	0.0	0.0	0.0
Stress Range, Nf/2	(Mpa)	0.0	0.0	0.0	0.0
" " "	(psi)	0.0	0.0	0.0	0.0
Mean Stress, Init	(Mpa)	0.0	0.0	0.0	0.0
" " "	(psi)	0.0	0.0	0.0	0.0
Mean Stress, Nf/2	(Mpa)	0.0	0.0	0.0	0.0
" " "	(psi)	0.0	0.0	0.0	0.0
Inel Stn Rng, Init		0.000000	0.000000	0.000000	0.000000
Inel Stn Rng, Nf/2		0.000000	0.000000	0.000000	0.000000

Life Results:

Initiation (0.030 in.)	(cycles)	4100.	1790.	9629.	1107.
5% Tensile Load Drop	(cycles)	5615.	2375.	15119.	1810.
10% Tensile Load Drop	(cycles)	5741.	2536.	15203.	1840.
50% Tensile Load Drop	(cycles)	5941.	2815.	15864.	2040.
Actual End of Test	(cycles)	8461.	6837.	19390.	2442.

B1900+HF MULTIAXIAL TESTS

TORSION ONLY, FAST RATE

Specimen Identification		209	221	203	219	212
Type of Specimen		Fig. 14C	Fig. 14C	Fig. 14C	Fig. 14C	Fig. 14C

Test Conditions:

		209	221	203	219	212
Temperature	(°C)	538.	538.	871.	871.	871.
"	(°F)	1000.	1000.	1600.	1600.	1600.
Axial Strain Range		0.000000	0.000000	0.000000	0.000000	0.000000
Axial Strain R-Ratio	(min/max)	0.000	0.000	0.000	0.000	0.000
Axial Strain Rate	(1/sec)	0.00E+00	0.00E+00	0.00E+00	0.00E+00	0.00E+00
Torsional Strain Range		0.010080	0.013620	0.008050	0.007290	0.010140
Torsional Strain R-Ratio	(min/max)	-0.998	-1.002	-1.002	-1.002	-1.000
Torsional Strain Rate	(1/sec)	3.36E-03	4.54E-03	2.68E-03	2.43E-03	3.38E-03
Strain Ratio (torsional/axial)		0.000	0.000	0.000	0.000	0.000
Strain Phase Angle	(degrees)	0.000	0.000	0.000	0.000	0.000
Frequency	(cyc/min)	10.000	10.000	10.000	10.000	10.000

Axial Stress-Strain Response:

		209	221	203	219	212
Stress Range, Init	(Mpa)	0.0	0.0	0.0	0.0	0.0
" " "	(psi)	0.0	0.0	0.0	0.0	0.0
Stress Range, Nf/2	(Mpa)	0.0	0.0	0.0	0.0	0.0
" " "	(psi)	0.0	0.0	0.0	0.0	0.0
Mean Stress, Init	(Mpa)	0.0	0.0	0.0	0.0	0.0
" " "	(psi)	0.0	0.0	0.0	0.0	0.0
Mean Stress, Nf/2	(Mpa)	0.0	0.0	0.0	0.0	0.0
" " "	(psi)	0.0	0.0	0.0	0.0	0.0
Inel Stn Rng, Init		0.000000	0.000000	0.000000	0.000000	0.000000
Inel Stn Rng, Nf/2		0.000000	0.000000	0.000000	0.000000	0.000000

Torsional Stress-Strain Response:

		209	221	203	219	212
Stress Range, Init	(Mpa)	659.2	853.9	410.9	405.7	564.2
" " "	(psi)	95599.9	123844.0	59600.0	58847.0	81824.9
Stress Range, Nf/2	(Mpa)	665.6	894.5	421.1	384.9	553.6
" " "	(psi)	96538.7	129729.0	61076.6	55829.1	80284.9
Mean Stress, Init	(Mpa)	-0.5	-0.2	-1.1	-4.3	-2.6
" " "	(psi)	-73.0	-24.0	-160.0	-629.5	-379.5
Mean Stress, Nf/2	(Mpa)	1.2	-1.4	-3.6	-9.0	0.4
" " "	(psi)	166.9	-205.5	-529.0	-1310.4	59.2
Inel Stn Rng, Init		0.000059	0.001129	0.000348	0.000176	0.000511
Inel Stn Rng, Nf/2		0.000055	0.000033	0.000629	0.000380	0.000726

Life Results:

		209	221	203	219	212
Initiation (0.030 in.)	(cycles)	20188.	1739.	8100.	40000.[1]	2337.
5% Tensile Load Drop	(cycles)	23500.	2019.	10530.	53000.[1]	3600.
10% Tensile Load Drop	(cycles)	23510.	2042.	10560.	58000.[1]	3650.
50% Tensile Load Drop	(cycles)	23590.	2213.	10820.	62000.[1]	3745.
Actual End of Test	(cycles)	24366.	2332.	11224.	45500.	3770.

Note: 1. Specimen 219 discontinued at 45,500 cycles; load drop lives estimated.

B1900+HF MULTIAXIAL TESTS

IN-PHASE TENSION-TORSION, FAST RATE

Specimen Identification		225	223	218	228	204	226
Type of Specimen		Fig. 14C	Fig. 14C	Fig. 14C	Fig. 14C	Fig. 14C	Fig. 14C

Test Conditions:

		225	223	218	228	204	226
Temperature	(°C)	538.	538.	871.	871.	871.	871.
"	(°F)	1000.	1000.	1600.	1600.	1600.	1600.
Axial Strain Range		0.003840	0.005090	0.002910	0.003070	0.003710	0.003550
Axial Strain R-Ratio	(min/max)	-1.002	-0.998	-1.001	-1.000	-1.002	-0.998
Axial Strain Rate	(1/sec)	1.28E-03	1.70E-03	9.70E-04	1.02E-03	1.24E-03	1.18E-03
Torsional Strain Range		0.005690	0.007750	0.004390	0.004570	0.005410	0.005440
Torsional Strain R-Ratio	(min/max)	-1.001	-1.001	-0.997	-1.000	-0.996	-0.996
Torsional Strain Rate	(1/sec)	1.90E-03	2.58E-03	1.46E-03	1.52E-03	1.80E-03	1.81E-03
Strain Ratio (torsional/axial)		1.482	1.523	1.509	1.489	1.458	1.532
Strain Phase Angle	(degrees)	0.000	0.000	0.000	0.000	0.000	0.000
Frequency	(cyc/min)	10.000	10.000	10.000	10.000	10.000	10.000

Axial Stress-Strain Response:

		225	223	218	228	204	226
Stress Range, Init	(Mpa)	611.3	861.1	427.8	403.6	437.6	482.6
" " "	(psi)	88662.9	124882.0	62041.9	58529.0	63471.9	69993.9
Stress Range, Nf/2	(Mpa)	614.1	872.0	424.0	399.3	420.5	485.8
" " "	(psi)	89059.1	126472.0	61495.2	57912.9	60983.2	70452.6
Mean Stress, Init	(Mpa)	0.4	0.0	-2.2	0.1	38.7	0.3
" " "	(psi)	58.5	0.0	-322.0	9.5	5613.0	39.0
Mean Stress, Nf/2	(Mpa)	6.9	1.4	141.9	-25.4	22.0	-13.4
" " "	(psi)	1005.0	204.9	20586.5	-3686.5	3188.1	-1941.1
Inel Stn Rng, Init		0.000071	0.000093	0.000136	0.000090	0.000260	0.000128
Inel Stn Rng, Nf/2		0.000033	0.000012	0.000132	0.000044	0.000150	0.000248

Torsional Stress-Strain Response:

		225	223	218	228	204	226
Stress Range, Init	(Mpa)	375.8	485.5	232.9	239.3	242.8	282.1
" " "	(psi)	54508.0	70409.9	33771.0	34706.0	35215.0	40920.0
Stress Range, Nf/2	(Mpa)	376.7	490.7	234.7	231.4	236.5	289.1
" " "	(psi)	54640.3	71167.6	34036.3	33565.7	34302.1	41935.0
Mean Stress, Init	(Mpa)	0.0	-2.8	-1.7	-6.1	-2.2	0.8
" " "	(psi)	0.0	-410.0	-248.5	-883.0	-313.5	118.0
Mean Stress, Nf/2	(Mpa)	-5.2	-3.2	-18.1	-3.8	-2.7	-13.3
" " "	(psi)	-761.2	-465.9	-2626.6	-554.1	-391.3	-1930.6
Inel Stn Rng, Init		0.000151	0.000022	0.000180	0.000036	0.000318	0.000026
Inel Stn Rng, Nf/2		0.000064	0.000114	0.000175	0.000175	0.000335	0.000296

Life Results:

		225	223	218	228	204	226
Initiation (0.030 in.)	(cycles)	6164.	1708.	6615.[1]	56000.[2]	350.[1]	5811.
5% Tensile Load Drop	(cycles)	7280.	2533.	9030.[1]	65000.[2]	609.[1]	7104.
10% Tensile Load Drop	(cycles)	7580.	2598.	9070.[1]	70000.[2]	639.[1]	7232.
50% Tensile Load Drop	(cycles)	9580.	2880.	9450.[1]	80000.[2]	714.[1]	8208.
Actual End of Test	(cycles)	11222.	6090.	9801.	39467.	1085.	9653.

Notes: 1. Low lives due to dross, inclusions (see text); not used for life model correlations.

2. Specimen 228 was discontinued at 39,467 cycles with 0.004 in. crack; all lives estimated.

B1900+HF MULTIAXIAL TESTS

OUT-OF-PHASE TENSION-TORSION, FAST RATE

Specimen Identification		214	202	206	205	227	216
Type of Specimen		Fig. 14C	Fig. 14C	Fig. 14C	Fig. 14C	Fig. 14C	Fig. 14C

Test Conditions:

Temperature	(°C)	538.	538.	538.	871.	871.	871.
"	(°F)	1000.	1000.	1000.	1600.	1600.	1600.
Axial Strain Range		0.005030	0.006800	0.006920	0.002940	0.004020	0.004940
Axial Strain R-Ratio	(min/max)	-0.998	-0.996	-0.999	-0.999	-0.999	-0.999
Axial Strain Rate	(1/sec)	1.68E-03	2.27E-03	2.31E-03	9.80E-04	1.34E-03	1.65E-03
Torsional Strain Range		0.007580	0.010270	0.010270	0.004430	0.006060	0.007420
Torsional Strain R-Ratio	(min/max)	-1.001	-0.993	-1.003	-1.003	-1.005	-0.986
Torsional Strain Rate	(1/sec)	2.53E-03	3.42E-03	3.42E-03	1.48E-03	2.02E-03	2.47E-03
Strain Ratio	(torsional/axial)	1.507	1.510	1.484	1.507	1.507	1.502
Strain Phase Angle	(degrees)	90.000	90.000	90.000	90.000	90.000	90.000
Frequency	(cyc/min)	10.000	10.000	10.000	10.000	10.000	10.000

Axial Stress-Strain Response:

Stress Range, Init	(Mpa)	856.5	1213.0	1120.8	460.0	521.6	737.4
" " "	(psi)	124214.0	175919.0	162546.0	66716.9	75654.9	106946.0
Stress Range, Nf/2	(Mpa)	867.6	1215.1	1113.7	451.7	514.2	718.4
" " "	(psi)	125837.0	176224.0	161523.0	65517.3	74579.6	104198.0
Mean Stress, Init	(Mpa)	0.3	7.1	9.0	0.4	-1.6	-5.8
" " "	(psi)	49.0	1026.5	1312.0	59.5	-233.5	-838.0
Mean Stress, Nf/2	(Mpa)	27.9	-1.4	5.2	-3.2	-12.3	121.4
" " "	(psi)	4049.9	-196.9	754.4	-470.5	-1789.5	17604.7
Inel Stn Rng, Init		0.000095	0.000167	0.000296	0.000057	0.000219	0.000030
Inel Stn Rng, Nf/2		0.000120	0.000071	0.000295	0.000104	0.000140	0.000028

Torsional Stress-Strain Response:

Stress Range, Init	(Mpa)	516.7	690.8	710.1	267.2	304.8	431.1
" " "	(psi)	74936.9	100186.0	102991.0	38745.9	44209.0	62525.0
Stress Range, Nf/2	(Mpa)	511.3	695.0	698.5	262.1	300.7	431.5
" " "	(psi)	74153.7	100801.0	101310.0	38009.5	43618.0	62581.5
Mean Stress, Init	(Mpa)	-0.2	6.4	12.0	-1.5	-1.3	-4.7
" " "	(psi)	-24.5	929.0	1747.5	-224.0	-189.5	-677.5
Mean Stress, Nf/2	(Mpa)	-6.0	-6.2	9.0	-5.9	-6.7	-15.8
" " "	(psi)	-873.2	-906.2	1311.2	-860.2	-972.6	-2292.1
Inel Stn Rng, Init		0.000194	0.000261	0.000859	0.000245	0.000100	0.000165
Inel Stn Rng, Nf/2		0.000173	0.000377	0.000734	0.000279	0.000112	0.000193

Life Results:

Initiation (0.030 in.)	(cycles)	5210.	240.[1]	1417.	11434.[1]	13794.	1313.
5% Tensile Load Drop	(cycles)	8060.	369.[1]	2505.	13819.[1]	15324.	1694.
10% Tensile Load Drop	(cycles)	8125.	395.[1]	2510.	14097.[1]	15648.	1729.
50% Tensile Load Drop	(cycles)	8625.	431.[1]	2544.	15389.[1]	18565.	1973.
Actual End of Test	(cycles)	9544.	543.	2544.	16504.	25300.	1973.

Note: 1. Low lives due to dross, inclusions (see text); not used for life model correlations.

B1900+HF MULTIAXIAL TESTS

SLOW RATE, TORSION ONLY AND OUT-OF-PHASE

Specimen Identification		210	211	215	213	207
Type of Specimen		Fig. 14C	Fig. 14C	Fig. 14C	Fig. 14C	Fig. 14C

Test Conditions:

Temperature	(°C)	871.	538.	538.	871.	871.
"	(°F)	1600.	1000.	1000.	1600.	1600.
Axial Strain Range		0.000000	0.005040	0.006810	0.004420	0.005000
Axial Strain R-Ratio	(min/max)	0.000	-1.000	-0.999	-0.998	-0.999
Axial Strain Rate	(1/sec)	0.00E+00	1.70E-04	2.30E-04	1.50E-04	1.70E-04
Torsional Strain Range		0.008040	0.007480	0.010240	0.006630	0.007560
Torsional Strain R-Ratio	(min/max)	-0.999	-1.002	-1.000	-0.999	-0.998
Torsional Strain Rate	(1/sec)	2.68E-04	2.49E-04	3.41E-04	2.21E-04	2.52E-04
Strain Ratio (torsional/axial)		0.000	1.484	1.504	1.500	1.512
Strain Phase Angle	(degrees)	0.000	90.000	90.000	90.000	90.000
Frequency	(cyc/min)	1.000	1.000	1.000	1.000	1.000

Axial Stress-Strain Response:

Stress Range, Init	(Mpa)	0.0	913.7	1170.2	542.2	639.3
" " "	(psi)	0.0	132517.0	169724.0	78632.9	92721.9
Stress Range, Nf/2	(Mpa)	0.0	911.3	1168.1	517.6	633.4
" " "	(psi)	0.0	132167.0	169416.0	75067.3	91860.2
Mean Stress, Init	(Mpa)	0.0	13.8	-14.2	-7.7	-12.3
" " "	(psi)	0.0	1998.4	-2056.0	-1109.5	-1787.0
Mean Stress, Nf/2	(Mpa)	0.0	-5.5	-10.1	1.5	-19.3
" " "	(psi)	0.0	-790.9	-1464.8	214.4	-2800.2
Inel Stn Rng, Init		0.000000	0.000135	0.000005	0.000190	0.000303
Inel Stn Rng, Nf/2		0.000000	0.000141	0.000024	0.000208	0.000358

Torsional Stress-Strain Response:

Stress Range, Init	(Mpa)	412.1	510.2	676.0	374.1	379.5
" " "	(psi)	59773.0	73994.9	98039.9	54254.0	55033.9
Stress Range, Nf/2	(Mpa)	388.8	505.5	673.7	352.2	365.8
" " "	(psi)	56390.0	73319.0	97713.6	51073.9	53050.5
Mean Stress, Init	(Mpa)	-5.8	-8.3	3.3	1.3	-2.4
" " "	(psi)	-847.5	-1210.5	478.0	189.0	-344.0
Mean Stress, Nf/2	(Mpa)	-9.2	-3.3	-0.2	-0.7	-0.7
" " "	(psi)	-1333.1	-477.8	-22.3	-94.9	-104.2
Inel Stn Rng, Init		0.000442	0.000238	0.000249	0.000319	0.000485
Inel Stn Rng, Nf/2		0.000753	0.000166	0.000203	0.000515	0.000546

Life Results:

Initiation (0.030 in.)	(cycles)	5440.	1454.	486.	1911.	327.
5% Tensile Load Drop	(cycles)	6800.[1]	1837.	805.	3728.	716.
10% Tensile Load Drop	(cycles)	7200.[1]	1946.	818.	3896.	731.
50% Tensile Load Drop	(cycles)	7500.[1]	2408.	873.	4368.	834.
Actual End of Test	(cycles)	5523.	3111.	918.	4682.	834.

Note: 1. Specimen 210 was discontinued at 5523 cycles; load drop lives estimated.

ENVIRONMENTAL SCREENING TESTS

AIR AND MODERATE PRESSURE OXYGEN

Specimen Identification		123B	124B	124D	123A	111C	111D	112A	112C
Type of Specimen		MERL 75	MERL 75	MERL 75	MERL 75	MERL 75	MERL 75	MERL 75	MERL 75
Test Conditions:									
Environment		LAB AIR	LAB AIR	LAB AIR	SHOP AIR	OXYGEN	OXYGEN	OXYGEN	OXYGEN
Temperature	(°C)	982.	982.	871.	871.	871.	982.	982.	982.
"	(°F)	1800.	1800.	1600.	1600.	1600.	1800.	1800.	1800.
Strain Range		0.004070	0.003993	0.005150	0.005130	0.005130	0.004030	0.004070	0.003943
Strain R-Ratio (min/max)		-0.983	-1.000	-0.977	-0.963	-0.961	-1.002	-0.974	-0.984
Strain Rate	(1/sec)	1.70E-04	1.66E-03	1.70E-04	1.70E-04	1.70E-04	1.70E-04	1.70E-04	1.64E-03
Frequency	(cyc/min)	1.248	12.500	1.000	0.996	0.996	1.260	1.248	12.500
Tension Hold	(sec)	0.000	0.000	0.000	0.000	0.000	0.000	0.000	0.000
Compression Hold	(sec)	0.000	0.000	0.000	0.000	0.000	0.000	0.000	0.000
Stress-Strain Response:									
Stress Range, Init	(Mpa)	452.9	487.9	676.0	688.5	695.4	477.1	470.1	505.2
"	(psi)	65690.4	70758.0	98044.2	99852.9	100858.0	69191.1	68184.7	73272.0
Stress Range, Nf/2	(Mpa)	442.9	485.1	647.9	659.7	748.2	428.4	456.9	547.0
"	(psi)	64236.3	70360.0	93965.7	95678.4	108518.0	62137.6	66264.9	79326.0
Mean Stress, Init	(Mpa)	-8.7	-8.2	-13.2	-10.8	-10.6	-9.6	-8.8	-6.2
"	(psi)	-1261.3	-1187.0	-1911.8	-1560.2	-1542.9	-1392.1	-1282.7	-895.0
Mean Stress, Nf/2	(Mpa)	2.9	-0.2	-19.3	-0.6	-18.1	-24.2	-6.2	5.1
"	(psi)	427.2	-30.0	-2796.3	-91.2	-2629.0	-3505.8	-893.0	737.0
Inel Stn Rng, Init		0.000654	0.000386	0.000192	0.000280	0.000150	0.000941	0.000716	0.000582
Inel Stn Rng, Nf/2		0.000759	0.000404	0.000355	0.000458	0.000487	0.001204	0.000939	0.000682
Life Results:									
Initiation	(cycles)	1320.	1560.	1350.	560.[1]	674.	559.	460.	924.[2]
5% Load Drop	(cycles)	2395.	4173.	4847.	1342.[1]	1869.	1143.	904.	2483.[2]
10% Load Drop	(cycles)	2444.	4254.	5199.	1380.[1]	2080.	1167.	951.	2562.[2]
50% Load Drop	(cycles)	2493.	4464.	5632.	1443.[1]	2245.	1216.	1000.	2641.[2]

Notes: 1. Life apparently reduced by foreign substances in air supply.

2. Specimen 112C failed at 958 cycles under the extensometer rods; load drop lives estimated.

PWA 1455 COATED ISOTHERMAL TESTS

PWA 286 OVERLAY COATING

Specimen Identification		117A	117B	117C	117D	118A	118B	118C	118D
Type of Specimen		MERL 75	MERL 75	MERL 75	MERL 75	MERL 73C	MERL 75	MERL 75	MERL 75
Test Conditions:									
Temperature (°C)		871.	982.	982.	982.	982.	982.	871.	871.
" (°F)		1600.	1800.	1800.	1800.	1800.	1800.	1600.	1600.
Strain Range		0.004904	0.005137	0.008023	0.005050	0.003981	0.003947	0.004959	0.004920
Strain R-Ratio (min/max)		0.014	0.000	-0.995	-0.999	-1.007	-0.990	0.002	0.012
Strain Rate (1/sec)		1.63E-03	1.71E-04	1.67E-03	1.70E-04	1.66E-04	1.05E-03	8.27E-05	1.30E-04
Frequency (cyc/min)		10.000	1.000	6.250	1.000	1.250	8.000	0.500	0.790
Tension Hold (sec)		0.000	0.000	0.000	0.000	0.000	0.000	0.000	60.000
Compression Hold (sec)		0.000	0.000	0.000	0.000	0.000	0.000	0.000	0.000
Stress-Strain Response:									
Stress Range, Init (Mpa)		642.6	569.0	807.6	484.0	420.9	481.0	672.4	680.4
" (psi)		93193.0	82525.0	117130.0	70193.8	61048.0	69754.6	97522.9	98675.9
Stress Range, Nf/2 (Mpa)		662.2	523.5	803.4	459.0	406.1	456.5	667.4	693.2
" (psi)		96047.0	75929.0	116513.0	66576.4	58897.1	66203.1	96798.9	100543.0
Mean Stress, Init (Mpa)		220.0	24.4	-9.9	-7.9	-2.0	8.9	190.6	184.7
" (psi)		31900.0	3543.0	-1435.0	-1150.9	-291.2	1292.4	27646.1	26794.3
Mean Stress, Nf/2 (Mpa)		163.8	1.7	-6.3	3.9	25.5	27.1	78.6	-43.7
" (psi)		23760.0	240.0	-918.0	559.5	3697.7	3923.9	11400.4	-6331.5
Inel Stn Rng, Init		0.000179	0.001244	0.002067	0.001010	0.000744	0.000339	0.000430	0.000562
Inel Stn Rng, Nf/2		0.000190	0.001424	0.002045	0.001154	0.000865	0.000524	0.000546	0.000529
Hold Sts Rlx, Init (Mpa)		0.0	0.0	0.0	0.0	0.0	0.0	0.0	-25.2
" (psi)		0.0	0.0	0.0	0.0	0.0	0.0	0.0	-3660.0
Hold Sts Rlx, Nf/2 (Mpa)		0.0	0.0	0.0	0.0	0.0	0.0	0.0	-28.4
" (psi)		0.0	0.0	0.0	0.0	0.0	0.0	0.0	-4120.0
Life Results:									
Initiation (cycles)		3799.	1780.	395.	>643.[1]	3409.	3857.	2349.	1618.[2]
5% Load Drop (cycles)		3920.	1840.	398.	>643.	3531.	5777.	2981.	3453.[2]
10% Load Drop (cycles)		3960.	1900.	412.	>643.	3685.	6011.	3102.	3566.[2]
50% Load Drop (cycles)		4041.	2000.	420.	>643.	3830.	6429.	3262.	3794.[2]

Notes: 1. Specimen 117D cracked under the extensometer rods at 643 cycles; no cracks visible in gage section.

2. Specimen 118D failed from cracks under the extensometer rods at 2147 cycles; load drop lives estimated.

PWA 1455 MEAN STRESS TESTING

LOAD CONTROLLED TMF

Specimen Identification		109C	110D	111B	114B	112B
Type of Specimen		MERL 73C	MERL 73C	MERL 73C	MERL 73C	MERL 73C

Test Conditions:

Cycle Type		IN	IN	IN	IN	OUT
Temperature Range	(°C)	538-871	538-871	538-871	538-871	538-871
" "	(°F)	1000-1600	1000-1600	1000-1600	1000-1600	1000-1600
Stress Range	(Mpa)	671.5	671.3	670.5	604.2	698.1
" "	(psi)	97382.6	97366.4	97238.7	87622.9	101251.0
Stress R-Ratio	(min/max)	-0.2503	-0.6678	-1.5063	-0.5002	-1.5002
Stress Rate	(Mpa/sec)	2.24E+01	2.24E+01	2.23E+01	2.01E+01	2.33E+01
" "	(psi/sec)	3.25E+03	3.25E+03	3.24E+03	2.92E+03	3.38E+03
Frequency	(cyc/min)	1.000	1.000	1.000	1.000	1.000
Tension Hold	(sec)	0.000	0.000	0.000	0.000	0.000
Compression Hold	(sec)	0.000	0.000	0.000	0.000	0.000

Stress-Strain Response:

Strain Range, Init		0.004150	0.004150	0.004040	0.003730	0.004230
Strain Range, Nf/2		0.004250	0.004310	0.003950	0.003740	0.004240
Mean Strain, Init		0.002040	0.001200	-.000090	0.000860	-.000590
Mean Strain, Nf/2		0.006570	0.005010	0.000520	0.007210	-.003790
Inel Stn Rng, Init		0.000200	0.000148	0.000176	0.000154	0.000193
Inel Stn Rng, Nf/2		0.000142	0.000185	0.000189	0.000124	0.000073

Life Results:

Initiation	(cycles)	177.	1914.	5611.	5765.	2684.
5% Load Drop	(cycles)	213.	2331.	>16503.[1]	7095.	6709.
10% Load Drop	(cycles)	218.	2380.	>16503.[1]	7244.	6850.
50% Load Drop	(cycles)	227.	2454.	>16503.[1]	7468.	7062.

Note: 1. Specimen 111B was discontinued at 16,503 cycles with a 0.071 in. crack.

INCO 718 FATIGUE TESTING

INITIAL ISOTHERMAL TESTS

Specimen Identification		718-1	718-2	718-3	718-4
Type of Specimen		MERL 75	MERL 75	MERL 75	MERL 75

Test Conditions:

		718-1	718-2	718-3	718-4
Temperature	(°C)	732.	732.	649.	649.
"	(°F)	1350.	1350.	1200.	1200.
Strain Range		0.007830	0.006460	0.007950	0.006460
Strain R-Ratio (min/max)		-1.007	-0.988	-0.994	-0.991
Strain Rate (1/sec)		2.60E-04	2.20E-04	2.60E-04	2.20E-04
Frequency (cyc/min)		1.000	1.000	1.000	1.000
Tension Hold (sec)		0.000	0.000	0.000	0.000
Compression Hold (sec)		0.000	0.000	0.000	0.000

Stress-Strain Response:

		718-1	718-2	718-3	718-4
Stress Range, Init (Mpa)		1143.5	1012.9	1240.4	1039.5
" " " (psi)		165849.0	146908.0	179896.0	150766.0
Stress Range, Nf/2 (Mpa)		956.1	888.1	1102.2	991.4
" " " (psi)		138668.0	128797.0	159862.0	143786.0
Mean Stress, Init (Mpa)		-15.1	1.4	-15.1	-5.7
" " (psi)		-2193.0	198.8	-2187.1	-829.3
Mean Stress, Nf/2 (Mpa)		9.8	1.9	-0.8	14.3
" " (psi)		1414.1	278.3	-117.0	2079.3
Inel Stn Rng, Init		0.000231	0.000125	0.000132	0.000121
Inel Stn Rng, Nf/2		0.001577	0.000810	0.001163	0.000354

Life Results:

		718-1	718-2	718-3	718-4
Initiation (cycles)		1339.	4719.	2122.	11066.
5% Load Drop (cycles)		2792.	6181.	2725.	13180.
10% Load Drop (cycles)		2851.	6311.	2782.	13224.
50% Load Drop (cycles)		2939.	6506.	2868.	13332.

REFERENCES

Moreno, V., Nissley, D. M., and Lin, L. S., 1984, "Creep Fatigue Life Prediction for Engine Hot Section Materials (Isotropic) – Second Annual Report," NASA CR-174844.

Nelson, R. S., Schoendorf, J. F., and Lin, L. S., 1986, "Creep Fatigue Life Prediction for Engine Hot Section Materials (Isotropic) – Interim Report," NASA CR-179550.

Swanson, G. A., Linask, I., Nissley, D. M., Norris, P. P., Meyer, T. G., and Walker K. P., 1987, "Life Prediction and Constitutive Models for Engine Hot Section Anisotropic Materials Program, " NASA CR-179594.

Vanderplaats, G. N., Sugimoto, H., and Sprague, C. M., 1983, "ADS-1: A New General Purpose Optimization Program," IAA 24 Structures, Structural Dynamics and Materials. Conference, Lake Tahoe, Nevada.

Report Documentation Page

1. Report No. NASA CR-189220	2. Government Accession No.	3. Recipient's Catalog No.
4. Title and Subtitle Creep Fatigue Life Prediction for Engine Hot Section Materials (Isotropic) - Interim Report		5. Report Date
		6. Performing Organization Code 590-21-11
7. Author(s) R.S. Nelson, G.W. Levan and J.F. Schoendorf		8. Performing Organization Report No. PWA-5894-
		10. Work Unit No.
9. Performing Organization Name and Address United Technologies Corporation Pratt & Whitney Commercial Engineering, East Hartford, CT 06108		11. Contract or Grant No. NAS3-23288
12. Sponsoring Agency Name and Address National Aeronautics and Space Administration Lewis Research Center 21000 Brookpark Rd. Cleveland, OH 44135		13. Type of Report and Period Covered Contractor Report-Interim 10/85-4/87
		14. Sponsoring Agency Code

15. Supplementary Notes

Project Manager: M. A. McGaw, NASA Lewis Research Center, Cleveland, Ohio

16. Abstract

A series of high temperature strain controlled fatigue tests have been completed to study the effects of thermomechanical fatigue, multiaxial loading, reactive environments, and imposed mean stresses. The baseline alloy used in these tests was cast B1900+Hf (with and without coatings); a small number of tests of wrought INCO 718 are also included. A strong path dependence was demonstrated during the thermomechanical fatigue testing, using in-phase, out-phase, and non-proportional (elliptical and "dogleg") strain-temperature cycles. The multiaxial tests also demonstrated cycle path to be a significant variable, using both proportional and non-proportional tension-torsion loading. Environmental screening tests were conducted in moderate pressure oxygen and purified argon; the oxygen reduced the specimen lives by two, while the argon testing produced ambiguous data. Both NiCoCrAlY overlay and diffusion aluminide coatings were evaluated under isothermal and TMF conditions; in general, the lives of the coated specimens were higher that those of uncoated specimens. Controlled mean stress TMF tests showed that small mean stress changes could change initiation lives by orders of magnitude; these results are not conservatively predicted using traditional linear damage summation rules. Microstructures were evaluated using optical, SEM and TEM methods.

17. Key Words (Suggested by Author(s)) Creep Fatigue, Crack initiation, Thermomechanical fatigue, Multiaxial, Life Prediction, Nickel-base Alloy, Cumulative Damage	18. Distribution Statement		
19. Security Classif. (of this report)	20. Security Classif. (of this page)	21. No. of pages	22. Price

NASA FORM 1626 OCT 86